Ionisation by Positron Impact

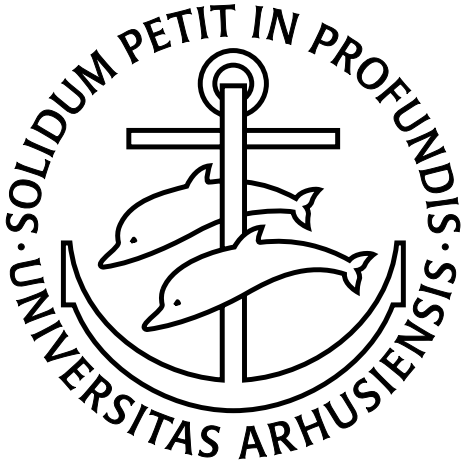

Henrik Bluhme

Institute of Physics and Astronomy
University of Aarhus, Denmark

April 2000

This thesis has been defended on May 25, 2000 at the Institute of Physics and Astronomy, University of Aarhus, Denmark.

External examiners:

Prof. Reinhold Schuch
Stockholm University, Sweden.

Prof. Paul G. Coleman
University of Bath, UK.

Internal examiner (chairman):

Sen. Assoc. Prof. Aksel S. Jensen
University of Aarhus, Denmark.

This version of the thesis is identical to the one submitted, except for the correction of a few minor misprints.

May 2000

This thesis has been printed at the Institute of Physics and Astronomy, University of Aarhus, Denmark.
It can be found in the Acrobat PDF file format on:
http://www.phys.au.dk/main/publications/PhD/home.shtm#2000

Preface

This thesis has been submitted to the Faculty of Science at the University of Aarhus, Denmark, in order to fulfill the requirements for the degree of Doctor of Philosophy (Ph.D.). The main part of the work presented in this thesis has been performed at the Institute of Physics and Astronomy, University of Aarhus, Denmark, under the supervision of Dr. Helge Knudsen. A part of the work has been obtained during a 10 months stay at the Department of Physics and Astronomy, University College London, UK, under the supervision of Dr. Gaetana Laricchia.

Acknowledgements

The past years spent as a Ph.D. student in the Positron group in Århus have been years filled with many interesting challenges and experiences. The number of members in the group has always been small. This has meant that I as a Ph.D. student have been trusted with a good share of the responsibility for the experiments conducted and also been shown a large degree of freedom in the daily work. At times when the experiments did not quite work out this could seem frustrating, but in the end it has proven to be highly educational and very rewarding. For this I would like to acknowledge a number of the people I have worked with over the years.

First of all I would like to thank my supervisor Dr. Helge Knudsen for taking me on as a Ph.D. student in the first place. Helge has always monitored the progress of my work and been the one who worried about the things that never occurred to me as being able of posing any problems. Helge is also acknowledged for teaching me about the framework of atomic collisions within which my work belongs.

Next I would like to extend a sincere thanks to Dr. Jon Merrison who for most of the years has been my primary companion in the lab. It was Jon who already in the spring of 1994 allowed me as an undergraduate to join in on some of the work in his lab. Since then he has taught me all the 'tricks of the trade', teaching me most of what I know about experimental positron physics. Many enjoyable coffee breaks and discussions over the occasional beer have been

spent with Jon. Both Jon and Helge are also acknowledged for proof reading this thesis.

Furthermore I would like to thank MSc Kim Nielsen who did the work for his master's thesis on my experiment, obtaining some of the results presented in this thesis. Two visiting exchange students from Leeds, UK, Robin Mitchell and Daniel Walker, are thanked for their help in obtaining some of the data as well.

The assistance of the technical staff in Århus is also acknowledged. This extends in particular to Poul Aggerholm who has provided help with things far beyond his normal work as an electronics technician. Thanks to the effort of Poul most thing in our lab were kept running smoothly. Furthermore H. J. Larsen is thanked for his good advice whenever I was about to hurt myself in his workshop.

During my stay in London I had the experience of working with another group of very talented people from within my field of research. Among these I would first of all thank Dr. Nella Laricchia for letting me join her group and for supervising me during my stay. Nella is also acknowledged for many useful discussions and comments on my work in general. Next to be acknowledged is my fellow Ph.D. student Dr. Vanita Kara and postdoc Dr. Karen Paludan, who's experiment I joined while there. These and other group members, Dr. Aysun Özen, Dr. David Cassidy and Dr. Andrew J. Garner, are thanked for making it an enjoyable stay in London. Furthermore from London (now at Swansea) is acknowledged Dr. Michael Charlton for providing useful comments and always paying a keen interest in our work in Århus.

Finally are all the people I have made friends with during my nearly 9 years at the University of Aarhus. Some of these have become my closest and most invaluable friends. They are all thanked for the fun times we have shared together over the past years.

Henrik Bluhme
April 2000

List of publications

The work presented in this thesis has been published in the following papers. When referring to any of these inside the thesis, the roman numerals below will be used.

[I] *'Strong suppression of the positronium channel in double ionization of noble gases by positron impact'*,
H. Bluhme, H. Knudsen, J. P. Merrison, and M. R. Poulsen,
Phys. Rev. Lett. **81**, 73 (1998).

[II] *'Non-dissociative and dissociative ionization of nitrogen molecules by positron impact'*,
H. Bluhme, N. P. Frandsen, F. M. Jacobsen, H. Knudsen, J. P. Merrison, K. Paludan, and M. R. Poulsen,
J. Phys. B: At. Mol. Opt. Phys. **31**, 4631 (1998).

[III] *'Double ionization of noble gases by positron impact'*,
H. Bluhme, H. Knudsen, and J. P. Merrison,
in *Proc. of 15th Int. Conf. on Application of Accelerators in Research and Industry 98*, AIP Conference Proceedings 475, edited by J. L. Duggan and I. L. Morgan (AIP, New York, 1999), p. 357.

[IV] *'Ionization of helium, neon and xenon by positron impact'*,
H. Bluhme, H. Knudsen, J. P. Merrison, and K. A. Nielsen,
J. Phys. B: At. Mol. Opt. Phys. **32**, 5237 (1999).

[V] *'Non-dissociative and dissociative ionization of CO, CO_2 and CH_4 by positron impact'*,
H. Bluhme, N. P. Frandsen, F. M. Jacobsen, H. Knudsen, J. P. Merrison, R. Mitchell, K. Paludan, and M. R. Poulsen,
J. Phys. B: At. Mol. Opt. Phys. **32**, 5825 (1999).

[VI] *'Ionization of argon and krypton by positron impact'*,
H. Bluhme, H. Knudsen, J. P. Merrison, and K. A. Nielsen,
J. Phys. B: At. Mol. Opt. Phys. **32**, 5835 (1999).

[VII] *'Atomic collisions involving pulsed positrons'*,
J. P. Merrison, H. Bluhme, D. Field, H. Knudsen, S. Lunt, K. A. Nielsen S. Stahl, and E. Uggerhøj,
in *The Physics of Electronic and Atomic Collisions, Proc. of XXI ICPEAC*, AIP Conference Proceedings 500, edited by Y. Itikawa, K. Okuno, H. Tanaka, A. Yagishita, and M. Matsuzawa (AIP, New York, 2000), p. 420.

[VIII] *'Positron impact ionisation of atomic hydrogen'*,
V. Kara, G. Laricchia, K. Paludan, H. Bluhme, J. Moxom, H. Knudsen, and J. Slevin,
submitted to J. Phys. B: At. Mol. Opt. Phys.

[IX] *'Ionisation of noble gases by positron impact'*,
K. A. Nielsen, H. Bluhme, H. Knudsen, and J. P. Merrison,
to appear in *Proc. of 1st Euro. Conf. on At. Phys. at Acc.*, Hyperfine Interact.

In addition I have during my Ph.D. participated in a number of experiments which will not be discussed in this thesis. This work has resulted in the following publications.

[X] *'Hydrogen formation by proton impact on positronium'*,
J. P. Merrison, H. Bluhme, J. Chevallier, B. I. Deutch, P. Hvelplund, L. V. Jørgensen, H. Knudsen, and M. R. Poulsen,
Phys. Rev. Lett. **78**, 2728 (1997).

[XI] *'Experimental demonstration of hydrogen formation following the interaction of protons with positronium'*,
J. P. Merrison, H. Bluhme, M. Charlton, H. Knudsen, and M. R. Poulsen,
Hyperfine Interact. **109**, 313 (1997).

[XII] *'Non-dissociative and dissociative ionization of O_2 molecules by impact of 40–1800 keV antiprotons'*,
H. Bluhme, H. Knudsen, U. Mikkelsen, E. Morenzoni, K. Paludan, S. P. Møller, and E. Uggerhøj,
J. Phys. B: At. Mol. Opt. Phys. **30**, 3417 (1997).

[XIII] *'Single, double and triple ionization of Ne, Ar, Kr and Xe by 30–1000 keV p^- impact'*,
K. Paludan, H. Bluhme, H. Knudsen, U. Mikkelsen, S. P. Møller, E. Uggerhøj, and E. Morenzoni,
J. Phys. B: At. Mol. Opt. Phys. **30**, 3951 (1997).

[XIV] *'Ionization of rare gases by particle-antiparticle impact'*,
K. Paludan, G. Laricchia, P. Ashley, V. Kara, J. Moxom, H. Bluhme, H. Knudsen, U. Mikkelsen, S. P. Møller, E. Uggerhøj, and E. Morenzoni,
J. Phys. B: At. Mol. Opt. Phys. **30**, L581 (1997).

[XV] *'Atomic spectroscopy and collisions using slow antiprotons'*,
T. Azuma *et al.* (44 authors),
CERN/SPS 97; 19 CERN/SPSC (1997).

[XVI] *'Measurement of the Barkas effect around the stopping-power maximum for light and heavy targets'*,
S. P. Møller, E. Uggerhøj, H. Bluhme, H. Knudsen, U. Mikkelsen, K. Paludan, and E. Morenzoni,
Nucl. Instr. and Meth. B **122**, 162 (1997).

[XVII] *'Direct measurements of the stopping power for antiprotons of light and heavy targets'*,
S. P. Møller, E. Uggerhøj, H. Bluhme, H. Knudsen, U. Mikkelsen, K. Paludan, and E. Morenzoni,
Phys. Rev. A **56**, 2930 (1997).

Outline of thesis

The contents of this thesis have been structured into chapters according to the different experiments performed. The chapters are therefore to a certain extent independent. Exceptions are when theory or experimental techniques are so related that a cross-reference between chapters are more appropriate than rewriting a whole section.

Chapter 1: The first part of this chapter gives a brief review of the field of atomic collisions with positrons and the work previously done within the field. The second part of the chapter serves to give a reader unfamiliar to the field an introduction to the basic techniques for production of low-energy positrons, as these will not be discussed in any detail in the experimental sections of the subsequent chapters.

Chapter 2: This chapter discusses the experiments performed on the noble gases. The main emphasis of these experiments has been on measuring the total double ionisation cross section with particular interest in positronium formation at near-threshold impact energies. In addition, new data on total single ionisation are also presented for some of the noble gases. This work has been published in the papers [I,IV,VI] and further presented in the conference contributions [III,VII,IX].

Chapter 3: This chapter starts with an introduction to Wannier theory and the Rost-Pattard model. It then treats the modified Rost-Pattard model developed for double ionisation cross sections for the noble gases presented in chapter 2. This work has been published in the paper [I] and further presented in the conference contributions [III,VII,IX].

Chapter 4: This chapter looks at the experiment performed at University College London which measured the direct and total ionisation cross sections of atomic deuterium by positron impact. The goal of this experiment has been to settle the dispute that exists in the literature concerning these cross sections. This work is to be published in the paper [VIII].

Chapter 5: This chapter contains a presentation of the measurements of the total non-dissociative and dissociative ionisation cross sections of a range of small molecules by positron impact. This work has been published in the papers [II,V].

The thesis is concluded by a summary which will recapitulate some of the conclusions of the previous chapters and make some more general observations on the results obtained.

Contents

1 Introduction **1**
- 1.1 Atomic collisions with positrons . . . 1
- 1.2 Slow positron beam production . . . 6
  - 1.2.1 Positron sources . . . 6
  - 1.2.2 Moderators . . . 7
  - 1.2.3 Beam transport . . . 10
  - 1.2.4 Accumulators and traps . . . 11
  - References . . . 12

2 Ionisation of noble gases **17**
- 2.1 Introduction . . . 17
  - 2.1.1 Single ionisation . . . 21
  - 2.1.2 Double ionisation . . . 25
- 2.2 Experimental technique . . . 30
  - 2.2.1 Experimental equipment . . . 31
  - 2.2.2 Data analysis . . . 36
- 2.3 Results and discussion . . . 40
  - 2.3.1 Single ionisation . . . 40
  - 2.3.2 Double ionisation . . . 44
  - References . . . 54

3 Modified Rost-Pattard theory **59**
- 3.1 Wannier theory . . . 59
- 3.2 Rost-Pattard theory . . . 64
- 3.3 MRP theory and discussion . . . 67
  - References . . . 71

4 Ionisation of atomic deuterium **75**
- 4.1 Introduction . . . 75
- 4.2 Experimental technique . . . 78
  - 4.2.1 Experimental equipment . . . 78

4.2.2 Data analysis 81
4.3 Results and discussion 82
References 86

5 Ionisation of molecules **89**
5.1 Introduction 89
5.2 Experimental technique 91
5.2.1 Experimental equipment 92
5.2.2 Data analysis 93
5.2.3 'Light-before-heavy' effect 95
5.3 Results and discussion 96
5.3.1 Non-dissociative ionisation 96
5.3.2 Dissociative ionisation 99
References 104

6 Summary **107**

Dansk resumé (Résumé in Danish) **111**

List of figures **115**

Chapter 1

Introduction

The existence of the positron (e^+) was predicted by Dirac in 1930 [1]. The first experimental observation of the particle was subsequently made by Anderson in 1932 [2]. Being the antiparticle of the electron (e^-), the properties of the positron can only be fully described through the theory of quantum electrodynamics (QED). However in the field of atomic collisions it is often sufficient to regard the positron as a particle of the same mass as the electron but with the opposite charge. The antiparticle nature of the positron needs only to be considered when discussing annihilation. The cross section for in flight annihilation of a positron with an electron at low energies is given by

$$\sigma_{\text{annih}} = \pi r_0^2 c/v \approx 1.26 \times 10^{-22}\text{cm}^2/\sqrt{E/\text{eV}}, \tag{1.1}$$

where r_0 is the classical electron radius and v the relative velocity between the particles [3]. Even though the effective number of electrons for a specific target can be high this cross section is usually at least a few orders of magnitude less than the typical scattering cross section. In flight annihilation is therefore normally ignored in these kinds of atomic collision experiments.

1.1 Atomic collisions with positrons

The first positron-gas experiments were conducted some 30 years ago. Despite this the field of atomic collisions with low-energy positrons is much less advanced than its electronic counterpart. The development of the field has always been closely linked to advances in the technology for producing beams of slow positrons. This technology is, as will be reviewed in section 1.2, very different from the techniques used for producing low-energy electrons. With beam intensities some 10 orders of magnitude less than those used in electron experiments, the type of experiments that can be performed with positrons are still today

limited. However the results that have been produced over the years have provided invaluable information about atomic collisions. This has lead to a better understanding of the mechanisms of atomic collisions not just with positrons, but also with electrons and heavier projectiles [4]. This improved understanding has spurred further developments in both experimental techniques and theory. The progress in the field has over the years been reviewed by several authors, see e.g. [5–8].

The positron being a positively charged particle can form a bound state with an electron. This special hydrogen 'isotope' is called positronium (Ps). Being a pure QED system, positronium is the simplest 'atom' that exists. With a reduced mass of half an electron mass, positronium has a binding energy of half that of hydrogen, 6.8 eV, and twice the radius, $2a_0$. The existence of positronium was predicted by Mohorovičić already in 1934 [9] and later discovered experimentally by Deutsch in 1951 [10,11]. Positronium is primarily formed in one of two ground states: The singlet (S = 0) para-positronium (p-Ps) or the triplet (S = 1) ortho-positronium (o-Ps). In a general collision p-Ps and o-Ps will be formed in a 1:3 ratio, as can be argued from the possible states of electron-positron spin orientations. Positronium is unstable in that the electron and positron can annihilate. Para-positronium normally decays into two 511 keV photons with a lifetime in vacuum of 125 ps. For ortho-positronium the two photon decay is forbidden due to its non-zero total angular momentum. Ortho-positronium therefore has to decay by a higher order process into at least three photons of total energy of 1.022 MeV. Ortho-positronium therefore has a longer lifetime than para-positronium of 142 ns.

Positronium has the ability just like hydrogen to bind a second electron to form a negative positronium ion, Ps^-. The existence of this system was first predicted by Wheeler in 1946 [12] and since then various properties of the ion have been studied theoretically. Among these is the total binding energy of 7.13 eV (see e.g. [13]). Much less is known experimentally. The existence of the ion was shown in an experiment by Mills in 1981 [14] who later also measured the ions annihilation decay rate [15].

The original use of the positron in atomic collisions was as a projectile. It was thought to complement electron experiments. It was hoped that positron experiments would produce more 'clean' results due to the lack of the exchange mechanism that often complicated comparison of electron experiments to theory. It was however soon realised that the process of positronium formation in collisions with positrons proved far more complicated to account for in theoretical calculations than exchange.

Today positrons are still used as projectiles to study processes in which positronium is just a reaction product often left undetected. However at the same time an entire field devoted to the atomic physics of positronium has appeared. This includes for example spectroscopy of transitions in positronium [16,17] and

experiments in which the positronium is used as an atomic target in collisions with charged particles, e.g. [X]. In these experiments the positronium is formed by the emission of positrons from a solid, like a heated silver foil. This is far more efficient than producing it in a positron-atom collision. Positronium has also recently been used as a projectile in positronium-atom collisions [18]. It has been found that positronium produced in a positron-atom collision is emitted mostly in the forward direction with a fairly well-defined energy with respect to the primary positron beam [19,20]. This has been utilised at University College London (UCL) to build a positronium beam for atomic collision studies [18].

The first positron impact cross sections to be measured were total scattering cross sections [21]. These included contributions from both elastic and inelastic processes. They were obtained by measuring the positron beam attenuation through the target gas. Great care had to be taken in these experiments to avoid systematic errors, particularly from small-angle forward scattering. Information about partial cross sections could only be extracted below the threshold for inelastic processes, under which the total scattering cross section was equal to the elastic scattering cross section.

Among some of the first experiments to follow the total scattering experiments were measurements of positronium formation cross sections. Different methods were used to measure these. At UCL a system to detect the unique three-photon signature of ortho-positronium annihilation was used [22–24]. Later it was however found that this system suffered from a serious systematic error [5]. The ortho-positronium would sometimes live long enough to travel to the walls of the experimental chamber. Upon collision with the wall, the positronium would be able to convert into para-positronium. This would decay by two-photon emission leading to a quenching of the observed three-photon signal. At Arlington a magnetic system was used which confined all positrons, scattered and unscattered, to the system [25]. The only way positrons could be lost were through positronium formation. By measuring the fraction of positrons that were lost to positronium formation relative to the total fraction of the initial beam scattered, the positronium formation cross section was determined relative to the total scattering cross section.

Around the same time experiments aiming to study the partial cross sections of inelastic processes (excitation and ionisation) appeared, see e.g. [26–29]. In general all of these experiments were based on a method suggested by Coleman *et al.* [30]. By using a time-of-flight method the energy of positrons which had passed through a gas cell was determined. Positrons which had collided inelasticly with the gas could be identified by having lower energy than the primary beam. In this way the cross section for inelastic scattering could be determined and through further analysis the cross sections for excitation and ionisation could be disentangled. However the large energy width of the positron beams complicated this technique and made it almost impossible to e.g. distinguish

different excitation channels. This was further complicated by a general inability for these experiments to distinguish energy loss and large angle scattering. In many of the experiments the collection of scattered positrons was also limited to an energy dependent forward scattering angle. There still are no other methods than the energy loss technique for studying excitation. Examples of recent experiments are published in [31,32]. Measuring excitation cross sections by observing the de-excitation photons emitted from a target in coincidence with a scattered positron has so far never been feasible due to the low intensity of positron beams. A study of simultaneous positronium formation and excitation in positron-molecule collisions is to date the closest to an attempt in this direction [33].

In 1986 Fromme *et al.* at Bielefeld introduced a new method for studying the partial cross sections for ionisation processes [34]. By detecting the ion created in coincidence with either the scattered or incident positron both direct and total ionisation cross sections could be measured. The positronium formation cross section could be deduced be subtracting the former from the latter. An important feature of this technique was the ability to single out a specific ionisation mechanism. By determining the charge-state of the ion to be e.g. singly charged the measured cross sections would be *single* ionisation cross sections. All previous measurements of ionisation/Ps formation cross sections had in principle been studies of the sum of all ionisation/Ps formation processes. Comparison between the old and new data was still possible due to the fact that single ionisation dominates over other ionisation processes by at least an order of magnitude. The new technique however allowed the first studies of *double* ionisation [35,36]. Today virtually all experiments studying ionisation use the ion detection technique.

All the experiments discussed so far have involved measurements of angular integrated cross sections. Emerging alongside these were experiments aiming to measure differential cross sections. Differential cross sections are from a theoretical point of view more interesting as they provide more stringent tests of theory. Differential cross sections often contain structures and effects that are washed out in the angular integrated cross section. Developments in experiments for measuring differential cross sections have been more strongly disabled by the low intensity of positron beams than other experiments. Having to detect positrons or ejected electrons scattered into a small solid angle severely reduces count rates. For this reason the most studied target has been argon, where the large cross section compensate somewhat for the lower detection efficiency. The first experiments measured differential elastic scattering cross sections [37,38]. This later evolved into experiments studying ionisation using simultaneous ion detection, as in e.g. [39]. With improving beam intensities it also became feasible to study double differential cross sections by energy analysing the positrons/electrons. Recent examples of such experiments are

[40,41]. Finally on the absolute boarder of feasibility can be found a single study of the triply differential cross section of molecular hydrogen [42].

In the early days of the field of atomic collisions with positrons there existed a regular gap between experiments and theory. This gap was mainly brought about by the difference in choice of systems studied. Experimentalists preferred to use easy-to-work-with targets like the noble gases or molecular gases, which also through their relatively large cross sections ensured reasonable count rates despite the low intensities of the positron beams. Theoreticians on the other hand preferred the simple but experimentally elusive atomic hydrogen target. Also the fact that differential measurements were so few, as discussed in the previous paragraph, did not improve the situation. Since then the gap has been somewhat bridged by both sides. Today many experimentalists still prefer to use noble or molecular gases, but some groups have taken on more 'untraditional' targets like the alkali metals and magnesium [43]. The previously elusive hydrogen target can also now be handled fairly comfortably due to the development of reliable hydrogen RF discharge sources [44].

At the present day new and exciting developments in the experimental technique promise to change the field and provide even more detailed data for atomic collisions with positrons. On the beam side the next generation of beam lines are becoming available. Utilising accumulators and traps, high intensity beams with low energy spread can be produced [45]. This type of beam will be reviewed further in section 1.2.4. The first experiment using this new type of beam has only recently appeared [32]. On the collision experiment side the introduction of recoil-ion momentum spectroscopy (RIMS) promises all the advantages that this technique has already demonstrated in e.g. electron and ion impact ionisation experiments. In general RIMS would be able to supply theory with more of the much requested differential cross section measurements. A general review of RIMS can be found in [46]. A progress report on one of the first experiments trying to use RIMS to study atomic collisions with positrons has recently been published [47].

The interest for positrons in Århus came about from two directions. The group was originally founded with the intention of studying ways to produce antihydrogen. The work in this direction still goes on today but is now done elsewhere. The direct experimental engagement in Århus in the project finished with the conclusion of the hydrogen test experiment [X,XI]. The other interest in positrons came from studies of ionisation cross section dependence on projectile charge and mass. Initial studies had been done with ion impact and were later successfully expanded using antiprotons a projectiles (for further discussion of this work, see Knudsen and Reading [4]). In order to expand the investigations to electron and positron impact for a more dramatic mass effect, a collaboration between UCL and Århus was established to provide the, at that time, missing positron cross sections. Several former master and Ph.D. students of this group

have contributed to this work [48–50]. The work presented in this thesis is to some extent a continuation along this line, involving ionisation studies of atoms and molecules. Compared to the new developments mentioned in the former paragraph, the experiments described in this thesis belong to the 'old' type. By this is meant that the experiments use the same technique as those used over the last decade to produce the bulk of the ionisation data available today. Even some of the beam lines used are the same or improved versions of those used back then. However today these techniques are well tested and known to produce reliable results, and by pushing them a little bit further new and exciting results can still be obtained.

1.2 Slow positron beam production

Behind every positron collision experiment is a beam line providing the positrons. It is not always discussed in the final publications, despite that much experimental work goes into the development of these beam lines. As mentioned in the previous section, the progress in experiments with positrons have been closely linked to the developments in beam production technology. An important feature of slow positron beams is that they can be built in 'table top' size using relatively simple technology. Since most of the interesting (atomic) physics occurs at energies below a few keV all acceleration voltages can be provided by simple power supplies. This has allowed quite a few groups around the world to build beam lines and participate in the field of atomic collisions with positrons. This section is meant as a brief introduction to beam production. A more complete and much cited review has been given by Schultz and Lynn [51] and another comprehensive review has more recently been given by Mills [52].

1.2.1 Positron sources

The main difference between positron and electron beams lies in the sources of the particles. While nearly unlimited amounts of electrons can be produced using a simple heated filament, this is not possible for positrons. This would require an antimatter filament. Instead positrons must be obtained from radioactive isotopes (β^+ emitters) or be produced by e^-- e^+ pair production which severely limits the number of particles produced.

The radioactive isotopes are produced by nuclear reactions using either an accelerator or a nuclear reactor. Some characteristics of the most commonly used isotopes are listed in table 1.1. The positron yield from a source depends on the isotopes positron branching ratio and the source activity. The maximum yield per area is limited by the self-absorption of the source. High-activity sources can be made by increasing the source area but this is not always desirable. The long-lived isotopes ^{22}Na and ^{58}Co are typically used in small lab-

Isotope	Half-life	β^+ branching ratio [%]	Maximum energy [keV]	Typical source activity [GBq]
^{22}Na	2.6 y	90.6	546	0.5–2
^{58}Co	70.8 d	15.0	474	5–20
^{64}Cu	12.7 d	19.3	657	∼50

Table 1.1: Commonly used radioactive isotopes. The β^+ branching ratio is the fraction of decays resulting in emission of a positron. The maximum energy is the maximum cut-off energy of the beta spectrum.

oratory beam lines where the source is mounted in a small capsule covered by a thin foil. A large fraction of the beam lines around the world use this type of source. The more short-lived isotope ^{64}Cu is normally used in conjunction with a nuclear reactor where the isotope is produced from ^{63}Cu by capture of thermal neutrons. The source can either be permanently mounted in the reactor core, from where the positrons then have to be transported or the source can be removed after irradiation and mounted in a separate beam line. Either way this usually requires specialised equipment and involves strict safety precautions.

To attain positron intensities higher than those available from radioactive sources one has to use pair production. In this production scheme an accelerator delivers a high-energy primary beam of e.g. 100 MeV electrons. This beam is implanted into a high-Z material resulting in emission of intense bremsstrahlung radiation as the particles are stopped. Some of the bremsstrahlung photons will in turn convert into electron-positron pairs by pair production in the high-Z material. Since both processes are strongly peaked in the forward direction with respect to the primary beam, an intense shower of positrons is created on the other side of the stopping material. Each primary projectile produces several positrons, the mean number depending on the projectile energy. The total number of positrons is determined by the energy and current of the primary beam. In principle unlimited intensities of positrons can be produced this way. One important feature of accelerator based beams is that the resulting positron beam inherit the time structure of the primary beam. This means that if the primary beam is pulsed (like from a LINAC) one gets a pulsed source of positrons which can be very advantageous in certain experiments.

1.2.2 Moderators

The positrons produced by the sources discussed in the previous section can not be used directly for atomic physics experiments. Positrons from radioactive sources have energies typically about half the maximum energy of the beta spectrum, i.e. a few 100 keV, while those produced in pair production can have

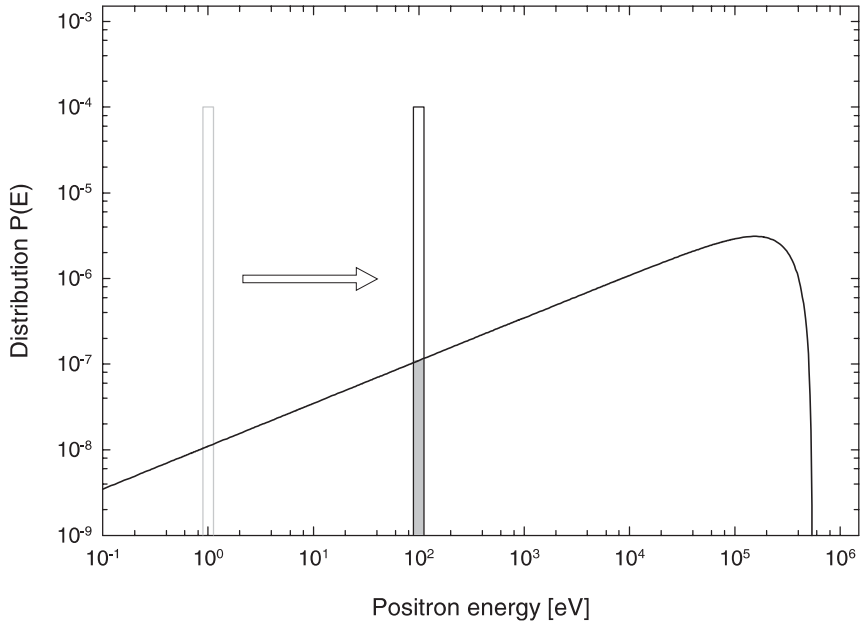

Figure 1.1: Advantage of moderation in production of 100 eV positrons. The curve is the normalised energy distribution for β^+ particles emitted from a ^{22}Na source. The shaded area shows the efficiency of velocity selection. The full bars show the efficiency of moderation and subsequent acceleration of the positrons using a typical source-moderator (polycrystalline tungsten) assembly.

mean energies of several MeV. These positrons are therefore not very useful for atomic physics where low-energy (≤ 1 keV) beams with well-defined energy are needed. One option would be to use velocity selection to choose low-energy positrons from the beta distribution. However as is illustrated in figure 1.1, the efficiency of this method can at maximum be in the range of 10^{-7}. A more desirable option would be to compress the entire beta distribution. According to Liouville's theorem such phase-space compression will require an irreversible process. The simplest of such processes would be stopping the positrons in a solid. Positrons implanted into a solid thermalise through collisions on a time scale of less than 10 ps. There the positrons will diffuse around in this hostile environment with an average lifetime of $\sim$100 ps against annihilation. It was realised by Madansky and Rasetti already in 1950 [53] that this would be sufficient time for some of the thermal positrons to diffuse back to the surface where they could be re-emitted. This method of making low-energy positrons has later become known as moderation. Madansky and Rasetti were not able

to observe the effect experimentally. Instead the first observation of reemitted low-energy positrons was done by Cherry in 1958 [54]. It was however not until 1972 that Canter *et al.* [55] discovered the first high-efficiency moderator, MgO. Being easy to produce and with an efficiency of $\sim 3 \times 10^{-5}$ this moderator could produce low-energy positrons more efficiently than any other method. The discovery of the MgO moderator is usually considered the onset of low-energy positron physics. Today numerous other and more efficient moderators are known. The advantage of moderators is illustrated in figure 1.1. A positron beam of any desired energy can be obtained just by accelerating the near-zero energy moderated positrons. Despite that moderators can be made reasonably efficient today, many positrons are still lost in the process. Together with the relatively weak sources, this loss is the reason for the weak intensities of positron beams and the experimental difficulties this gives rise to. Typical intensities of positron beams are in the order of 10^4–10^6 e^+/s for source based beams, depending on source strength, moderator and beam transport. For accelerator based beams this number can go as high as 10^{10} e^+/s.

Moderators can generally be classified into two groups: Negative work function materials and wide band gap materials. The first efficient moderators discovered belonged to the negative work function materials. It was noted that the positrons emitted from these solids in general had mean energies a few eV higher than expected for a thermal distribution. That meant that the positrons *gained* energy leaving the solid, giving rise to the name 'negative work function materials'. The theoretical explanation for this phenomenon (in metals) was given by Tong in 1972 [56]. The work functions for electrons and positrons can be viewed as having two contributions: One is the chemical potential of the particle. For electrons this is the energy required to lift an electron from the Fermi level and into vacuum. For the positrons a similar 'binding energy' arises from the sum of the repulsive interaction with the ion cores in the solid and the correlation potential from the attractive interaction with the electrons of the solid. The second contribution to the work functions arise from the effect of the solid surface dipole layer. At the surface the electron distribution tends to spill out into the vacuum. Together with the ion cores inside the surface, these electrons create a dipole layer at the surface. The effect of this layer on an electron is to decelerate it as it leaves the solid, making it harder to remove. For the positrons the effect is the opposite. Positrons get accelerated by the surface layer which counters the binding effect of the chemical potential. For some materials the contribution from the dipole layer is larger than the one from the chemical potential, making the positron work function negative.

Among the negative work function materials tungsten (W(110)) has the highest reported efficiency of $\sim 3 \times 10^{-3}$ [57]. A moderator should in general be a single crystal solid. This is because defects tend to attract and trap positrons, preventing them from diffusing to the surface. To avoid this problem the mod-

erator can be prepared by heating it to high temperatures (annealing) which removes vacancies and dislocations. The width of the energy distribution of positrons emitted from a well-prepared single crystal is in the order of 0.5 eV (FWHM) or less. Popular alternatives to single crystals are polycrystalline tungsten foils or commercially available meshes. These are easier to prepare and handle and they allow for moderation in transmission mode as opposed to a thick crystal. However being polycrystalline the efficiency of these moderators is lower ($\sim 10^{-4}$) and the energy width larger (1–2 eV FWHM).

The other group of moderators, the wide band gap materials, was discovered later than the negative work function moderators. Of this kind of moderator the rare gas solids are the most studied, but also diamond can be used. These materials are all insulators characterised by large band gaps (> 5 eV). When a high-energy positron enters such a material it will only be able to lose energy efficiently as long as its energy is larger than the width of the band gap. Within the band gap energy loss can no longer take place by excitation, but only by the far more inefficient phonon scattering. For this reason positrons slowed down in one of these materials are not thermalised completely and are considered to be 'hot'. These hot positrons have a longer diffusion length, so more of them will make it to the surface of the moderator. At the surface the positron work function does not necessarily need to be negative for the positrons to be emitted from the solid. Since the positrons are hot, they may possess enough energy to overcome a positive work function and leave the solid. For these reasons the wide band gap materials have a higher positron yield than the typical negative work function material of around a factor of 10. One drawback is that being hot the emitted positrons have a wider energy distribution of some 2–5 eV (FWHM). Of all moderators solid neon has the highest reported efficiency of $\sim 7 \times 10^{-3}$ [58]. Disadvantages of using rare gas solids are that they are not easy to produce and have limited lifetimes. The production requires cryostatic cooling to a few Kelvin for the rare gases to solidify. The lifetime is determined by how fast the surface of the moderator gets contaminated by other elements and is therefore dependent on vacuum conditions. Typical lifetimes are in the range of hours. More experimentation with diamond could bring a solution to these problems.

1.2.3 Beam transport

The simplest way to guide a low-energy positron beam is to apply a magnetic field along the direction of transportation. If a positron in the beam has a velocity component perpendicular to the beam direction it will be kept confined to the beam by the cyclotron motion induced by the magnetic field. As a result the positron will follow a spiraling trajectory along the magnetic field lines. Since the positrons are so light and low in energy this guidance can be achieved

by using even a modest magnetic field, which can be produced by for example a solenoid or Helmholtz coils suitably placed along the beam line.

For some experiments however one may want to avoid having magnetic fields present. An alternative is to use purely electrostatic guidance. The confinement of the beam in this case is not as good as in a magnetic beam which may cause loss of positrons during transport. However the electrostatic beam optics are well understood and can be simulated in advance to minimise any loss.

One final thing should be mentioned about beam transport. This is the need to shift or deflect the slow positron beam out of the direct line of sight to the source. This serves two purposes: Firstly, gamma radiation from the source is prevented from reaching the experimental region at the end of the beam line. Secondly by making the deflection energy/velocity dependent one ensures that the beam is monoenergetic and does not contain other components like for example high-energy positrons from the source which have not been stopped in the moderator. Such deflection can be done in various ways. In magnetic systems one can have a soft bend in the beam line and the confining magnetic field. Another popular choice for magnetic beams is to use an $\mathbf{E} \times \mathbf{B}$ velocity filter with cylindrical (trochoidal) electrodes as devised by Hutchins *et al.* [59]. In electrostatic beam line the deflection is usually done by a simple electrostatic analyser.

1.2.4 Accumulators and traps

As mentioned in section 1.1 a new generation of beam lines is emerging. Characterising these beams is not that they devise new and more efficient ways of making slow positrons, but rather make better and more economic use of the limited amount of positrons available from the existing sources. The development of positron accumulators has been pioneered by the group of Surko in San Diego. In their scheme positrons are caught using a Penning trap filled with a thin buffer gas (N_2). Positrons are admitted into the trap at the top of the trap potential. Through inelastic collisions with the buffer gas the positrons lose energy and fall deeper into the potential and are trapped. In this way new positrons can be stored on top of those previously trapped. Using this scheme the San Diego group has been able to accumulate as much as 10^8 positrons. One way to use the stored positrons would be to release them all at once creating a very intense pulse. This could be used to study effects unobservable with the intensity available from conventional beams. In San Diego they have instead devised a scheme where the positrons are allowed to slowly spill over the top of the trap potential. In this way a beam with an energy resolution much better than normal can be created. Energy widths of 18 meV (FWHM) have been achieved in this way [45]. This allows new high-resolution studies of e.g. excitation [32].

An alternative or further development of the San Diego accumulator would be to use a Penning trap with the magnetic field supplied by a superconducting magnet. In such an intense magnetic field positrons would lose energy by emitting synchrotron radiation. This would eliminate the need for a buffer gas. The positrons would be able to cool down to the ambient temperature which in a helium cooled trap would be only a few Kelvin. If released from the trap this would produce a beam with unprecedented intensity and energy resolution. Such a technique is presently being developed by the Århus positron group [VII].

References

[1] P. A. M. Dirac, Proc. Roy. Soc. Lond. A **126**, 360 (1930).

[2] C. D. Anderson, Science **76**, 238 (1932).

[3] W. Heitler, *The Quantum Theory of Radiation*, 3rd ed. (Dover Publications, New York, 1984), p. 270.

[4] H. Knudsen and J. F. Reading, Phys. Rep. **212**, 107 (1992).

[5] M. Charlton, Rep. Prog. Phys. **48**, 737 (1985).

[6] M. Charlton and G. Laricchia, J. Phys. B: At. Mol. Opt. Phys. **23**, 1045 (1990).

[7] W. Raith, in *Photonic, Electronic and Atomic Collisions, Proc. of XX ICPEAC*, edited by F. Aumayr and H. Winter (World Scientific, Singapore, 1998), p. 341.

[8] G. Laricchia and M. Charlton, Phil. Trans. Roy. Soc. Lond. A **357**, 1259 (1999).

[9] St. Mohorovičić, Astron. Nachr. **253**, 94 (1934).

[10] M. Deutsch, Phys. Rev. **82**, 455 (1951).

[11] M. Deutsch, Phys. Rev. **83**, 866 (1951).

[12] J. A. Wheeler, Ann. NY Acad. Sci. **48**, 219 (1946).

[13] Y. K. Ho, Phys. Rev. A **48**, 4780 (1993).

[14] A. P. Mills, Jr., Phys. Rev. Lett. **46**, 717 (1981).

[15] A. P. Mills, Jr., Phys. Rev. Lett. **50**, 671 (1983).

[16] S. Chu and A. P. Mills, Jr., Phys. Rev. Lett. **48**, 1333 (1982).

[17] S. Chu, A. P. Mills, Jr., and J. L. Hall, Phys. Rev. Lett. **52**, 1689 (1984).

[18] A. J. Garner, G. Laricchia, and A. Özen, J. Phys. B: At. Mol. Opt. Phys. **29**, 5961 (1996).

[19] G. Laricchia, M. Charlton, S. A. Davies, C. D. Beling, and T. C. Griffith, J. Phys. B: At. Mol. Phys. **20**, L99 (1987).

[20] G. Laricchia, S. A. Davies, M. Charlton, and T. C. Griffith, J. Phys. E: Sci. Instrum. **21**, 886 (1988).

[21] D. G. Costello, D. E. Groce, D. F. Herring, and J. Wm. McGowan, Can. J. Phys. **50**, 23 (1972).

[22] M. Charlton, T. C. Griffith, G. R. Heyland, K. S. Lines, and G. L. Wright, J. Phys. B: At. Mol. Phys. **13**, L757 (1980).

[23] M. Charlton, G. Clark, T. C. Griffith, and G. R. Heyland, J. Phys. B: At. Mol. Phys. **16**, L465 (1983).

[24] T. C. Griffith, in *Positron Scattering in Gases*, edited by J. W. Humberston and M. R. C. McDowell (Plenum Press, New York, 1983), p. 53.

[25] L. S. Fornari, L. M. Diana, and P. G. Coleman, Phys. Rev. Lett. **51**, 2276 (1983).

[26] T. C. Griffith, G. R. Heyland, K. S. Lines, and T. R. Twomey, J. Phys. B: At. Mol. Phys. **12**, L747 (1979).

[27] P. G. Coleman and J. T. Hutton, Phys. Rev. Lett. **45**, 2017 (1980).

[28] P. G. Coleman, J. T. Hutton, D. R. Cook, and C. A. Chandler, Can. J. Phys. **60**, 584 (1982).

[29] O. Sueoka, J. Phys. Soc. Japan **51**, 3757 (1982).

[30] P. G. Coleman, T. C. Griffith, G. R. Heyland, and T. L. Killeen, J. Phys. B: At. Mol. Phys. **8**, L454 (1975).

[31] S. Mori and O. Sueoka, J. Phys. B: At. Mol. Opt. Phys. **27**, 4349 (1994).

[32] S. J. Gilbert, R. G. Greaves, and C. M. Surko, Phys. Rev. Lett. **82**, 5032 (1999).

[33] G. Laricchia, M. Charlton, and T. C. Griffith, J. Phys. B: At. Mol. Opt. Phys. **21**, L227 (1988).

[34] D. Fromme, G. Kruse, W. Raith, and G. Sinapius, Phys. Rev. Lett. **57**, 3031 (1986).

[35] M. Charlton, L. H. Andersen, L. Brun-Nielsen, B. I. Deutch, P. Hvelplund, F. M. Jacobsen, H. Knudsen, G. Laricchia, M. R. Poulsen, and J. O. Pedersen, J. Phys. B: At. Mol. Opt. Phys. **21**, L545 (1988).

[36] M. Charlton, L. Brun-Nielsen, B. I. Deutch, P. Hvelplund, F. M. Jacobsen, H. Knudsen, G. Laricchia, and M. R. Poulsen, J. Phys. B: At. Mol. Opt. Phys. **22**, 2779 (1989).

[37] P. G. Coleman and J. D. McNutt, Phys. Rev. Lett. **42**, 1130 (1979).

[38] G. M. A. Hyder, M. S. Dababneh, Y.-F. Hsieh, W. E. Kauppila, and C. K. Kwan, Phys. Rev. Lett. **57**, 2252 (1986).

[39] T. Falke, T. Brandt, O. Kühl, W. Raith, and M. Weber, J. Phys. B: At. Mol. Opt. Phys. **30**, 3247 (1997).

[40] A. Schmitt, U. Cerny, H. Möller, W. Raith, and M. Weber, Phys. Rev. A **49**, R5 (1994).

[41] Á. Kövér, R. M. Finch, M. Charlton, and G. Laricchia, J. Phys. B: At. Mol. Opt. Phys. **30**, L507 (1997).

[42] Á. Kövér and G. Laricchia, Phys. Rev. Lett. **80**, 5309 (1998).

[43] T. S. Stein, J. Jiang, W. E. Kauppila, C. K. Kwan, H. Li, A. Surdutovich, and S. Zhou, Can. J. Phys. **74**, 313 (1996).

[44] J. Slevin and W. Stirling, Rev. Sci. Instrum. **52**, 1780 (1981).

[45] S. J. Gilbert, C. Kurz, R. G. Greaves, and C. M. Surko, Appl. Phys. Lett. **70**, 1944 (1997).

[46] J. Ullrich, R. Moshammer, R. Dörner, O. Jagutzki, V. Mergel, H. Schmidt-Böcking, and L. Spielberger, J. Phys. B: At. Mol. Opt. Phys. **30**, 2917 (1997).

[47] R. D. DuBois, J. Phys. IV France **9**, Pr6, 195 (1999).

[48] L. Brun-Nielsen, Master's thesis, University of Aarhus, 1990.

[49] N. P. Frandsen, Master's thesis, University of Aarhus, 1993.

[50] K. Paludan, Ph.D. thesis, University of Aarhus, 1997.

[51] P. J. Schultz and K. G. Lynn, Rev. Mod. Phys. **60**, 701 (1988).

[52] A. P. Mills, Jr., in *Atomic, Molecular and Optical Physics: Charged Particles*, Vol. 29A of *Exp. Meth. Phys. Sci.*, edited by F. B. Dunning and R. G. Hulet (Academic Press, San Diego, 1995), p. 39.

[53] L. Madansky and F. Rasetti, Phys. Rev. **79**, 397 (1950).

[54] W. H. Cherry, Ph.D. thesis, Princeton University, 1958.

[55] K. F. Canter, P. G. Coleman, T. C. Griffith, and G. R. Heyland, J. Phys. B: At. Mol. Phys. **5**, L167 (1972).

[56] B. Y. Tong, Phys. Rev. B **5**, 1436 (1972).

[57] A. Vehanen, K. G. Lynn, P. J. Schultz, and M. Eldrup, Appl. Phys. A **32**, 163 (1983).

[58] A. P. Mills, Jr. and E. M. Gullikson, Appl. Phys. Lett. **49**, 1121 (1986).

[59] S. M. Hutchins, P. G. Coleman, R. J. Stone, and R. N. West, J. Phys. E: Sci. Instrum. **19**, 282 (1986).

Chapter 2

Ionisation of noble gases

2.1 Introduction

The noble gases are among the most studied targets in atomic collisions with positrons. Ionisation studies of these gases have over the last decade improved our understanding of ionisation processes greatly and helped the development of what is now referred to as the 'standard picture of ionisation' [1]. Nevertheless there are still processes, particularly in multiple ionisation, for which our knowledge is poor experimentally as well as theoretically. The main motivation for the experiments presented in this chapter has been to provide data for a better understanding of double ionisation by positron impact. Along with these, new data for single ionisation were obtained for the heavier noble gases.

In single ionisation of a noble gas, A, by positron impact, one of two fundamental processes takes place: Ionisation without and with positronium formation, i.e.

$$e^+ + A \rightarrow A^+ + e^- + e^+, \tag{2.1}$$

$$e^+ + A \rightarrow A^+ + Ps. \tag{2.2}$$

The two processes will in this thesis be referred to as direct single ionisation and single ionisation with positronium formation. In ion impact ionisation the process corresponding to (2.1) is often called 'pure ionisation'. The process (2.2) is sometimes referred to as transfer or capture. The ions produced in (2.1) and (2.2) could in principle end up in an excited state (A^{*+}) but these processes are generally not discerned from the above as only the charge state of the ion is normally determined in experiments.

The partial cross sections corresponding to the processes (2.1) and (2.2) will be denoted σ_I^+ and σ_{Ps}^+ respectively. If one performs a single ionisation experiment in which it is not discerned whether positronium is formed or not,

the measured cross section will be the total single ionisation cross section, $\sigma_{\rm tot}^{+}$, which is equal to the sum of $\sigma_{\rm I}^{+}$ and $\sigma_{\rm Ps}^{+}$. It is important not to confuse $\sigma_{\rm tot}^{+}$ with the total *scattering* cross section which is sometimes denoted $\sigma_{\rm tot}$.

The two processes (2.1) and (2.2) have different threshold energies. The threshold, $E_{\rm I}^{+}$, of the direct ionisation channel is the ionisation potential of the atom. The threshold, $E_{\rm Ps}^{+}$, of the positronium formation channel lies 6.8 eV below $E_{\rm I}^{+}$. This difference is due to the energy gained from the binding of the positronium. In this thesis, the gap between $E_{\rm Ps}^{+}$ and $E_{\rm I}^{+}$ is referred to as the Ore gap [2]. The strict definition of the Ore gap is the energy region in which positronium formation is the only inelastic channel open. This means that the gap is the region between $E_{\rm Ps}^{+}$ and the first excitation energy, $E_{\rm ex}$, of the atom, provided that $E_{\rm ex}$ is larger than $E_{\rm Ps}^{+}$ as is the case in the noble gases. Otherwise the gap does not exist. However in ionisation studies where excitation is of no interest the definition of the Ore gap is usually broadened to include the entire gap between $E_{\rm Ps}^{+}$ and $E_{\rm I}^{+}$. Within the entire gap $\sigma_{\rm tot}^{+}$ equals $\sigma_{\rm Ps}^{+}$.

In double ionisation processes similar to (2.1) and (2.2) exist:

$$\mathrm{e}^{+} + \mathrm{A} \quad \rightarrow \quad \mathrm{A}^{2+} + 2\mathrm{e}^{-} + \mathrm{e}^{+}, \tag{2.3}$$

$$\mathrm{e}^{+} + \mathrm{A} \quad \rightarrow \quad \mathrm{A}^{2+} + \mathrm{e}^{-} + \mathrm{Ps}. \tag{2.4}$$

Analogous to single ionisation the two processes (2.3) and (2.4) will be referred to as direct double ionisation and double ionisation with positronium formation. In some works the positronium formation channel is also referred to as transfer ionisation. Following the notation for the single ionisation cross sections, the partial cross sections corresponding to the two processes (2.3) and (2.4) are denoted $\sigma_{\rm I}^{2+}$ and $\sigma_{\rm Ps}^{2+}$ respectively. Similarly the threshold energies are $E_{\rm I}^{2+}$ and $E_{\rm Ps}^{2+}$. The same 6.8 eV difference found between $E_{\rm Ps}^{+}$ and $E_{\rm I}^{+}$, exists between $E_{\rm Ps}^{2+}$ and $E_{\rm I}^{2+}$. Extending the analogy from single ionisation this gap is sometimes referred to as the second Ore gap or just the Ore gap when it is implicit that double ionisation is being discussed.

Apart from the two processes above, double ionisation may also take place by a third process. This involves the formation of the negative positronium ion:

$$\mathrm{e}^{+} + \mathrm{A} \quad \rightarrow \quad \mathrm{A}^{2+} + \mathrm{Ps}^{-}. \tag{2.5}$$

The process has threshold energy $E_{\rm Ps^-}^{2+}$ which lies 0.3 eV below $E_{\rm Ps}^{2+}$ due to the extra binding energy of the second electron. The corresponding cross section should be denoted $\sigma_{\rm Ps^-}^{2+}$. Due to the energy resolution of our positron beam and the nature of our detection method, as will be described in section 2.2, we can not separate the Ps^{-} channel (2.5) from the Ps channel (2.4). Other groups doing similar experiments completely omit a discussion of this channel despite that their experiments suffer from the same problem (see e.g. [3,4]). The total double ionisation cross section, $\sigma_{\rm tot}^{2+}$, is equal to the sum of $\sigma_{\rm I}^{2+}$, $\sigma_{\rm Ps}^{2+}$ and $\sigma_{\rm Ps^-}^{2+}$, except within the second Ore gap where $\sigma_{\rm I}^{2+}$ is zero.

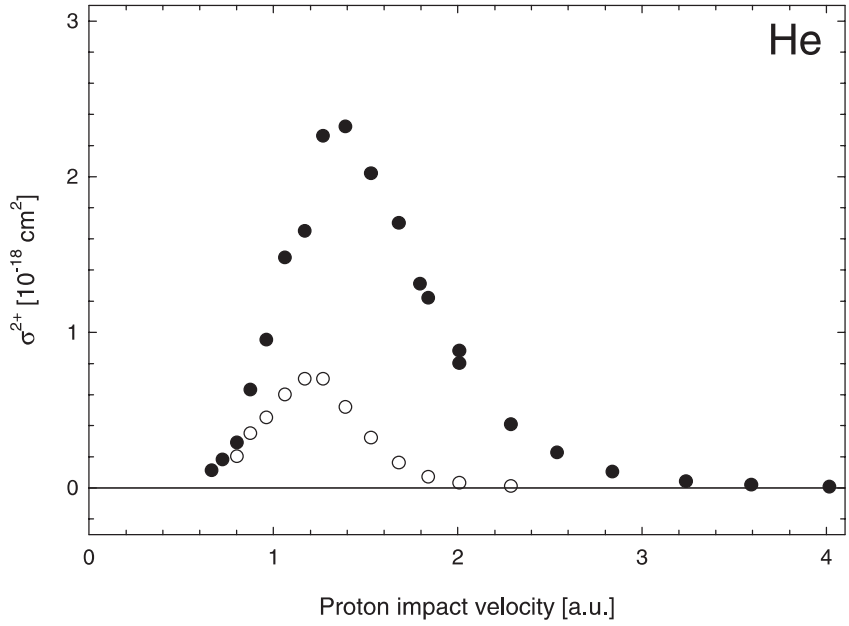

Figure 2.1: Capture in double ionisation of helium by proton impact. (●) σ_{H}^{2+} by Shah and Gilbody [5] and Shah *et al.* [6]; (○) $\sigma_{\mathrm{H}^-}^{2+}$ by Barnett *et al.* [7]. Proton impact velocity given in atomic units.

There exist no experimental or theoretical estimates of how important the Ps^- channel is relative to the Ps channel in double ionisation. The only estimate that can be obtained is through a comparison with the similar two processes in proton impact on helium:

$$\mathrm{p} + \mathrm{He} \rightarrow \mathrm{He}^{2+} + \mathrm{e}^- + \mathrm{H}, \tag{2.6}$$

$$\mathrm{p} + \mathrm{He} \rightarrow \mathrm{He}^{2+} + \mathrm{H}^-. \tag{2.7}$$

Measurements of the cross sections, σ_{H}^{2+} and $\sigma_{\mathrm{H}^-}^{2+}$, for the two processes are shown in figure 2.1. The cross sections are plotted as function of proton *impact* velocity. One way to estimate the importance of Ps^- formation would be to assume that the behaviour of the positron cross sections are the same as the proton ones at a given impact velocity. From figure 2.1 one sees that double electron capture is only important at impact velocities below ∼2 a.u. Viewed this way the Ps^- channel is of no importance since a positron travelling at a velocity of 2 a.u. or less has energy less than $E_{\mathrm{Ps}^-}^{2+}$ which therefore is insufficient to doubly ionise helium. It is the much smaller mass of the positron that causes this difference to protons.

Comparison of positrons to protons at low velocities is however, not as straight forward as described above. As suggested by e.g. Raith [8], who looked at positronium/hydrogen formation in single ionisation, it would be more realistic to compare positron and proton collisions with the same projectile *exit* velocity. This is because at these velocities the positrons (unlike the protons which hardly change their velocity) suffer a dramatic change in velocity during the collision. This difference is again caused by the smaller mass of the positrons. The effect is that positrons, at higher impact velocities, are more efficient in capturing a target electron (in single ionisation) than protons are. As the positrons lose a large fraction of their total energy and suffer larger deflection during the collision it is more likely for them to achieve the right matching of velocity with the released electron. This is the all important condition for a capture process to take place. By comparing positrons and protons with the same exit velocity this effect can to a certain extent be taken into account.

For the proton cross sections in figure 2.1 there is only an insignificant change. The large mass of the proton makes the energy loss in the collision insignificant and the exit velocity is virtually the same as the impact velocity. For the positrons the calculation of the exit velocity for a given impact energy is more complicated. Ignoring the 0.3 eV difference between $E^{2+}_{\mathrm{Ps}^-}$ and E^{2+}_{Ps}, one first has to subtract E^{2+}_{Ps} from the impact energy. Next one has to remember that Ps^- is 1.5 times heavier than Ps. This makes the exit velocity of Ps ∼22% higher than that of Ps^- formed from positrons with the same impact energy. In figure 2.1 one sees that the maximum of $\sigma^{2+}_{\mathrm{H}^-}$ is around 1.2 a.u. This corresponds to a positron impact energy of ∼131 eV (∼59 eV exit energy Ps^-). It should be compared to σ^{2+}_{H} at 1.22×1.2 a.u. ≈ 1.46 a.u. This gives an estimate of the Ps to Ps^- formation ratio of approximately 3 to 1. At positron impact energies of ∼100 eV and ∼200 eV respectively this ratio is 5 to 1 and at ∼250 eV it is 10 to 1. So viewed in this way one has to say that the Ps^- channel should give a contribution which, compared to that of the Ps channel, is significant from E^{2+}_{Ps} and up to some 100–150 eV above it.

However it is not clear if one can make these kinds of comparisons between double ionisation by positron and proton impact in either the impact or exit velocity estimations. There is no experimental or theoretical evidence for this. Neither is it certain that these estimates done for a helium target can be used for the other noble gases. In conclusion we have to say that whenever, in the remainder of this chapter, Ps formation is discussed, we actually mean the sum of Ps *and* Ps^- formation. We do however expect the contribution from the latter process to be smaller than or even insignificant as compared to the contribution of the former.

We will now turn to an introduction of the standard picture of ionisation and a brief review of some of the previous work done on single and double ionisation of the noble gases by positron impact. The standard picture of ionisation has

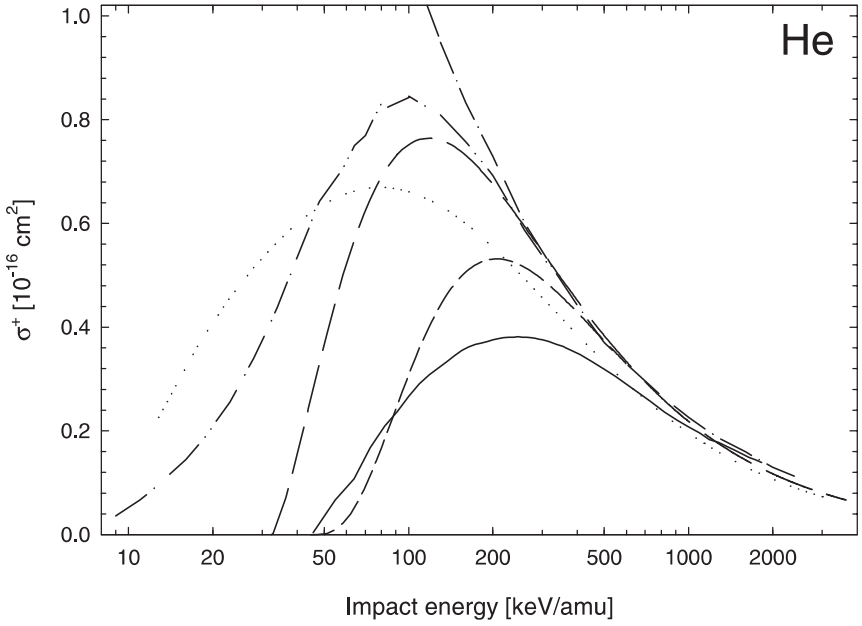

Figure 2.2: Curves or smoothed curves fitted through measurements of the single ionisation cross sections of helium. Positron impact: (——) $\sigma^+_{\rm tot}$ by Moxom *et al.* [10], (– – – –) $\sigma^+_{\rm I}$ by Jacobsen *et al.* [11] and Moxom *et al.* [12]. Electron impact: (——) $\sigma^+_{\rm I}$ by Krishnakumar and Srivastava [13]. Proton impact: (—·—) $\sigma^+_{\rm tot}$, (—··—) $\sigma^+_{\rm I}$ both by Shah *et al.* [5,6]. Antiproton impact: (·····) $\sigma^+_{\rm I}$ by Andersen *et al.* [14] and Hvelplund *et al.* [15].

mainly been developed through comparisons of the cross sections for impact by the four projectiles: e^+, e^-, p and $\bar{p}$ [1]. In the introduction below we will be discussing various effects in terms of all four projectiles. However as the main motivation of the present work has been to investigate the importance of the positronium channel in double ionisation (2.4), comparison of our data with proton and antiproton data will be limited in the later discussion. Investigations of that kind have previously been discussed in the thesis and papers by Paludan *et al.* [9,XIII,XIV]. Threshold theories, like the Wannier theory, will not be discussed below as chapter 3 is devoted to this.

2.1.1 Single ionisation

In figures 2.2 and 2.3 the single ionisation cross section for helium is plotted for impact by various projectiles (e^+, e^-, p and $\bar{p}$). These figures will be used

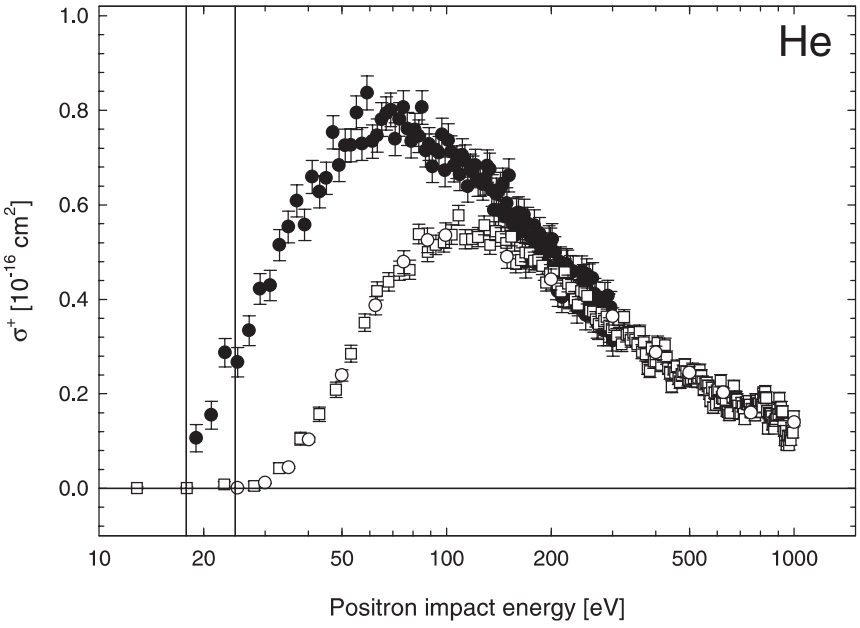

Figure 2.3: Single ionisation cross sections of helium by positron impact. (●) $\sigma^+_{\rm tot}$ by Moxom *et al.* [10], (○) $\sigma^+_{\rm I}$ by Jacobsen *et al.* [11], (□) $\sigma^+_{\rm I}$ by Moxom *et al.* [12]. The two vertical lines indicate $E^+_{\rm Ps}$ and $E^+_{\rm I}$ respectively.

to illustrate the discussion below. In figure 2.2 the cross sections are plotted as a function of impact energy divided by the projectile mass. This equals a half times the projectile velocity squared and is therefore effectively a velocity scale. This is the usual scale used for comparisons between light and heavy projectiles. In figure 2.3 the cross sections for the light projectiles are plotted as a function of impact energy, which is the more natural scale for discussing some of the effects of interest in this chapter.

At projectile impact velocities, v, much higher than the typical velocity of a target electron, $v_{\rm e}$, the single ionisation cross section behaves as predicted by the first Born approximation:

$$\sigma^+ \propto q^2 \frac{\ln v}{v^2}, \; v \gg v_{\rm e}, \tag{2.8}$$

where q is the projectile charge. This cross section behaviour is derived from the assumption that the projectile has a brief, weak interaction with the atom such that first order perturbation theory can be used. One observes from (2.8) that the cross section depends on the projectile charge *squared*, meaning that

it is independent of the sign of the charge. Furthermore if plotted on a velocity (or E/m) scale there is no mass dependence either. In such a plot the cross sections of all (singly charged) projectiles whether positively or negatively charged or whether light or heavy, should agree in this velocity regime. This behaviour can be observed in figure 2.2. However this should be taken with reservation. When measuring cross sections experimentalists often rely on the validity of (2.8) to compare their data at high velocities with those of others to obtain an absolute scale for their cross section. As a result most absolute cross sections are normalised, sometimes indirectly, to the same set of measurements (Rapp and Englander-Golden [16]). The good agreement can therefore be an artifact of the normalisation. On the other hand one observes in figure 2.2 that the *shape* of the cross sections agree, which indicates the validity of (2.8) and that the normalisation is sound. Capture processes are unimportant at high impact velocities. As discussed before, these usually require $v \approx v_e$. Therefore $\sigma_{tot}^+ = \sigma_I^+$ at these impact velocities.

At projectile velocities lower than those above but which are still larger than v_e, the projectile-atom interaction time becomes long enough for the target to be polarised prior to ionisation. This polarisation is caused by the incoming projectile attracting or repelling the target electrons depending on the projectile charge. The effect is independent of projectile mass and only depends on the sign and size of the charge. Classically speaking the positive projectile attracts the electrons, increasing the chance of ionisation, while the opposite happens for the negative ones. This is reflected by the cross sections in figure 2.2 with the cross sections of the positrons and protons rising above those of the electrons and antiprotons at velocities below ∼1000 keV/amu. One observes that this is a charge and not a mass dependent effect as the positron and proton (electron and antiproton) cross sections stay merged below this velocity. This picture persists until ∼500 keV/amu below which it is blurred by a mass dependent effect setting in.

The electron and positron carry 1836 times less kinetic energy than equivelocity protons/antiprotons. As the projectile impact velocity deceases, this starts to make the light projectiles less efficient at ionising the atom. Due to this 'lack of energy' effect one observes that the (direct ionisation) cross sections of the light projectiles fall below that of their heavier counterpart. Also in this velocity regime capture (Ps and H formation) starts to set in making σ_{tot}^+ rise above σ_I^+. As discussed earlier this happens at higher velocities for positrons than for protons, again due to the mass/energy effect.

At projectile velocities of the same order of magnitude as v_e several new effects start to influence the cross sections. As the velocity decreases, close collisions become more important. For the proton and antiproton this gives rise to a number of effects. One is the 'binding/antibinding' effect where the proton/antiproton pass inside the electron cloud of the target, leading to an

increase/decrease of the central charge in the atom as viewed by the electrons. This changes the binding of the electrons making them harder/easier to ionise.

Another important effect comes from the electrostatic Coulomb interaction between the projectile and the core/nucleus of the atom. The velocity of the projectile is now so low that this Coulomb interaction may change the trajectory of the incoming projectile. This 'Coulomb trajectory' effect causes the protons to be decelerated and deflected away from the atom, while antiprotons get accelerated further in towards the atom. Thirdly capture in proton impact is at its maximum probability at $v \approx v_e$. This leads to an overall increase in the total ionisation cross section for protons but at the cost of a decrease in the direct ionisation cross section as capture is relatively more likely to take place. The sum of these three effects results in the direct ionisation cross section of the protons decreasing below that of the antiprotons leading to a cross-over between the two. This is what is observed in figure 2.2 at around 45 keV/amu.

For the electrons and positrons the picture is somewhat similar but with a few important differences. Due to the lower mass, the Coulomb trajectory effect is expected to be more important as the light projectiles are easier to accelerate and deflect. The capture process has the same effect of raising the positron cross section $\sigma_{\mathrm{tot}}^{+}$ and lowering σ_{I}^{+} as on the proton ones. Contrary to antiprotons, electrons are subject to the exchange mechanism, which tend to have the same effect of lowering the electron cross section as capture has on the positron direct ionisation cross section. The above effects cause the same cross-over of the electron and positron direct ionisation cross sections as observed between the proton and antiproton ones. However the most important effect for the light projectiles is the ever increasing significance of the 'lack of energy' effect. This causes the cross sections of both projectiles to decrease even further until a velocity corresponding to E_{I}^{+} is reached below which $\sigma_{\mathrm{I}}^{+} = 0$. As discussed earlier the same happens at E_{Ps}^{+} for $\sigma_{\mathrm{tot}}^{+}$ for positrons.

The plots in figure 2.3 are better suited for emphasising the behaviour of the Ps formation channel. One should remember that σ_{Ps}^{+} is the difference between the plotted σ_{I}^{+} and $\sigma_{\mathrm{tot}}^{+}$. The two threshold energies E_{Ps}^{+} and E_{I}^{+} are indicated by the two vertical lines in the figure and the region in between is the Ore gap. A few things in the figure should be noted: First of all Ps formation only gives a significant contribution to the total cross section at energies below 200–300 eV. In this region however the channel grows with decreasing projectile energy to become the dominant one, contributing some 50% at the maximum of $\sigma_{\mathrm{tot}}^{+}$. Secondly one should note the threshold behaviour of σ_{Ps}^{+}. One observes that in the Ore gap σ_{Ps}^{+} (or $\sigma_{\mathrm{tot}}^{+}$) seems to start rising *sharply* from zero at E_{Ps}^{+} and reach a significant value of $\sim 30\%$ of the maximum value of $\sigma_{\mathrm{tot}}^{+}$ already at E_{I}^{+}. This should be compared to the *slow* rise from zero of σ_{I}^{+} above E_{I}^{+}. This observation of the near-threshold behaviour of Ps formation becomes important when we later turn to discuss our results on double ionisation.

Previous work on single ionisation of the noble gases by positron impact has to a large extent focused on measuring direct ionisation cross sections as it is these that can be directly compared to electron impact. For helium the two sets of measurements by Jacobsen *et al.* [11] and Moxom *et al.* [12] shown in figure 2.3 are the most recent ones and are also considered to be the most reliable. The same groups (Århus and UCL) have also performed measurements of σ_{I}^{+} for the other noble gases: Ne [11,17], Ar [11,12], Kr [12,17] and Xe [17]. The good agreement seen in figure 2.3 between the results of the two groups for helium is also found for the other gases.

As mentioned in section 1.1, positronium formation cross sections, σ_{Ps}^{+}, have earlier been measured directly by several different groups. At UCL σ_{Ps}^{+} was determined for all the noble gases [18,19], but as discussed earlier these data suffered from a systematic error. More confidence is placed in the measurements from the group at Arlington, who measured σ_{Ps}^{+} for all the five noble gases [20–25]. In another experiment by Fromme *et al.* [26], σ_{Ps}^{+} was deduced from simultaneous measurements of σ_{I}^{+} and $\sigma_{\mathrm{tot}}^{+}$. And finally using the same technique as in the Arlington experiment Overton *et al.* [27] also measured σ_{Ps}^{+} for helium.

When it comes to measurements of the total ionisation cross section, $\sigma_{\mathrm{tot}}^{+}$, the amount of published data is far more scarce. This despite the fact that these cross sections (in principle) should be easier to measure than σ_{I}^{+} and σ_{Ps}^{+} as there is no need to discriminate between ionisation channels by e.g. detecting the scattered positrons. Apart from the experiment by Fromme *et al.* [26] mentioned in the previous paragraph all other measurements have been done by the group at UCL. Cross sections for helium and argon have been published by Moxom *et al.* [10,28] of which the helium data are those shown in figure 2.3. These data are in full agreement with the older data by Fromme *et al.* It should however be noted that Moxom *et al.* used the data by Fromme *et al.* for normalisation. Measurements of $\sigma_{\mathrm{tot}}^{+}$ for all the gases have also been published in another study by Moxom *et al.* [29]. The emphasis of this experiment was to study σ_{Ps}^{+} by measuring $\sigma_{\mathrm{tot}}^{+}$ in the Ore gap and so the data are limited to the near-threshold region. The measurements have however been extended up to higher energies [30], but apart form the argon data, which has briefly been presented in a conference paper [31], and the neon data, which has been made available especially for us by Laricchia [30], the rest have remained unpublished. We will return to these cross sections in the discussion of our own results. Particular attention will be given to the argon data as a discrepancy exists between these data and those published by Moxom *et al.*

2.1.2 Double ionisation

The standard picture of ionisation is far less developed for double ionisation than it is for single ionisation. Most of what is known concerns direct ionisation

at high projectile impact velocities. Much less is known about the low velocity range and about capture processes. When studying double ionisation it has been customary not to investigate the cross sections directly but rather focus on the ratio:

$$R^{(2)} \equiv \frac{\sigma^{2+}}{\sigma^{+}}. \tag{2.9}$$

Experimentally this has certain advantages as we will return to later, but there are also theoretical advantages to using this ratio. It has long been known that the key mechanism in double ionisation is the correlation between the two target electrons. In collisions at very high projectile impact velocity the projectile has time for only a single interaction with the atom, just like in single ionisation. It is then electron-electron correlation that gives rise to double ionisation of the atom. One could therefore state that the double ionisation cross section is equal to the single ionisation cross section times a factor depending on the electron-electron correlation. As it is the correlation that has been of interest in many previous studies, it has made sense to study the ratio $R^{(2)}$ since it isolates the behaviour due to correlation mechanisms from the 'trivial' projectile-atom interaction. However, as it is the positronium formation channel (2.4) which is of our main interest, we will tend to present our double ionisation data as absolute cross sections and only discuss them in terms of $R^{(2)}$ when it is more convenient for comparison with previous experiments. However since single ionisation is well-understood it is obvious that in the discussion of double ionisation below, it makes little difference whether we use the terms σ^{2+} or $R^{(2)}$.

In the discussion of double ionisation mechanisms the governing parameter is q/v, where as before q and v are the projectile charge and impact velocity respectively. When comparing double ionisation data of light and heavy projectiles, a velocity (or E/m) scale is again the appropriate choice. In figure 2.4 the ratio for direct ionisation, $R_{\mathrm{I}}^{(2)}$, for e^+, e^-, p and $\bar{p}$ impact on helium are plotted. This figure will be used to illustrate some of the concepts in the following discussion.

As mentioned above, double ionisation at very high projectile impact velocities ($v \gg v_e$) takes place through a single projectile-atom interaction in conjunction with correlation effects within the atom. It is customary to distinguish between two different mechanisms: Shake-off (SO) and two-step 1 (TS1). In shake-off the first electron is (instantly) removed by the interaction with the projectile. The remaining electron is left with a wave function which is *not* an eigenstate of the residual ion. In the subsequent rearrangement (shake) of the ionic wave function there is a finite probability for the second electron to end up in a continuum state, thereby doubly ionising the atom. SO is a one-step mechanism in that it can take place within the first Born approximation. Contrary to this TS1, as the name indicates, is a two-step mechanism. This means that a second order Born term is needed to calculate the contribution from

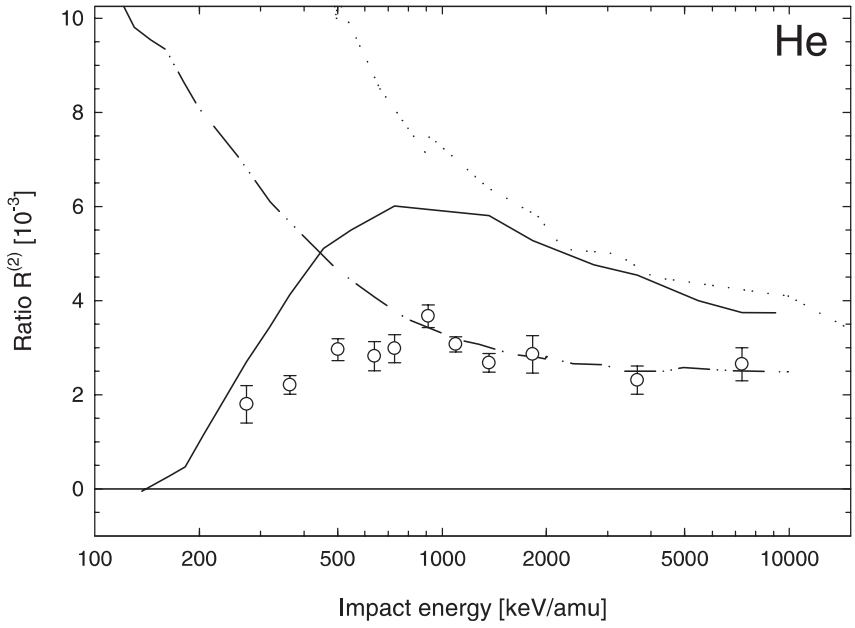

Figure 2.4: Ratio $R_{\mathrm{I}}^{(2)}$ for helium. Positron impact: (O) by Charlton *et al.* [32]. Electron impact: (——) by Charlton *et al.* [32]. Proton impact: (—··—) by Shah *et al.* [5,6] and Hvelplund *et al.* [15]. Antiproton impact: (·····) by Hvelplund *et al.* [15] and Andersen *et al.* [33,34]. Other measurements exist of the electron and proton ratios. However the advantage of those shown here (except those of [5,6]) is that they have been measured using the same type gas cell as in the positron and antiproton experiments. This should help eliminate systematic errors in the comparison between the different curves

this mechanism. In TS1 the electron that interacts with the projectile leaves the atom slowly enough to interact with the other electron and ionising it as well. It is these two separate events that makes it a second order Born term. From the point of view of many-body perturbation theory (MBPT) diagrams, the correlation in TS1 is an electron-electron interaction while in SO it is an electron-hole interaction.

It is the interplay between SO and TS1 which determines the asymptotic value of $R_{\mathrm{I}}^{(2)}$ at high velocities. Since both mechanisms rely on a single projectile-atom interaction the double ionisation cross section in this velocity region is proportional to the single ionisation cross section and $R_{\mathrm{I}}^{(2)}$ a constant. The constant is for the same reason independent of the projectile charge as the double ionisation cross section depends on the charge squared just like the single

ionisation cross section. For charged particle impact on helium the asymptotic value is found to be around 2.6×10^{-3} both experimentally and theoretically, see discussions in e.g. [1,35]. The velocity region in which this value is reached is outside the range in figure 2.4.

It is not quite clear how high the exit velocity of the first electron has to be for SO to be dominant over TS1. Experimentally it may not be possible to distinguish the two. At least not in the simple ion-counting type experiments we perform. New experiments using RIMS (see discussion in section 1.1) may in the future be able to do so through detecting different distribution patterns for the two mechanisms in the recoil spectra. It is however certain that both are important in determining the limiting value of $R_{\mathrm{I}}^{(2)}$. Even at very high impact velocities the primary ejected electron tends to leave slow enough for TS1 to be important. This can be seen for example from comparison with the corresponding ratio, $R_{\gamma}^{(2)}$, for ionisation by high-energy photons. In photon impact nearly all the energy of the photon tends to be deposited with the primary electron which leaves very fast. The difference to charged particle impact is seen in that the limiting value of $R_{\gamma}^{(2)}$ is around 1.7×10^{-2} [35].

In figure 2.4 we are clearly below the asymptotic limit. One observes that the ratios of all the projectiles have not yet merged to a common constant. Rather the electron ratio seems merged with the antiproton ratio down to $\sim$2000 keV/amu, while the positron and proton ones stay merged down to $\sim$1000 keV/amu. Since all the *single* ionisation cross sections are merged at these energies, as can be seen from figure 2.2, this difference lies entirely in the double ionisation cross sections. The effect causing this difference depends on the projectile charge, particularly the *sign* of it. It arises from another mechanism named two-step 2 (TS2) coming into play at these lower velocities (but still $v > v_{\mathrm{e}}$). It was McGuire, who first suggested that it could be the interference between SO, TS1 and TS2 that gave rise to the observed difference [36]. In TS2 the projectile is moving slowly enough to have time to interact with both target electrons, ionising them individually. Since two separate events take place, TS2 is a second order Born mechanism just like TS1. However the major difference from TS2 to SO and TS1 is that it is *not* correlation but direct interaction with the projectile that causes the double ionisation. This means that in a theory with no correlation within the atom, TS2 would be the lowest order double ionisation mechanism. Similarly SO would be the only one in a first Born calculation.

Since TS2 is the result of two separate electron ionisations, the cross section behaves similarly to the product of two single ionisation cross sections. This means that the cross section depends on the projectile charge to the fourth power. However this should not result in any difference between the double ionisation cross sections for impact of positively and negatively charged projectiles. This only appears in the following interference model. Looking at the

probability amplitudes, a, of the three mechanisms, we have that

$$a_{\mathrm{SO/TS1}} \propto q/v, \tag{2.10}$$

$$a_{\mathrm{TS2}} \propto (q/v)^2 . \tag{2.11}$$

In a velocity region where all mechanisms are important both (2.10) and (2.11) have to be included in the total probability amplitude

$$\begin{aligned} a &= a_{\mathrm{SO/TS1}} + a_{\mathrm{TS2}} \\ &= c_1\, q/v + c_2\, (q/v)^2 , \end{aligned} \tag{2.12}$$

resulting in an observable probability, P, which is

$$P = |a|^2 = |c_1|^2\, (q/v)^2 + |c_2|^2\, (q/v)^4 + Re(c_1 c_2)\, (q/v)^3 , \tag{2.13}$$

where c_1 and c_2 are independent of q and v. The expression in (2.12) corresponds to an expansion of a in a Born series in q/v. The probability in (2.13) translates approximately (ignoring the slowly varying $\ln v$ terms) into the ratio

$$R_{\mathrm{I}}^{(2)} = C_1 + C_2\, (q/v)^2 + C_3\, q/v. \tag{2.14}$$

In (2.14) we observe that due to the interference between $a_{\mathrm{SO/TS1}}$ and a_{TS2} there is a term linear in q. This can explain the observations in figure 2.4. Theoretical calculations also indicate that C_3 in (2.14) is negative [37] in agreement with the observation that the electron and antiproton ratios lie above the positron and proton ones.

Finally it should be noted that the interference model is only a qualitative explanation for the observed effect. For a quantitative calculation one would have to include the correlation in an even more complete way. For example in the lowest order MBPT picture this would mean that one had to include ground state correlation, in which the electron-electron interaction takes place *before* the interaction with the projectile. This is the opposite of what happens in SO and TS1, which are due to final state correlation. Another approach to the problem is the 'forced impulse method', which has been very successful for the heavy projectiles (see e.g. [38]).

We should also here mention inner shell contributions stemming from Auger and Coster-Kronig processes. These are of course not relevant for helium but may contribute to double ionisation in the other noble gases. The processes may be viewed as SO where the two ejected electrons come from different shells/subshells. Helms *et al.* have made predictions of the contribution to double ionisation by electron and positron impact from inner shell processes [39] based on the theory by Lotz [40,41] and measurements by Carlson *et al.* [42]. Further discussion of the model and conclusions of Helms *et al.* will be postponed to section 2.3.2.

In the velocity region below ∼1000 keV/amu the situation becomes much more complicated as differences in the single ionisation cross sections also start to affect the $R_{\mathrm{I}}^{(2)}$ ratios. In general we can only say that the double ionisation cross sections and the ratios for the light projectiles again start to fall below the corresponding values for heavy projectile impact. This is due to the same 'lack of energy' effect as in single ionisation. The effect is even stronger in double ionisation as the ionisation threshold energy is higher and more outgoing particles have to share the excess energy.

All of the above discussion involves direct double ionisation. When it comes to double ionisation with positronium formation, little theory exist. This is mainly because of the lack of data for this process and double ionisation in general. Prior to our experiments the general conception of the behaviour of $\sigma_{\mathrm{Ps}}^{2+}$ was that it behaved just like the corresponding single ionisation cross section, i.e. rising sharply at the threshold E_{Ps}^{2+}, reaching a significant value at E_{I}^{2+} and being a dominant contribution to $\sigma_{\mathrm{tot}}^{2+}$ at low energies. We will discuss this further in section 2.3.2.

As stated before, prior to our experiments on the noble gases few double ionisation measurements by positron impact existed. The first ever experiment was done by Charlton *et al.* who measured $R_{\mathrm{I}}^{(2)}$ for He, Ne and Ar [32,43]. Inspired by this Kruse *et al.* measured the same ratio for xenon [44]. The first measurement of the total double ionisation cross section was done by Helms *et al.* who measured $R_{\mathrm{tot}}^{(2)}$ for Ar, Kr and Xe [3,39]. Later they were the first to deduce an absolute double ionisation cross section [45] by multiplying their own ratio for argon by a $\sigma_{\mathrm{tot}}^{+}$ constructed by adding measurements of σ_{Ps}^{+} [20,46] to measurements of σ_{I}^{+} [11]. In a recent experiment, Kara *et al.* measured both the ratio $R_{\mathrm{I}}^{(2)}$ and the absolute cross section σ_{I}^{2+} for Ne, Kr and Xe [17]. Further discussion of the results of the above experiments, plus those of an even more recent experiment [4], together with our results will be given in section 2.3.2. Finally we should mention an experiment by Falke *et al.* in which $\sigma_{\mathrm{Ps}}^{2+}$ for Ar and Kr was measured directly [47–49]. This study however was differential without means of absolute normalisation. This study can therefore not say anything about the significance of the positronium formation channel, but can only claim to show its existence.

2.2 Experimental technique

All of our ionisation experiments on the noble gases have been performed using the Århus electrostatic slow positron beam line. Six separate series of measurements were performed in all: One on each of the gases He, Ne, Ar, and Kr and two on Xe. In time the experiments span some $2\frac{1}{2}$ years from the first data on helium to the last measurement on argon. During this time the experimental

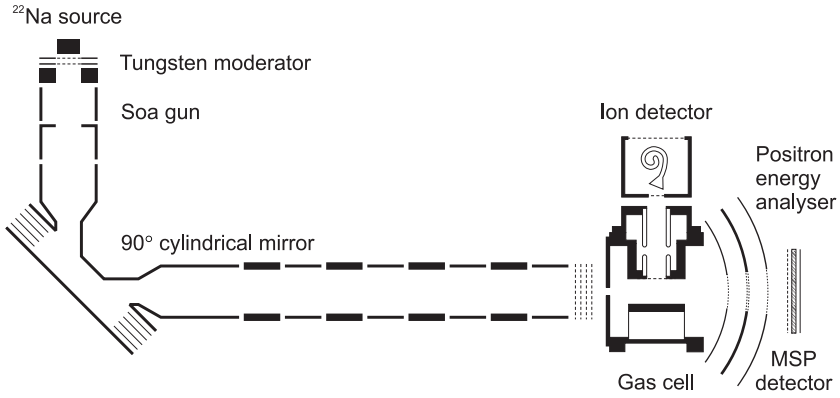

Figure 2.5: Schematic of the Århus electrostatic beam line and gas cell. The additional magnetic steering rods and Helmholtz coils are not shown. The lens elements are made from 38 mm steel tube and the beam line is around 1 m long as measured from the source to the grids at the end.

technique has to a large extent remained the same. As will be discussed below, the main difference has been that the Ar, Kr and second Xe experiments were performed using a gas mixture allowing us to measure both the absolute single as well as the absolute double ionisation cross sections of these gases. Adjustments and improvements have also been made to the equipment, but these have mostly served to improve the stability and intensity of the positron beam and to reduce background. In the data analysis the introduction of mixed gases caused some differences, but apart from this the main development has been the ability to take more and more experimental uncertainties into account in the error estimation.

2.2.1 Experimental equipment

A schematic of the Århus electrostatic slow positron beam line is shown in figure 2.5. The beam is source based, using a ^{22}Na source. The activity of the source was at the beginning of the experiments roughly 1.4 GBq (40 mCi) which over the years has decayed to half the value of $\sim$0.7 GBq. The positrons are moderated in a tungsten moderator made from a stack of four high-transmission grids which have been carefully annealed prior to installation. The source is always held at a potential of a few volts higher than the moderator in order to drive slow moderated positrons emitted from the moderator in the backwards direction, back into the grids. The source and moderator are mounted in a Soa gun [50], which takes care of the initial acceleration and focusing of the slow

positrons. These are focused onto the 10 mm entrance hole of a 90° cylindrical electrostatic mirror. This mirror serves to bend the beam out of the direct line of sight to the source, preventing (together with lead shielding) the intense gamma radiation from the source from reaching the gas cell at the end of the beam line. The mirror also acts as a crude energy analyser (∼200 eV energy acceptance window) removing from the beam any residual high-energy positrons not stopped in the moderator.

On the exit side of the mirror, the beam gets transported and further focused by a series of Einzel lenses. Four pairwise coupled conducting rods placed along the beam direction around the outside of the vacuum tubing generates a weak transverse magnetic field providing additional steering. At the end of the beam line, the positrons traverse four grids. The two central ones were originally connected, but in the later experiments on Ar, Kr, and Xe, one grid was removed, leaving only one central grid. The purpose of these grids is to decelerate the beam. All potentials for the beam line are provided by a high-voltage supply divided down by a resistive chain. The energy at which the positrons are transported through the beam line is set by the potential of the moderator, which is usually held at around 960 V. The ground potential ($V_{\mathrm{f.gnd}}$) of the high-voltage supply and the resistive chain can be floated by an additional voltage supply. Internally in the beam line this does not change the transport of the positrons as all potentials are set with respect to $V_{\mathrm{f.gnd}}$. However at the end of the beam line, the last grid is permanently connected to the true ground. If $V_{\mathrm{f.gnd}}$ is set to be negative, the positrons will suffer a deceleration as they traverse this last grid. The final energy of the beam can therefore be set solely by adjusting $V_{\mathrm{f.gnd}}$.

The beam enters the gas cell through a 10 mm aperture. In the region of the gas cell there are no means of steering the beam except for the Helmholtz coils around the chamber. These are usually used to make the interaction region free of magnetic fields, but since this is of no importance to our experiments, the coils can be used to steer the beam. This is achieved by raising the field along the beam direction to its maximum of a few Gauss, keeping the beam more focused while entering and passing the gas cell. The beam exits the gas cell through a spherical retarding field analyser mounted on the downstream side of the cell. The positrons can finally be detected by a multi-sphere-plate (MSP) detector. The DC beam intensity has at high energies been measured on this detector to be around 3×10^4 e^+/s. From ∼300 eV and down to 50 eV the intensity falls by a factor of 10. Below 50 eV it remains at a constant level again. This beam loss is probably due to defocusing in the deceleration of the beam in the grids, causing a loss of positrons in the entrance aperture of the gas cell.

In runs below 110 eV, the beam energy distribution is measured directly using the retarding field analyser. Stepping the voltage on the central grids of

the analyser using a multi-scaler, the integrated beam energy distribution can be measured on the MSP detector. A typical beam energy spread of around 1.5 eV (FWHM) has been found. The beam energy at higher energies is set through extrapolation of $V_{\mathrm{f.gnd}}$ from the low energies.

During experiments the beam was run in a pulsed mode. This was done by pulsing the voltage applied to the cylindrical mirror. Due to the wide energy acceptance window of the mirror, the voltage had to be switched down by $\sim$200 V to turn the beam off completely. The positrons were pulsed on for 1 μs with a repetition time of the order of 10 μs, reducing the effective beam intensity by a factor of 10. In the He, Ne and first Xe experiments, a grid placed immediately after the moderator was used simultaneously with the bend to pulse the beam. The grid was however found to be superfluous and therefore removed before the subsequent experiments.

During measurements target gases were admitted into the gas cell through a needle valve. The pressure was set depending on the gas, ranging from 2 mTorr for He and down to 0.2 mTorr for Xe. These low pressures were maintained in order to ensure single collision conditions, i.e. that each positron would at most only scatter once. Due to the low beam intensity and high pulsing rate, each positron pulse contained much less than one ($\sim$0.03) positron. Together with the low pressures this meant that only one ion was created per pulse, allowing for single ion detection methods to be used. This was tested for all gases by performing measurements at half the pressure, yielding consistent results.

The interaction region of the gas cell has been constructed as two parallel extraction plates. During the passage of the positron pulse, these plates were held at zero potential in order not to deflect and accelerate the positrons. Right after the passage of the beam, extraction voltages of equal size but opposite sign were applied to the plates. The size and duration of the extraction pulse varied from gas to gas but were generally in the order of 150–200 V lasting 1–1.5 μs. Any ions created would be extracted out of the interaction region through a grid-covered hole in the negative plate and into a flight tube before finally being detected by a Ceratron detector. By using a time-to-amplitude converter (TAC) and a multi-channel analyser (MCA) the time-of-flight (TOF) between the onset of the extraction and the detection of the ion was measured. The flight time identified the mass/charge ratio of each ion. An example of a TOF spectrum can be seen in figure 2.6.

During the time from the end of the ion extraction pulse and to the passage of the next positron pulse, the extraction plates were in the early experiments held at zero potential. Later in the mixed gas experiments it was found that applying a sweep pulse to the extraction plates reduced the general background in the TOF spectra. This is the background that just barely can be seen between the peaks in figure 2.6. Reduction of this background was very important for the signal to noise ratio in near-threshold measurements. The sweep pulse was

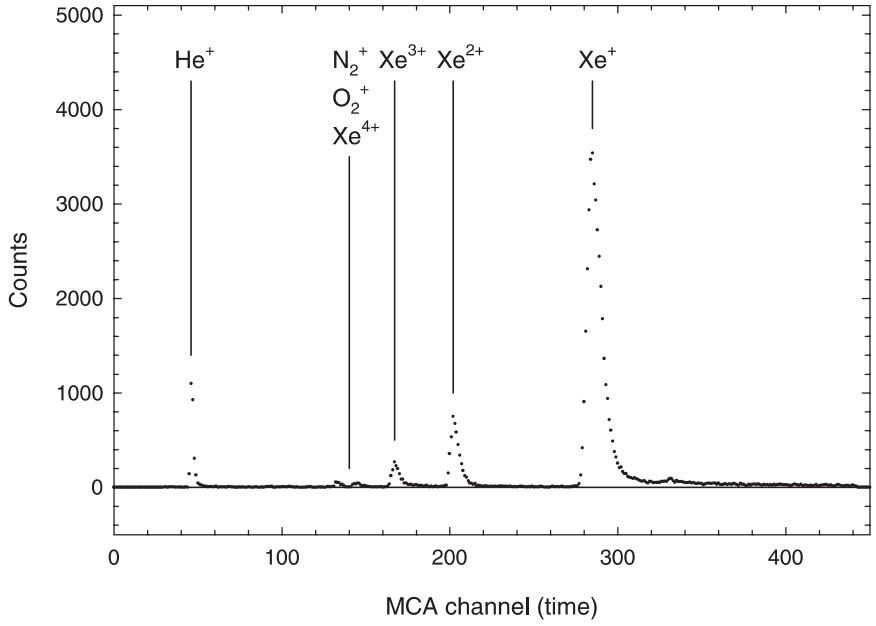

Figure 2.6: Time-of-flight MCA spectrum from mixed gas (xenon-helium) experiment at 300 eV positron impact energy. The peaks can be identified by using that their positions follow the relation: Channel $= a\sqrt{\mathrm{M/Q}} + b$, where M and Q are the mass and charge of the ion, while a and b are constants found by calibration. The small nitrogen and oxygen peaks are due to residual background gas in the chamber.

generated by applying a positive pulse to the negative extraction plate in the time gap between one extraction and the next positron pulse. Apart from clearing up the TOF spectra, the sweep pulse also ensured that the interaction region was free of any spurious ions prior to the admission of the positrons.

The optics of the extraction have been designed to provide both spatial and temporal focusing of the ions. This means that the ions are spatially focused onto the detector and that ions of the same kind arrive at the detector simultaneously no matter from where in the interaction region they are extracted, thus giving sharp peaks in the TOF spectrum. One observes in figure 2.6 that the peaks are fairly well-defined except for a tail towards larger times. These tails are due to the extracted ions undergoing collisions with the target gas resulting in the processes:

$$\mathrm{A_I^+ + A_{II}} \rightarrow \mathrm{A_I + A_{II}^+}, \tag{2.15}$$

$$\mathrm{A_I^{2+} + A_{II}} \rightarrow \mathrm{A_I + A_{II}^{2+}}. \tag{2.16}$$

The new ions created this way are initially nearly at rest and are subsequently accelerated towards the ion detector. Such ions give a tail on the ion peaks in the TOF spectrum. Evidence that the tails are caused by (2.15) and (2.16) are found in their pressure dependence. If one reduces the target pressure by a factor of 2 one observes the count rate of the main peak to go down by a factor of 2 as expected due to the lower target density. The count rate in the tail on the other hand goes down by the factor of 2 squared i.e. 4 as both the number of potential 'projectiles' and target atoms in (2.15) and (2.16) are reduced by a factor of 2 each.

In general we always observed a significant tail on the single ionisation peak, indicating the importance of (2.15). Tails were only observed in the double ionisation peak for the heavier gases as they were taken at relatively high pressures. The tails do not cause any problems themselves as they just have to be included in the total number of counts. However one could fear that a doubly charged ion having a collision, instead of ending up in the tail due to (2.16) would be lost due to the process:

$$\mathrm{A}_{\mathrm{I}}^{2+} + \mathrm{A}_{\mathrm{II}} \quad \rightarrow \quad \mathrm{A}_{\mathrm{I}}^{+} + \mathrm{A}_{\mathrm{II}}^{+}. \tag{2.17}$$

This process could potentially lead to an underestimation of the double ionisation count rate. For helium we know that at the velocity the ions attain during extraction and in the TOF region, the cross section for (2.17) is an order of magnitude smaller than the cross section of (2.16) [7]. For the other gases we have not obtained such an estimate but have relied upon experimental tests. One would expect (2.17) to behave just like (2.16) with respect to the target gas pressure. Since measurements at half the pressure yielded consistent results, we can conclude that any loss due to (2.17) is insignificant in these experiments.

Already during preliminary tests for the helium experiment it was found that a spurious background was present in the TOF spectra. It could be observed by performing runs at positron energies below the threshold E_{Ps}^{2+}. At these energies double ionisation should not be energetically possible and yet a very small amount of counts were observed in the double ionisation peak in the TOF spectra. Further investigations into this background revealed that it stemmed from an *electron* component in the beam. It was found that the electrons have an energy, E_-, corresponding to $E_- = E_0 - E_+$, where E_+ is the positron impact energy and $E_0 \approx 960$ eV i.e. the electrons will be high-energy when running low-energy positrons. The energy relation seems to indicate that the electrons are generated by positrons hitting the last lens element or more likely one of the first three grids in the decelerator. These are always held at $V_{\mathrm{f.gnd}}$ or at a potential very close to $V_{\mathrm{f.gnd}}$, explaining the value of E_0. Since the grids act as a decelerator for the positrons, the electrons would instead be accelerated by the grids right into the gas cell with an energy corresponding to the positron deceleration i.e. E_-.

By using the MSP detector we found the electron current, n_-, to be fairly constant over all positron energies below 600 eV. At first this seemed surprising as one would expect it to be proportional to the positron current, n_+, which as mentioned before is *not* constant. However one has to remember that the electrons are generated by the positrons in the first grids *before* the deceleration. Since the transport conditions inside the beam line is the same at all energies, one would expect a constant amount of positrons reaching the first grids, explaining the observed n_-. The electron current could not be measured with the MSP detector for positron energies above 600 eV. However in this energy range the exact behaviour of n_- is not important since the ion background induced by the electrons should be small compared to the number of ions produced by positron impact. We therefore assume that n_- stays constant up until $V_{\mathrm{f.gnd}} \approx 0$.

Using our knowledge about n_- and n_+ we can correct for the background in the data analysis as will be discussed in the next section.

2.2.2 Data analysis

The quantity measured in the pure gas experiments on He, Ne and Xe, was the ratio, N^{2+}/N^+, between the number of counts in the double ionisation peak, N^{2+}, to the number of counts in the single ionisation peak, N^+. Both N^+ and N^{2+} are corrected for the general background in the TOF spectrum. In our experiments there were no means of determining the final state of the positron. Therefore N^+ contained counts from ions produced by both the processes (2.1) and (2.2). Similarly with N^{2+} and the processes (2.3) and (2.4) (and (2.5)) i.e. with Ps formation included.

The ratio N^{2+}/N^+ is related to the ratio $R^{(2)}_{\mathrm{tot}}$ by

$$R^{(2)}_{\mathrm{tot}} \equiv \frac{\sigma^{2+}_{\mathrm{tot}}}{\sigma^{+}_{\mathrm{tot}}} = \epsilon \, \frac{N^{2+}}{N^+}. \tag{2.18}$$

The factor ϵ has been put in to correct for the difference in detector efficiency for the singly and doubly charged ions. Andersen *et al.* have found that the detector efficiency for a Ceratron depends on the impact velocity of the ion on the detector [33]. Due to the doubly charged ions being accelerated to a velocity $\sqrt{2}$ times higher than the singly charged ions, the detector efficiency changes with the charge state, except for the light ions. For helium and neon the ions have irrespectively of the charge state sufficiently high velocity for the relative detector efficiency to be 1 [33], i.e. $\epsilon = 1$.

The advantage of measuring $R^{(2)}_{\mathrm{tot}}$ (or N^{2+}/N^+) is that it is independent of the accumulation time, beam intensity, gas pressure and the geometry of the interaction region. The absolute total double ionisation cross section, $\sigma^{2+}_{\mathrm{tot}}$, can later be deduced from $R^{(2)}_{\mathrm{tot}}$ by multiplication with known values of the

total single ionisation cross section. Unfortunately things were not as straight forward in our experiments due to the electron induced background discussed in the previous section. Instead of (2.18) we had the relation

$$\frac{n_+\sigma_{\rm tot}^{2+}(E_+) + n_-\sigma_{\rm I}^{2+}(E_-)}{n_+\sigma_{\rm tot}^{+}(E_+) + n_-\sigma_{\rm I}^{+}(E_-)} = \epsilon\,\frac{N^{2+}}{N^+}, \tag{2.19}$$

where n_-, n_+, E_- and E_+ are the currents and energies defined in section 2.2.1. $\sigma_{\rm tot}^{+}(E_+)$ and $\sigma_{\rm tot}^{2+}(E_+)$ are like before the positron cross sections, while $\sigma_{\rm I}^{+}(E_-)$ and $\sigma_{\rm I}^{2+}(E_-)$ are the corresponding electron cross sections at the energy E_-. From equation (2.19) one can isolate $\sigma_{\rm tot}^{2+}(E_+)$. However before we could deduce values of $\sigma_{\rm tot}^{2+}$ we needed an absolute calibration of the ratio n_+/n_-, for which only the shape was known (assuming n_- constant and n_+ a known function of E_+). This could be achieved using data taken at energies below $E_{\rm Ps}^{2+}$ where $\sigma_{\rm tot}^{2+} = 0$. At these energies (2.19) reduces to

$$\frac{\sigma_{\rm I}^{2+}(E_-)}{\frac{n_+}{n_-}\sigma_{\rm tot}^{+}(E_+) + \sigma_{\rm I}^{+}(E_-)} = \epsilon\,\frac{N^{2+}}{N^+}, \tag{2.20}$$

from which n_+/n_- could be calibrated. Using this in (2.19) the absolute total double ionisation cross sections by positron impact were deduced.

Values of $\sigma_{\rm tot}^{+}(E_+)$, $\sigma_{\rm I}^{+}(E_-)$ and $\sigma_{\rm I}^{2+}(E_-)$ were found in the literature. For all our noble gas experiments the electron cross sections of Krishnakumar and Srivastava [13] were used, except in the helium experiment where cross sections by Shah *et al.* [51] were used. For helium the values of $\sigma_{\rm tot}^{+}(E_+)$ shown in figure 2.3 were used, while for neon the unpublished data by Laricchia [30] shown in figure 2.7 were used. In figure 2.7 are also plotted data for $\sigma_{\rm I}^{2+}$ just to illustrate that the single ionisation cross section for neon behave completely analogous to those of helium and in accordance with the discussion in section 2.1.1. For xenon however we were faced with a problem as no data for $\sigma_{\rm tot}^{+}$ were available. To resolve this problem we turned to doing experiments using mixed gases.

In the mixed gas experiments, a mixture of the heavy noble gas under investigation and helium was admitted into the gas cell. The idea was to determine both the total single and total double ionisation cross section of the heavy gas (e.g. xenon) by measuring these relative to the known total single ionisation cross section of helium. For a heavy noble gas, A, we would therefore instead of (2.18) be measuring the ratio

$$R_{\rm tot,AHe}^{(k)} \equiv \frac{\sigma_{\rm tot,A}^{k+}}{\sigma_{\rm tot,He}^{+}} = \epsilon^{(k)}\rho_{\rm AHe}\frac{N_{\rm A}^{k+}}{N_{\rm He}^{+}},\ k = 1, 2. \tag{2.21}$$

Like before $N_{\rm A}^{k+}$ and $N_{\rm He}^{+}$ are the ion count rates of the specified gases. $\epsilon^{(k)}$ corrects for the difference in detector efficiency between the ions of the heavy

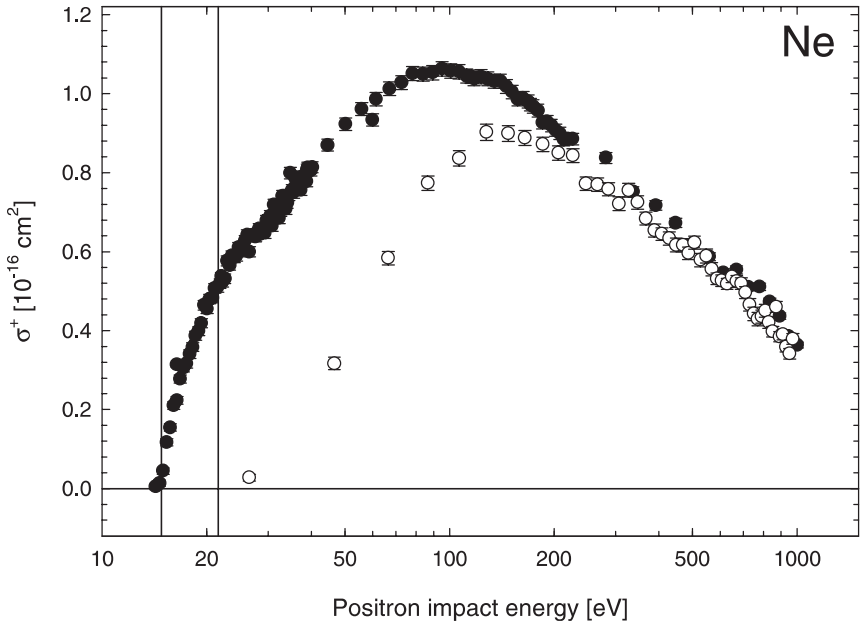

Figure 2.7: Single ionisation cross sections of neon by positron impact. (●) $\sigma^+_{\rm tot}$ by Laricchia [30], (○) $\sigma^+_{\rm I}$ by Kara *et al.* [17]. This cross section has also been measured by Jacobsen *et al.* [11], but as their results agree with those of Kara *et al.* they are not shown in this figure. The two vertical lines indicate $E^+_{\rm Ps}$ and $E^+_{\rm I}$ respectively.

gas and the He^+ ions. The factor $\rho_{\rm AHe}$ is the ratio between target densities of the two gases. This arises from two terms: First is the mixture ratio in the gas bottle used. In all of our experiments we had a nominal ratio of 70% helium and 30% of the heavy gas. Secondly the target densities also depended on how fast the gases diffused out of the gas cell. For thermal diffusion this would imply that $\frac{1}{2}{\rm M}v^2_{\rm diff} = $ constant, meaning that the diffusion velocity $v_{\rm diff}$ depends inverse proportionally on the square root of the mass of the gas, i.e. lighter gases escape faster than heavy ones.

Just as in the case of the pure gas experiments, corrections due to electron induced background had to be made and (2.21) replaced by

$$\frac{n_+\sigma^{k+}_{\rm tot,A}(E_+) + n_-\sigma^{k+}_{\rm I,A}(E_-)}{n_+\sigma^{+}_{\rm tot,He}(E_+) + n_-\sigma^{+}_{\rm I,He}(E_-)} = \epsilon^{(k)}\rho_{\rm AHe}\frac{N^{k+}_{\rm A}}{N^{+}_{\rm He}},\ k = 1, 2. \tag{2.22}$$

All factors are as defined before. Calibration of n_+/n_- was again performed

using below threshold double ionisation data. This calibration was then used to deduce both single and double ionisation cross sections.

For double ionisation the factor $\epsilon^{(2)}$ was calculated using estimates for the detector efficiencies from the curve of Andersen *et al.* [33] just like in the pure gas experiments. For the ions Ar^{2+}, Kr^{2+} and Xe^{2+} values of the detector efficiency (relative to the He^{2+} ion) of 0.95, 0.90 and 0.80 respectively were used, all with an estimated uncertainty of 0.05. In single ionisation a different approach was used. Here the entire factor of $\epsilon^{(1)}\rho_{\mathrm{AHe}}$ was determined through direct normalisation of our data to the ratio $\sigma^{+}_{\mathrm{I,A}}/\sigma^{+}_{\mathrm{I,He}}$ for electrons at impact energies above 700 eV. As discussed in section 2.1.1 this is a common approach based on the first Born approximation for normalisation of single ionisation cross sections. From the values of $\epsilon^{(1)}$ detector efficiencies for all the singly charged heavy ions could be deduced and compared to the curve of Andersen *et al.* For Kr^{+} and Xe^{+} this yielded detector efficiencies of 0.80 ± 0.05 and 0.63 ± 0.03 respectively in good agreement with the results of Andersen *et al.* However for Ar^{+} we found a value of 1.21 ± 0.07. This either meant that Ar^{+} was detected more efficiently than He^{+} in our experiment in disagreement with the findings of Andersen *et al.* or more likely something else was going on. At first we suspected that a problem with the gas mixture ratio had led us to use a wrong ρ_{ArHe} in our deduction of $\epsilon^{(1)}$. However the final argon data were taken over two separate runs using *different* gas bottles. These yielded results which only exhibited a difference in absolute magnitude so small that it was within the expected variation on the gas mixture ratio. This at least showed that the two bottles contained similar mixtures. In the final data an average was taken using overlapping high-energy points in the two sets in order to obtain better mixture accuracy. As another check on the mixture ratio, we deduced the double ionisation cross section for argon using the nominal gas mixture ratio and detector efficiency of Andersen *et al.* which, as will be seen in section 2.3.2, agrees well with several previous experiments. This indicates that the problem is not with the gas mixture and that it was limited to the Ar^{+} ion. Another explanation of the problem could therefore be pick-up from electronic noise or other contamination of the Ar^{+} peak, though no traces of such were observed. The nature of the problem therefore remained unresolved and as a consequence the normalisation constant of Ar^{+} can not be satisfactorily interpreted in terms of experimental factors. However since the normalisation to electron data yielded good agreement with previous single ionisation data for argon (see section 2.3.1) we believe it to be reliable.

In all the mixed gas experiments cross-checks were made of the detector efficiencies using electrons. This was done by setting the positron deceleration voltage so high that all positrons were stopped at the end of the beam line and only the background current of electrons would pass through the gas cell. This situation corresponds to $n_{+} = 0$ in equation (2.22). The efficiencies measured

had unfortunately rather poor statistics due to the way they were obtained. For argon we found values of 1.68 ± 0.43 and 0.80 ± 0.38 for Ar^+ and Ar^{2+} ions respectively. For krypton the two values were 0.71 ± 0.19 and 1.51 ± 0.51 and for xenon 0.64 ± 0.12 and 0.82 ± 0.18 respectively. The high value for the Ar^+ ion could be related to the problem discussed above. The remaining values agree reasonably well with the values we used. Best agreement is seen in xenon.

Finally it should be remarked that one data point in the mixed gas xenon experiment was taken at an energy *below* E^+_{Ps} for helium. However assuming (2.22) valid even when $\sigma^+_{\mathrm{tot,He}}(E_+) = 0$, the point could still be normalised.

2.3 Results and discussion

Our results for the total single and total double ionisation cross sections of the noble gases by positron impact are presented in the two following sections. All cross sections have been deduced as discussed in section 2.2.2 from relative measurements using the known σ^+_{tot} for helium shown in figure 2.3. Exceptions are $\sigma^{2+}_{\mathrm{tot}}$ for neon which has been deduced using the σ^+_{tot} for neon shown in figure 2.7, and the pure gas $\sigma^{2+}_{\mathrm{tot}}$ for xenon which has been deduced using our own σ^+_{tot} from the mixed gas xenon experiment.

The error bars on our data do not represent the same quantity in all of the following figures. For $\sigma^{2+}_{\mathrm{tot}}$ for helium and neon they only represent the statistical uncertainty whereas in the other cross sections they include all accumulated uncertainty i.e. statistical uncertainty and uncertainty introduced by background correction and normalisation to an absolute scale. This difference from the light gases to the heavy ones does not reflect any limitations imposed by the physics, but merely a development in our data treatment capabilities. The error bars in helium and neon could have been recalculated, but we have chosen to present the data here as they were originally published. In all cases the statistical uncertainty is the dominant contribution to the error bars.

2.3.1 Single ionisation

Our results for the total single ionisation cross sections of argon, krypton and xenon by positron impact are presented in figures 2.8, 2.9 and 2.10 respectively. In figure 2.8 are also plotted a previous measurement of σ^+_{tot} by Laricchia [31]. In all the figures are, for comparison, included data for σ^+_{I} by either Jacobsen *et al.* [11] or Kara *et al.* [17]. Extrapolated curves through these direct ionisation cross sections have been added to measurements of σ^+_{Ps} by Fornari *et al.* [20] and Diana *et al.* [24,25] to provide an estimate of σ^+_{tot} at low energies. Finally in all figures the measurements of σ^+_{I} for electron impact by Krishnakumar and Srivastava [13], which have been used for normalisation of our data, have been included.

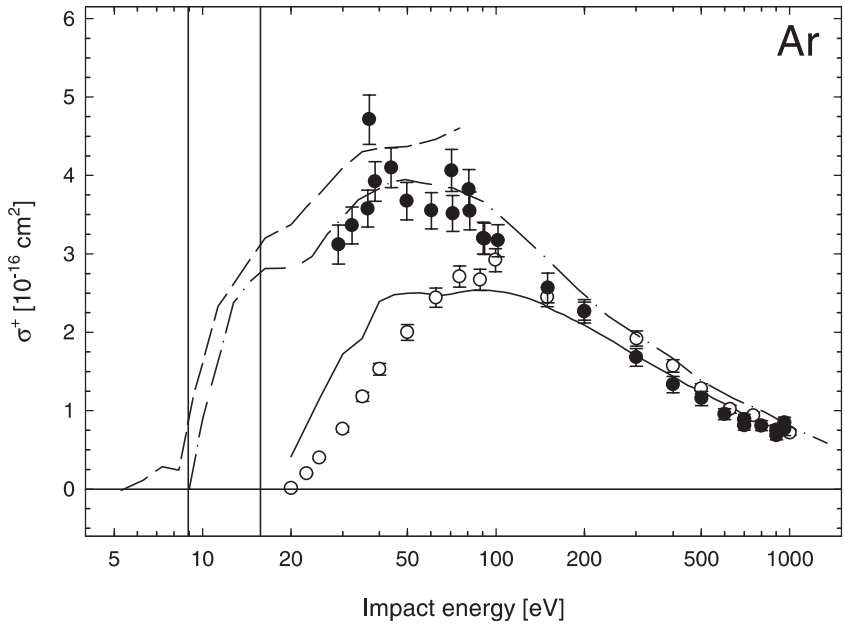

Figure 2.8: Single ionisation cross sections of argon. Positron impact: (●) $\sigma^+_{\rm tot}$ present results, (○) $\sigma^+_{\rm I}$ by Jacobsen *et al.* [11]. This cross section has also been measured by Moxom *et al.* [12], but as their results agree with those of Jacobsen *et al.*, they are not shown in this figure. (—·—) $\sigma^+_{\rm tot}$ by Laricchia [31]. This cross has also been measured by Moxom *et al.* [10], see the discussion in the text. (— —) $\sigma^+_{\rm tot}$ sum of $\sigma^+_{\rm Ps}$ by Fornari *et al.* [20] and $\sigma^+_{\rm I}$ by Jacobsen *et al.* [11]. Electron impact: (——) $\sigma^+_{\rm I}$ by Krishnakumar and Srivastava [13]. The two vertical lines indicate $E^+_{\rm Ps}$ and $E^+_{\rm I}$ respectively.

The behaviour of the cross sections are very similar for all three gases and can be discussed as one. However, first we have to turn our attention to figure 2.8. Here one observes a good agreement between the present data and the measurement by Laricchia [31]. One also sees a reasonable merger between our data and the curve for $\sigma^+_{\rm tot}$ estimated as the sum of $\sigma^+_{\rm Ps}$ by Fornari *et al.* [20] and $\sigma^+_{\rm I}$ by Jacobsen *et al.* [11]. Both observations indicate of that our single ionisation data for argon have been normalised correctly despite the problem discussed in section 2.2.2.

Regarding the data by Laricchia one has to remark that another set of data for $\sigma^+_{\rm tot}$ for argon was published by the same group nearly simultaneously with those shown in figure 2.8 in a paper by Moxom *et al.* [10]. The measurements by Moxom *et al.* are normalised differently than our data and those by Laricchia,

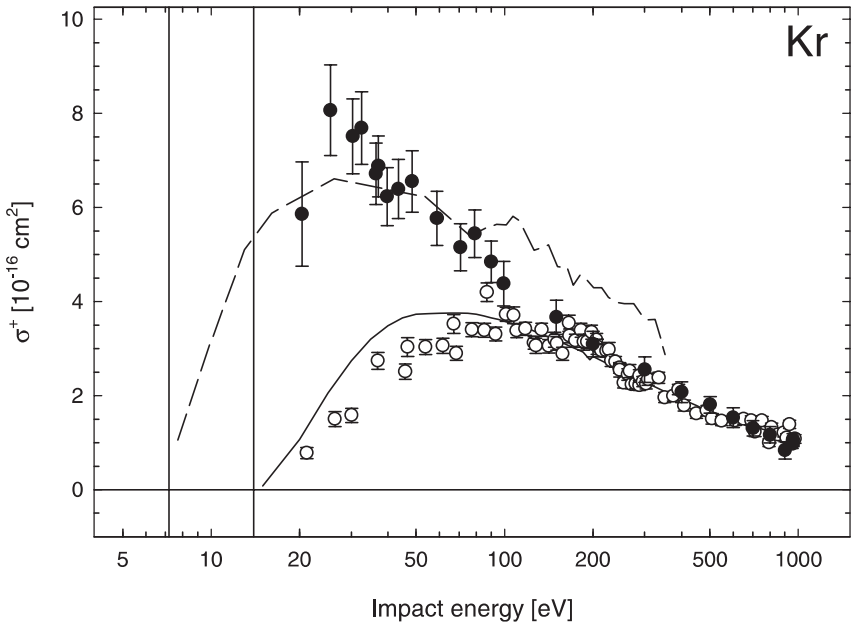

Figure 2.9: Single ionisation cross sections of krypton. Positron impact: (●) $\sigma^+_{\rm tot}$ present results, (○) $\sigma^+_{\rm I}$ by Kara *et al.* [17]. This cross section has also been measured by Moxom *et al.* [12], but as their results agree with those of Kara *et al.*, they are not shown in this figure. (——) $\sigma^+_{\rm tot}$ sum of $\sigma^+_{\rm Ps}$ by Diana *et al.* [24] and $\sigma^+_{\rm I}$ by Kara *et al.* [17]. Electron impact: (——) $\sigma^+_{\rm I}$ by Krishnakumar and Srivastava [13]. The two vertical lines indicate $E^+_{\rm Ps}$ and $E^+_{\rm I}$ respectively.

making them slightly larger than these at high energies. However at the cross section maximum they are a factor of 2 higher than the Laricchia data which is far more than can be accounted for by the different normalisation (factor of ∼1.4). This discrepancy has never been discussed by any of the authors from the UCL group and remains unresolved. We choose in figure 2.8 to plot the data by Laricchia as they are the most recent and are to be published together with the cross sections for Ne, Kr and Xe in a forthcoming paper [30].

The single ionisation cross sections of the three heavy noble gases are seen to behave in the same way as those of helium and neon in figures 2.3 and 2.7 in accordance with the discussion in section 2.1.1. At high impact energies the cross sections for electrons and positrons are merged, due to the normalisation used. However one also observes that the *shape* of the cross sections are similar, indicating that we are in an energy region where the first Born approximation is valid.

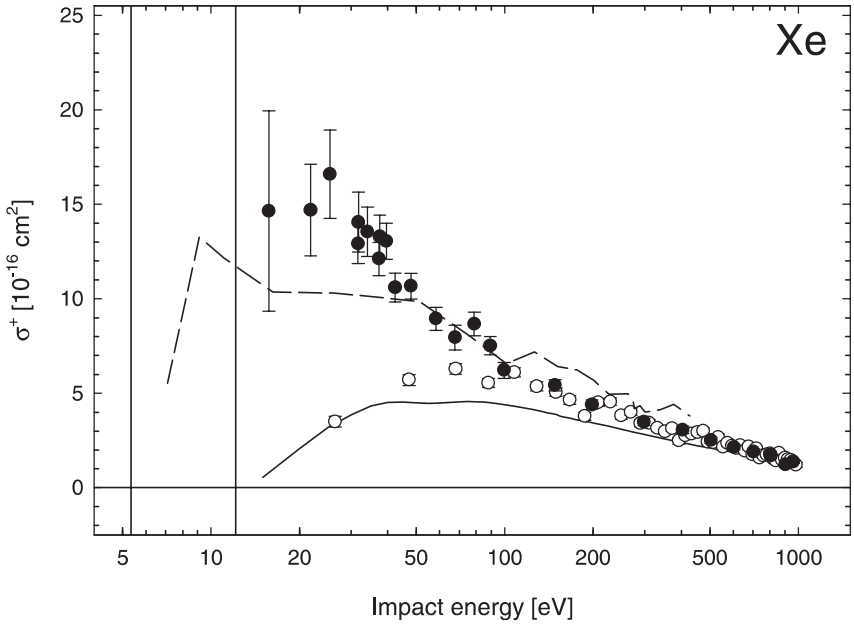

Figure 2.10: Single ionisation cross sections of xenon. Positron impact: (●) $\sigma^+_{\rm tot}$ present results, (○) $\sigma^+_{\rm I}$ by Kara *et al.* [17], (— —) $\sigma^+_{\rm tot}$ sum of $\sigma^+_{\rm Ps}$ by Diana *et al.* [25] and $\sigma^+_{\rm I}$ by Kara *et al.* [17]. Electron impact: (——) $\sigma^+_{\rm I}$ by Krishnakumar and Srivastava [13]. The two vertical lines indicate $E^+_{\rm Ps}$ and $E^+_{\rm I}$ respectively.

Below ∼100 eV the present data for $\sigma^+_{\rm tot}$ start to rise above the corresponding $\sigma^+_{\rm I}$ due to the growing importance of the positronium formation channel (2.2). At the maximum of $\sigma^+_{\rm tot}$ positronium formation contributes around half of the total cross section. Despite that our data do not extend all the way down to threshold, their general trend seems to indicate a significant contribution from positronium formation in the Ore gap. This is supported by the curves for $\sigma^+_{\rm tot}$ estimated from $\sigma^+_{\rm Ps}$ and $\sigma^+_{\rm I}$. These all show that $\sigma^+_{\rm tot}$ should rise sharply at the threshold $E^+_{\rm Ps}$ and reach a value close to that of the cross section maximum already at $E^+_{\rm I}$. This shows that positronium formation is even more important at low energies in these gases than in helium and neon. The present data merge reasonably with the estimated curves. Best agreement is seen for krypton in figure 2.9. In both krypton and xenon one observes that the estimated curves overshoot our data at energies above ∼100 eV. This is because Diana *et al.* [24,25] find $\sigma^+_{\rm Ps}$ to be non-zero at these energies, while a comparison between the present data and those for $\sigma^+_{\rm I}$ indicates the opposite. In argon the estimate does not reach so high an energy. However if we had extended it by supplementing

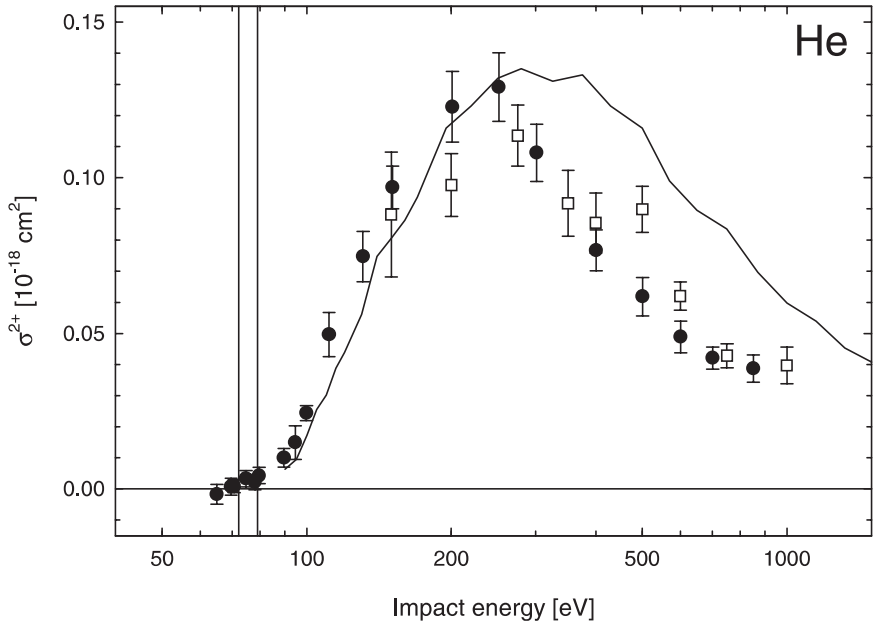

Figure 2.11: Double ionisation cross sections of helium. Positron impact: (●) $\sigma_{\mathrm{tot}}^{2+}$ present results, (□) σ_{I}^{2+} derived from $R_{\mathrm{I}}^{(2)}$ by Charlton *et al.* [32] using σ_{I}^{+} by Jacobsen *et al.* [11]. Electron impact: (——) σ_{I}^{2+} by Shah *et al.* [51]. The two vertical lines indicate E_{Ps}^{2+} and E_{I}^{2+} respectively.

the σ_{Ps}^{+} by Fornari *et al.* [20] with the high-energy data for argon by Diana *et al.* [22] the same would have been seen there. As discussed before it is not in general believed today that positronium formation contributes significantly to $\sigma_{\mathrm{tot}}^{+}$ at such high energies. This is also what is known from helium.

In conclusion we may say that the present data for the total single ionisation cross section of argon, krypton and xenon by positron impact exhibit no surprising features.

2.3.2 Double ionisation

Our results for the total double ionisation cross sections of the noble gases by positron impact are presented in figures 2.11 to 2.15. In figure 2.15 the present results for xenon are plotted as two separate sets: One from the pure gas experiment and another from the mixed gas experiment. In figure 2.13 for argon is also plotted the previous measurement of $\sigma_{\mathrm{tot}}^{2+}$ by Hippler *et al.* [45]. For comparison data for σ_{I}^{2+} are included in all the figures. For Ne, Kr

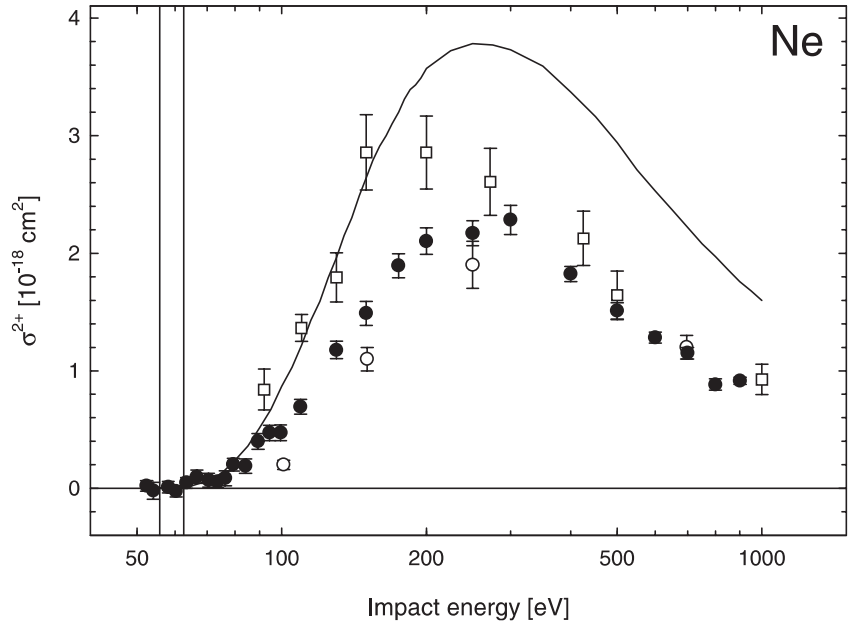

Figure 2.12: Double ionisation cross sections of neon. Positron impact: (●) $\sigma_{\rm tot}^{2+}$ present results, (○) $\sigma_{\rm I}^{2+}$ by Kara *et al.* [17], (□) $\sigma_{\rm I}^{2+}$ derived from $R_{\rm I}^{(2)}$ by Charlton *et al.* [43] using $\sigma_{\rm I}^{+}$ by Jacobsen *et al.* [11]. Electron impact: (——) $\sigma_{\rm I}^{2+}$ by Krishnakumar and Srivastava [13]. The two vertical lines indicate $E_{\rm Ps}^{2+}$ and $E_{\rm I}^{2+}$ respectively.

and Xe we have plotted the $\sigma_{\rm I}^{2+}$ measured by Kara *et al.* [17] and for He, Ne and Ar are included values of $\sigma_{\rm I}^{2+}$ derived from $R_{\rm I}^{(2)}$ by Charlton *et al.* [32,43] using $\sigma_{\rm I}^{+}$ by Jacobsen *et al.* [11]. Finally data for double ionisation by electron impact are included. In figure 2.11 for helium it is the results by Shah *et al.* [51] that are shown while in the remaining figures the results by Krishnakumar and Srivastava [13] are being displayed.

Before turning to discuss the detailed behaviour of the cross sections we start with two more general remarks: First one observes in figure 2.13 for argon that there is a good agreement between the present results and those by Hippler *et al.* [45] over the entire energy range, verifying our experimental technique. It also shows that all aspects of the data analysis are well understood including the normalisation of the double ionisation data. The normalisation problem discussed in section 2.2.2 is therefore clearly limited to the argon single ionisation data. The second observation one makes is in figure 2.15 for xenon. Here one notes a good agreement between the present results obtained in the pure

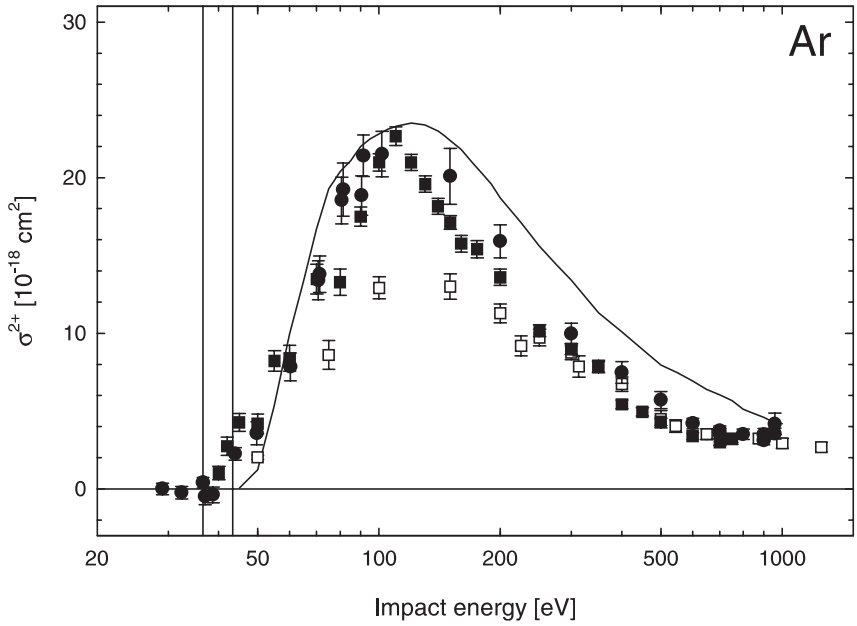

Figure 2.13: Double ionisation cross sections of argon. Positron impact: (●) $\sigma_{\rm tot}^{2+}$ present results, (■) $\sigma_{\rm tot}^{2+}$ by Hippler *et al.* [45], (□) $\sigma_{\rm I}^{2+}$ derived from $R_{\rm I}^{(2)}$ by Charlton *et al.* [43] using $\sigma_{\rm I}^{+}$ by Jacobsen *et al.* [11]. Electron impact: (——) $\sigma_{\rm I}^{2+}$ by Krishnakumar and Srivastava [13]. The two vertical lines indicate $E_{\rm Ps}^{2+}$ and $E_{\rm I}^{2+}$ respectively.

gas experiment and those from the mixed gas experiment. Of course one has to remember here that the pure gas data have been normalised using our own mixed gas xenon single ionisation data shown in figure 2.10. Both sets of data are therefore in essence normalised to $\sigma_{\rm tot}^{2+}$ for helium. It however still shows a consistency between our two methods and verifies our technique for measuring $R_{\rm tot}^{(2)}$ in the pure gas experiment.

Starting at high energies one sees that the present cross sections behave much as expected. In all gases there is a merger between $\sigma_{\rm tot}^{2+}$ and $\sigma_{\rm I}^{2+}$. In contrast to single ionisation this behaviour is not an artifact of some common normalisation and shows that there is no significant contribution from double ionisation with positronium formation (2.4) to $\sigma_{\rm tot}^{2+}$ at these energies. A few minor deviations from the merger between the two cross sections are seen in krypton and xenon. In figure 2.14 for krypton one observes that $\sigma_{\rm I}^{2+}$ falls below $\sigma_{\rm tot}^{2+}$ at energies between 300 and 500 eV. We believe that this is due to a few anomalously low points in $\sigma_{\rm I}^{2+}$ rather than being an indication of positronium

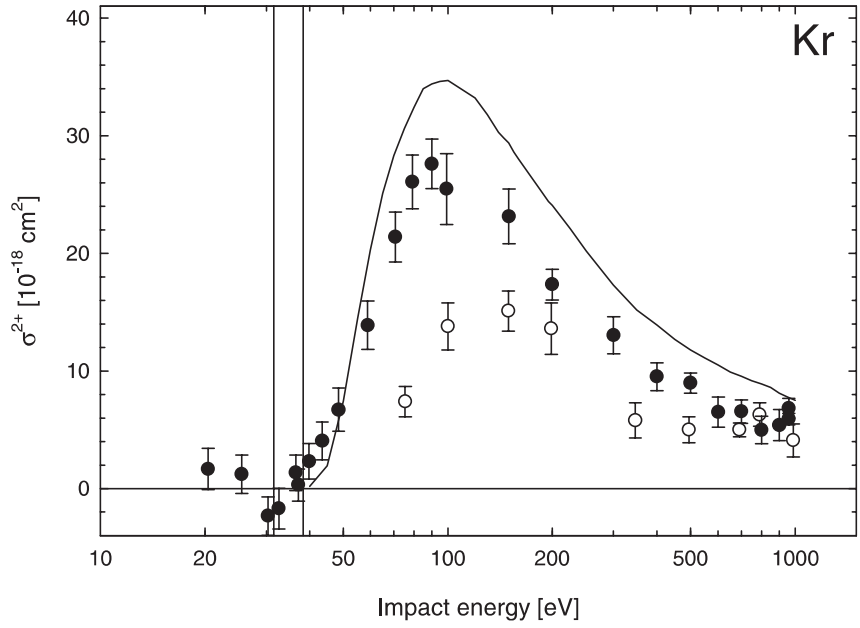

Figure 2.14: Double ionisation cross sections of krypton. Positron impact: (●) $\sigma^{2+}_{\rm tot}$ present results, (○) $\sigma^{2+}_{\rm I}$ by Kara *et al.* [17]. Electron impact: (——) $\sigma^{2+}_{\rm I}$ by Krishnakumar and Srivastava [13]. The two vertical lines indicate $E^{2+}_{\rm Ps}$ and $E^{2+}_{\rm I}$ respectively.

formation. In figure 2.15 for xenon one observes that the present data have a slight 'bump' at energies from 300 to 1000 eV which the corresponding $\sigma^{2+}_{\rm I}$ does not exhibit. This could possibly again be attributed to a few deviating points. The observed bump is closely related to a structure seen in the ratio $R^{(2)}_{\rm tot}$. As can be seen in figure 4 in Bluhme *et al.* [IV] the $R^{(2)}_{\rm I}$ by Kara *et al.* [17] as well as other previous measurements of $R^{(2)}_{\rm tot}$ [39] and $R^{(2)}_{\rm I}$ [44] all exhibit similar structure. As there is no difference between between $\sigma^{+}_{\rm I}$ and $\sigma^{+}_{\rm tot}$ at these energies (see figure 2.10) one would expect the bump to be present in $\sigma^{2+}_{\rm I}$ as well. The conclusiveness of this is however limited by the scarcity of the $\sigma^{2+}_{\rm I}$ data.

The origin of the high-energy bump in $\sigma^{2+}_{\rm tot}$ for xenon could be attributed to inner shell ionisation processes in which an inner shell electron is ionised by the interaction with the positron followed by an Auger or Coster-Kronig process which leaves the atom doubly ionised. As already mentioned in section 2.1.2 Helms *et al.* [39] have developed an estimate of the contribution to $\sigma^{2+}_{\rm tot}$ from inner shell processes based on the semi-empirical cross sections by Lotz [40,41]

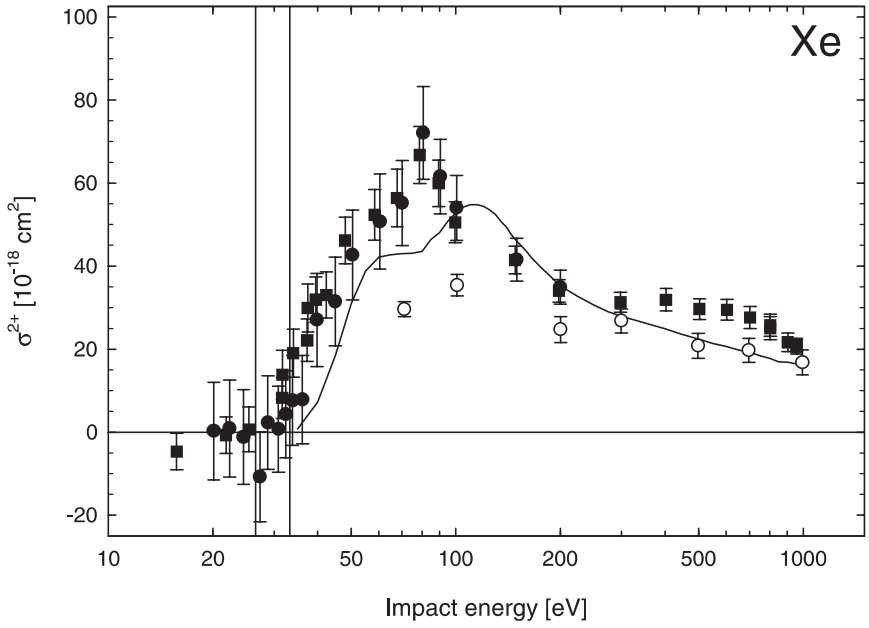

Figure 2.15: Double ionisation cross sections of xenon. Positron impact: (●) $\sigma_{\rm tot}^{2+}$ present results, pure gas, (■) $\sigma_{\rm tot}^{2+}$ present results, mixed gas, (○) $\sigma_{\rm I}^{2+}$ by Kara *et al.* [17]. Electron impact: (——) $\sigma_{\rm I}^{2+}$ by Krishnakumar and Srivastava [13]. The two vertical lines indicate $E_{\rm Ps}^{2+}$ and $E_{\rm I}^{2+}$ respectively.

and the branching ratios by Carlson *et al.* [42]. Comparing the estimates to their measured ratios $R_{\rm tot}^{(2)}$ for Ar, Kr and Xe Helms *et al.* conclude that inner shell processes are responsible for most of the double ionisation at high energies. However there are several pitfalls in such a comparison: First of all comparing of ratios instead of absolute cross sections makes it hard to discern effects due to $\sigma_{\rm tot}^{2+}$ from those arising from $\sigma_{\rm tot}^{+}$. As shown by the same group in a later paper [45] the picture may change somewhat when comparing absolute double ionisation cross sections instead. Secondly it is unclear how well inner shell cross sections are described by the Lotz model [52]. Finally there is the use of the branching ratios by Carlson *et al.* The ratios were measured using x-rays to create the inner shell vacancies in the atoms and are therefore effectively measurements of $R_{\gamma}^{(2)}$ for inner shell ionisation. However as discussed in section 2.1.2 then it is generally known that there can be a large difference in magnitude between $R_{\gamma}^{(2)}$ and $R^{(2)}$ for charged particle impact. It is therefore questionable whether or not the data by Carlson *et al.* can be applied in this situation.

Finally it should be remarked that one would expect an inner shell contribution in the electron cross section as well. However as discussed by Helms *et al.* [39] the contribution need not be the same for electrons as for positrons due to the influence of the Coulomb trajectory effect (see section 2.1.1) which affects the two projectiles in opposite ways. This can explain why we do not observe a bump in the electron cross section at the same energy.

Going down to intermediate energies the cross sections of the five gases start to differ in their behaviour. In figure 2.11 for helium one observes that at these energies there is *still* no difference between $\sigma_{\mathrm{tot}}^{2+}$ and σ_{I}^{2+}, indicating insignificant amounts of double ionisation with positronium formation. This suppression of the positronium channel (2.4) in helium is very surprising as it is opposite to what is observed in single ionisation and therefore also generally expected for double ionisation (see section 2.1.2). Continuing to figure 2.12 for neon one notices the disagreement between the two measurements of σ_{I}^{2+} by Charlton *et al.* [43] and Kara *et al.* [17] respectively. Kara *et al.* attributed this difference to inadequate discrimination against positronium formation in the experiment by Charlton *et al.* However such a lack of discrimination should only have put the data by Charlton *et al.* somewhere *between* the σ_{I}^{2+} by Kara *et al.* and the present results for $\sigma_{\mathrm{tot}}^{2+}$. A contribution from $\sigma_{\mathrm{Ps}}^{2+}$ could never raise a σ_{I}^{2+} above our data unless these somehow should be in error for which we have no indications. It therefore remains unexplained what, in the experiment by Charlton *et al.*, has caused the disagreement. However even when comparing the present $\sigma_{\mathrm{tot}}^{2+}$ to the σ_{I}^{2+} by Kara *et al.* one finds none or at least very little positronium formation at intermediate energies just like in helium. This is again unexpected. Turning to the three heavy gases one observes a change. In the figures 2.13, 2.14 and 2.15 there is a clear difference between the present $\sigma_{\mathrm{tot}}^{2+}$ and the σ_{I}^{2+} indicating that a contribution from positronium formation is present at intermediate energies for all three gases. For argon and krypton this is in agreement with the findings by Falke *et al.* [48], who observed the existence of positronium formation in this energy range.

Descending to the threshold region and the second Ore gap one finds that the trend in helium and neon from the intermediate energies continues. In the second Ore gap where $\sigma_{\mathrm{tot}}^{2+}$ equals $\sigma_{\mathrm{Ps}}^{2+}$ we find values for the cross section consistent with zero in the entire gap for both gases, showing a clear lack of double ionisation with positronium formation at threshold. The cross sections show no indication of a sharp rise at E_{Ps}^{2+} similar to that seen in $\sigma_{\mathrm{tot}}^{+}$ at E_{Ps}^{+}. Instead the cross sections only start to rise slowly above E_{I}^{2+} in a manner more like the behaviour of σ_{I}^{+} above E_{I}^{+}. It was this observation for the helium and neon targets that first spurred our interest in the double ionisation threshold behaviour and lead us to conduct similar measurements on the three heavy gases. Prior to our measurements Helms *et al.* [39] had seen an indication of a rise in their ratios $R_{\mathrm{tot}}^{(2)}$ for Ar, Kr and Xe within the second Ore gap. However

it could be doubtful whether this was due to positronium formation or an effect of the poor energy resolution of their positron beam (∼6 eV FWHM [53]). In argon one sees that the present results show a small rise within the second Ore gap in agreement with the $\sigma_{\rm tot}^{2+}$ derived by Hippler *et al.* [45] from the $R_{\rm tot}^{(2)}$ by Helms *et al.* However the rise is still not as sharp that seen in single ionisation. In krypton our data are a bit inconclusive. In the second Ore gap the points seem to be consistent with zero, while the points right above $E_{\rm I}^{2+}$ indicate a small rise within the gap. When looking at the mixed gas results for xenon, which have the smallest error bars, there are a few points within the gap clearly above zero. This shows that there must be a rise, which is also supported by the general trend of the data above $E_{\rm I}^{2+}$.

Our observations on the threshold behaviour have been supported by more recent data. Inspired by our first paper on helium and neon [I] Moxom *et al.* [4] devised an experiment which would focus on the low-energy region. With a mixed gas technique similar to ours they have measured $\sigma_{\rm tot}^{2+}$ for Ne, Ar, Kr and Xe with a better resolution. This was achieved by using a Penning trap-like setup to increase the effective interaction length by several orders of magnitude over ours [54]. Their results are shown separately together with the present results in figure 2.16. In general there is a good agreement between the present results and those by Moxom *et al.* An exception is in krypton where our data are a bit lower than theirs at energies between 5 and 40 eV above $E_{\rm Ps}^{2+}$. In neon the agreement is also a bit artificial. Moxom *et al.* perform a normalisation of their data using previous measurements. In neon they use our present results for normalisation, explaining the observed agreement in absolute magnitude of the cross sections. In the remaining gases they use values deduced from the ratios by Helms *et al.* [39]. One observes that the results by Moxom *et al.* confirm our conclusions about the behaviour of $\sigma_{\rm tot}^{2+}$ at threshold: In neon they also find values of $\sigma_{\rm tot}^{2+}$ consistent with zero in the entire second Ore gap. In the three heavy gases they see a small rise within the gap indicating the presence of double ionisation with positronium formation. The rise above $E_{\rm Ps}^{2+}$ is however the same slow one as we observe. If one takes the value of $\sigma_{\rm tot}^{2+}$ at $E_{\rm I}^{2+}$ relative to the value at the cross section maximum as a measure of the importance of the positronium channel (2.4), one sees that it increases with the mass of the target atom. However in double ionisation it never attains values as high as the corresponding ratio in single ionisation, e.g. ∼15% compared to ∼75% for argon and krypton (see figures 2.8 and 2.9).

To briefly summarise we have found that double ionisation with positronium formation is suppressed in helium and neon at *all* energies while in argon, krypton and xenon a contribution from this channel is seen at low and intermediate energies. The threshold behaviour exhibited in these gases is different from that seen in single ionisation. It should be remarked that a more quantitative discussion of $\sigma_{\rm Ps}^{2+}$ is mostly limited by the quality of data available on $\sigma_{\rm I}^{2+}$.

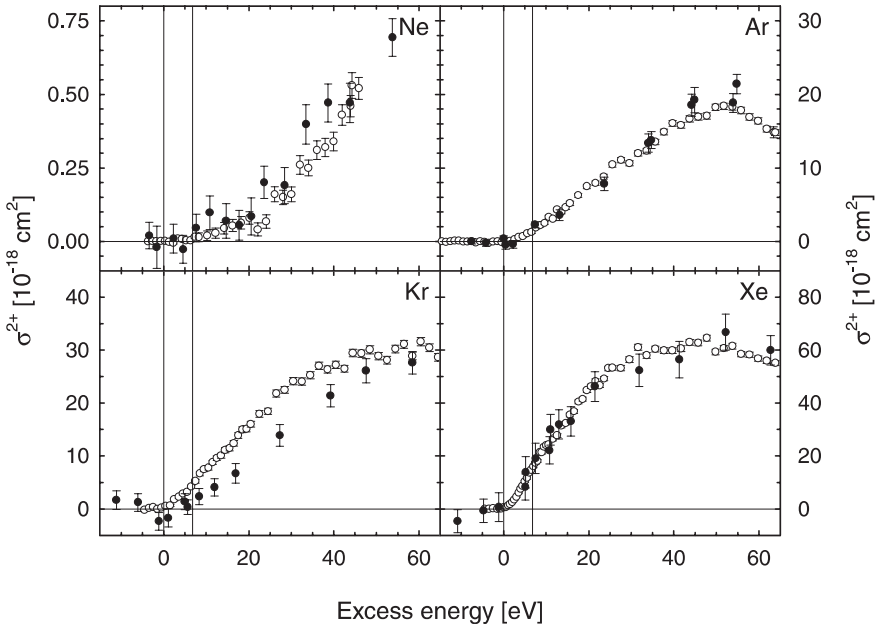

Figure 2.16: Threshold behaviour of the total double ionisation cross sections of the noble gases Ne, Ar, Kr and Xe. (●) $\sigma^{2+}_{\rm tot}$ present results, (○) $\sigma^{2+}_{\rm tot}$ by Moxom *et al.* [4]. In xenon only the present mixed gas results are shown. The cross sections are plotted as a function of positron excess energy above $E^{2+}_{\rm Ps}$. The two vertical lines indicate in all the figures $E^{2+}_{\rm Ps}$ and $E^{2+}_{\rm I}$ respectively.

In a very recent paper Humberston and Van Reeth [55] have given a possible explanation for the observed behaviour of $\sigma^{2+}_{\rm Ps}$ at threshold. In their model they look at the recapture process:

$$\mathrm{Ps} + \mathrm{A}^{2+} \quad \rightarrow \quad \mathrm{A}^{+} + \mathrm{e}^{+}. \tag{2.23}$$

Arguing that the positronium formed in double ionisation travels at slower velocities than the simultaneously escaping electron, the Ps will be left behind in the near vicinity of the doubly charged ion. In this situation there is a probability for the process (2.23) to occur. This would lead to a reduction in the number of doubly charged ions produced and to a suppression of the Ps channel (2.4). The quantity describing the strength of the Coulomb field felt by the Ps and thereby also the probability for (2.23) to occur, is the energy, ΔE, released in the process. This is given by $\Delta E = E^{2+}_{\rm I} - E^{+}_{\rm I} - 6.8$ eV $= E^{2+}_{\rm Ps} - E^{+}_{\rm I}$. The ΔE for the five noble gases are given in table 2.1. One sees that the values of ΔE for helium and neon are somewhat larger than the values for the other gases.

	He	Ne	Ar	Kr	Xe
ΔE [eV]	47.62	34.16	20.83	17.56	14.41

Table 2.1: Values of ΔE for the noble gases.

According to Humberston and Van Reeth this should make the suppression of positronium formation stronger in helium and neon than in the other noble gases. This is in agreement with the experimental observations. Furthermore Humberston and Van Reeth consider what happens as the positron energy is raised well above $E_{\rm Ps}^{2+}$. Here they expect the velocity of the Ps to be larger than it is near threshold, thereby reducing the probability of recapture. This explains the rise within the second Ore gap and the Ps formation at intermediate energies observed in Ar, Kr and Xe. However for helium and neon they suggest that the recapture probability remains high enough up to $E_{\rm I}^{2+}$ for Ps formation to be suppressed in the entire second Ore gap as observed. Even beyond $E_{\rm I}^{2+}$ the recapture rate could remain high up to energies where the *formation* probability for the Ps starts to be suppressed. The net result would be a suppression of double ionisation with positronium formation at *all* energies in agreement with our observations. A disadvantage of the Humberston and Van Reeth model is that they do not concern themselves with the formation of the positronium in any great detail. This mechanism could be as important for the behaviour of $\sigma_{\rm Ps}^{2+}$ as the recapture process.

Finally Humberston and Van Reeth make an observation on positronium formation in general. Recapture should, just like in double ionisation, occur in single ionisation. The recapture there would be the reverse process of (2.2). However the energy released in such a process would be equal to $E_{\rm Ps}^{+}$, and so only a relatively small suppression would be expected. The two authors make a remarkable observation when plotting values of $\sigma_{\rm Ps}^{+}$ and $\sigma_{\rm Ps}^{2+}$ measured within the Ore gaps against the released energy i.e. $E_{\rm Ps}^{+}$ and ΔE respectively. In such a plot the positronium formation cross sections seem to fit the relation:

$$\sigma_{\rm Ps}^{k+} = \frac{A\exp(-BE_r)}{k^2},\ k = 1, 2. \tag{2.24}$$

E_r is the released energy and A and B are constants. The formula is purely empirical and the factor of k^2 added *ad hoc*. However the formula fits cross sections ranging over five orders of magnitude which would indicate an underlying mechanism. The validity of (2.24) will be tested in the near-future by Moxom *et al.* [56] by looking at triple ionisation ($k = 3$). One use of (2.24) would be to predict the value of $\sigma_{\rm Ps}^{2+}$ for helium a few eV above $E_{\rm Ps}^{2+}$. This yields approximately 1×10^{-22} cm^2 [56] which is an order of magnitude smaller than the error bars on the zero value we find ($(2.2 \pm 2.5) \times 10^{-21}$ cm^2 at 78 eV).

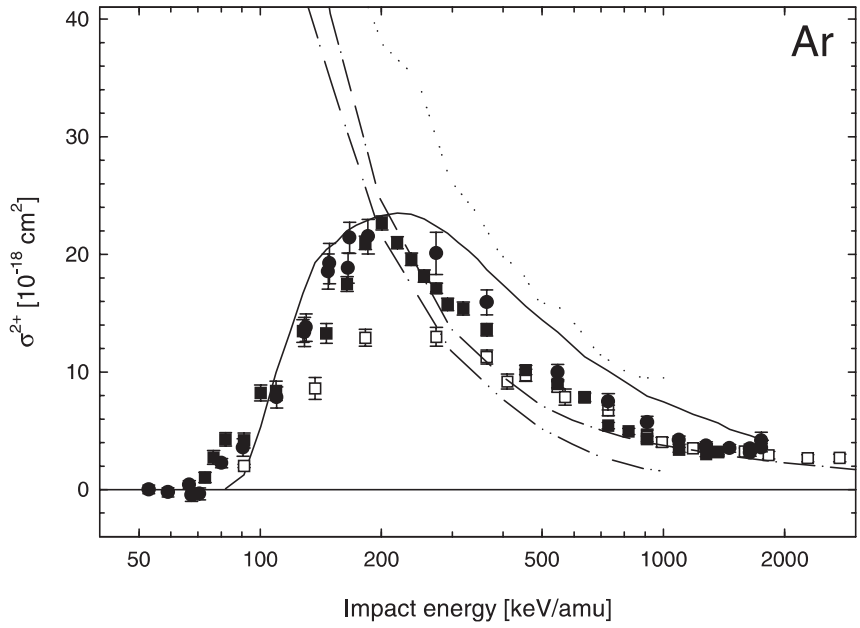

Figure 2.17: Double ionisation cross sections of argon. Positron impact: (●) $\sigma^{2+}_{\rm tot}$ present results, (■) $\sigma^{2+}_{\rm tot}$ by Hippler *et al.* [45], (□) $\sigma^{2+}_{\rm I}$ derived from $R^{(2)}_{\rm I}$ by Charlton *et al.* [43] using $\sigma^{+}_{\rm I}$ by Jacobsen *et al.* [11]. Electron impact: (——) $\sigma^{2+}_{\rm I}$ by Krishnakumar and Srivastava [13]. Proton impact: (—·—) $\sigma^{2+}_{\rm tot}$, (—··—) $\sigma^{2+}_{\rm I}$ both from DuBois and Manson [57] and references within. Antiproton impact: (·····) $\sigma^{2+}_{\rm I}$ by Paludan *et al.* [XIII,XIV].

Concluding this chapter we shall briefly return to the standard picture of ionisation. In all the figures 2.11 to 2.15 are included data for electron impact double ionisation. For all the gases, except xenon, there is no merger at high energies between the positron and electron data as predicted in section 2.1.2. The data for argon and krypton show signs of a possible merger at energies slightly above those in our figures. In all four gases the electron data lie above the positron data indicating that the constant C_3 in (2.14) is negative. To emphasise this we plot in figure 2.17 the data for argon from figure 2.13 on a velocity scale together with double ionisation cross sections for proton and antiproton impact. One observes that the cross sections in figure 2.17 stay merged towards lower velocities according to the sign of the projectile charge. This is the same behaviour as observed in figure 2.4 and confirms the interference model. Finally in figure 2.15 for xenon one sees a somewhat different behaviour at high energies with our data lying above the electron ones. This is however

due to the bump in our data discussed earlier on. If caused by inner shell processes this is clearly something not accommodated by the standard picture of ionisation and therefore the deviation is quite understandable.

References

[1] H. Knudsen and J. F. Reading, Phys. Rep. **212**, 107 (1992).

[2] A. Ore, University of Bergen Yearbook, Naturvitensk. rekke Nr. 9, 1949.

[3] S. Helms, U. Brinkmann, J. Deiwiks, R. Hippler, H. Schneider, D. Segers, and J. Paridaens, J. Phys. B: At. Mol. Opt. Phys. **27**, L557 (1994).

[4] J. Moxom, D. M. Schrader, G. Laricchia, Jun Xu, and L. D. Hulett, Phys. Rev. A **60**, 2940 (1999).

[5] M. B. Shah and H. B. Gilbody, J. Phys. B: At. Mol. Phys. **18**, 899 (1985).

[6] M. B. Shah, P. McCallion, and H. B. Gilbody, J. Phys. B: At. Mol. Opt. Phys. **22**, 3037 (1989).

[7] C. F. Barnett, J. A. Ray, E. Ricci, M. I. Wilker, E. W. McDaniel, E. W. Thomas, and H. B. Gilbody, *Atomic Data for Controlled Fusion Research* ORNL 5206 (Oak Ridge National Laboratory, Oak Ridge, TN, 1977), Vol. 1.

[8] W. Raith, in *Atomic Physics with Positrons*, edited by J. W. Humberston and E. A. G. Armour (Plenum Press, New York, 1987), p. 1.

[9] K. Paludan, Ph.D. thesis, University of Aarhus, 1997.

[10] J. Moxom, G. Laricchia, and M. Charlton, J. Phys. B: At. Mol. Opt. Phys. **28**, 1331 (1995).

[11] F. M. Jacobsen, N. P. Frandsen, H. Knudsen, U. Mikkelsen, and D. M. Schrader, J. Phys. B: At. Mol. Opt. Phys. **28**, 4691 (1995).

[12] J. Moxom, P. Ashley, and G. Laricchia, Can. J. Phys. **74**, 367 (1996).

[13] E. Krishnakumar and S. K. Srivastava, J. Phys. B: At. Mol. Opt. Phys. **21**, 1055 (1988).

[14] L. H. Andersen, P. Hvelplund, H. Knudsen, S. P. Møller, J. O. P. Pedersen, S. Tang-Petersen, E. Uggerhøj, K. Elsener, and E. Morenzoni, Phys. Rev. A **41**, 6536 (1990).

[15] P. Hvelplund, H. Knudsen, U. Mikkelsen, E. Morenzoni, S. P. Møller, E. Uggerhøj, and T. Worm, J. Phys. B: At. Mol. Opt. Phys. **27**, 925 (1994).

[16] D. Rapp and P. Englander-Golden, J. Chem. Phys. **43**, 1464 (1965).

[17] V. Kara, K. Paludan, J. Moxom, P. Ashley, and G. Laricchia, J. Phys. B: At. Mol. Opt. Phys. **30**, 3933 (1997).

[18] M. Charlton, G. Clark, T. C. Griffith, and G. R. Heyland, J. Phys. B: At. Mol. Phys. **16**, L465 (1983).

[19] T. C. Griffith, in *Positron Scattering in Gases*, edited by J. W. Humberston and M. R. C. McDowell (Plenum Press, New York, 1983), p. 53.

[20] L. S. Fornari, L. M. Diana, and P. G. Coleman, Phys. Rev. Lett. **51**, 2276 (1983).

[21] L. M. Diana, S. C. Sharma, L. S. Fornari, P. G. Coleman, P. K. Pendleton, D. L. Brooks, and B. E. Seay, in *Positron Annihilation*, edited by P. C. Jain, R. M. Singru, and K. P. Gopinathan (World Scientific, Singapore, 1985), p. 428.

[22] L. M. Diana, P. G. Coleman, D. L. Brooks, P. K. Pendleton, D. M. Norman, B. E. Seay, and S. C. Sharma, in *Positron (Electron)-Gas Scattering*, edited by W. E. Kauppila, T. S. Stein, and J. M. Wadehra (World Scientific, Singapore, 1986), p. 296.

[23] L. M. Diana, P. G. Coleman, D. L. Brooks, P. K. Pendleton, and D. M. Norman, Phys. Rev. A **34**, 2731 (1986).

[24] L. M. Diana, P. G. Coleman, D. L. Brooks, and R. L. Chaplin, in *Atomic Physics with Positrons*, edited by J. W. Humberston and E. A. G. Armour (Plenum Press, New York, 1987), p. 55.

[25] L. M. Diana, D. L. Brooks, P. G. Coleman, R. L. Chaplin, and J. P. Howell, in *Positron Annihilation*, edited by L. Dorikens-Vanpraet, M. Dorikens, and D. Segers (World Scientific, Singapore, 1989), p. 311.

[26] D. Fromme, G. Kruse, W. Raith, and G. Sinapius, Phys. Rev. Lett. **57**, 3031 (1986).

[27] N. Overton, R. J. Mills, and P. G. Coleman, J. Phys. B: At. Mol. Opt. Phys. **26**, 3951 (1993).

[28] J. Moxom, G. Laricchia, and M. Charlton, J. Phys. B: At. Mol. Opt. Phys. **26**, L367 (1993).

[29] J. Moxom, G. Laricchia, M. Charlton, Á. Kövér, and W. E. Meyerhof, Phys. Rev. A **50**, 3129 (1994).

[30] G. Laricchia, private communication.

[31] G. Laricchia, in *The Physics of Electronic and Atomic Collisions, Proc. of XIX ICPEAC*, AIP Conference Proceedings 360, edited by L. J. Dubé, J. B. A. Mitchell, J. W. McConkey, and C. E. Brion (AIP Press, New York, 1995), p. 385.

[32] M. Charlton, L. H. Andersen, L. Brun-Nielsen, B. I. Deutch, P. Hvelplund, F. M. Jacobsen, H. Knudsen, G. Laricchia, M. R. Poulsen, and J. O. Pedersen, J. Phys. B: At. Mol. Opt. Phys. **21**, L545 (1988).

[33] L. H. Andersen, P. Hvelplund, H. Knudsen, S. P. Møller, A. H. Sørensen, K. Elsener, K.-G. Rensfelt, and E. Uggerhøj, Phys. Rev. A **36**, 3612 (1987).

[34] L. H. Andersen, P. Hvelplund, H. Knudsen, S. P. Møller, J. O. P. Pedersen, S. Tang-Petersen, E. Uggerhøj, K. Elsener, and E. Morenzoni, Phys. Rev. A **40**, 7366 (1989).

[35] J. H. McGuire, N. Berrah, R. J. Bartlett, J. A. R. Samson, J. A. Tanis, C. L. Cocke, and A. S. Schlachter, J. Phys. B: At. Mol. Opt. Phys. **28**, 913 (1995).

[36] J. H. McGuire, Phys. Rev. Lett. **49**, 1153 (1982).

[37] L. Végh and J. Burgdörfer, Phys. Rev. A **42**, 655 (1990).

[38] J. F. Reading, T. Bronk, and A. L. Ford, J. Phys. B: At. Mol. Opt. Phys. **29**, 6075 (1996).

[39] S. Helms, U. Brinkmann, J. Deiwiks, R. Hippler, H. Schneider, D. Segers, and J. Paridaens, J. Phys. B: At. Mol. Opt. Phys. **28**, 1095 (1995).

[40] W. Lotz, Astrophys. J. Suppl. **14**, 207 (1967).

[41] W. Lotz, Z. Phys. **216**, 241 (1968).

[42] T. A. Carlson, W. E. Hunt, and M. O. Krause, Phys. Rev. **151**, 41 (1966).

[43] M. Charlton, L. Brun-Nielsen, B. I. Deutch, P. Hvelplund, F. M. Jacobsen, H. Knudsen, G. Laricchia, and M. R. Poulsen, J. Phys. B: At. Mol. Opt. Phys. **22**, 2779 (1989).

[44] G. Kruse, A. Quermann, W. Raith, G. Sinapius, and M. Weber, J. Phys. B: At. Mol. Opt. Phys. **24**, L33 (1991).

[45] R. Hippler, S. Helms, U. Brinkmann, J. Deiwiks, H. Schneider, and D. Segers, Can. J. Phys. **74**, 373 (1996).

[46] T. S. Stein, W. E. Kauppila, C. K. Kwan, S. P. Parikh, and S. Zhou, Hyperfine Interact. **73**, 53 (1992).

[47] T. Falke, W. Raith, and M. Weber, Phys. Rev. Lett. **75**, 3418 (1995).

[48] T. Falke, T. Brandt, O. Kühl, W. Raith, and M. Weber, J. Phys. B: At. Mol. Opt. Phys. **30**, 3247 (1997).

[49] T. Brandt, T. Falke, and W. Raith, Nucl. Instr. and Meth. B **149**, 201 (1999).

[50] K. F. Canter, P. H. Lippel, W. S. Crane, and A. P. Mills, Jr., in *Positron Studies of Solids, Surfaces, and Atoms*, edited by A. P. Mills, Jr., W. S. Crane, and K. F. Canter (World Scientific, Singapore, 1986), p. 199.

[51] M. B. Shah, D. S. Elliott, P. McCallion, and H. B. Gilbody, J. Phys. B: At. Mol. Opt. Phys. **21**, 2751 (1988).

[52] J. M. Rost, private communication.

[53] J. Paridaens, D. Segers, M. Dorikens, and L. Dorikens-Vanpraet, Nucl. Instr. and Meth. A **287**, 359 (1990).

[54] J. Moxom, J. Xu, G. Laricchia, L. D. Hulett, D. M. Schrader, Y. Kobayashi, B. Somieski, and T. A. Lewis, Nucl. Instr. and Meth. B **143**, 112 (1998).

[55] J. W. Humberston and P. Van Reeth, J. Phys. B: At. Mol. Opt. Phys. **33**, L97 (2000).

[56] J. W. Humberston, private communication.

[57] R. D. DuBois and S. T. Manson, Phys. Rev. A **35**, 2007 (1987).

Chapter 3

Modified Rost-Pattard theory

In chapter 2 we looked at the total double ionisation cross section of the noble gases by positron impact. Comparison with theory was limited as virtually none exists for total double ionisation. However one of the conclusions in chapter 2 was that positronium formation is suppressed in double ionisation of helium and neon, particularly at threshold. Therefore our $\sigma_{\mathrm{tot}}^{2+}$ for helium and neon must be approximately equal to σ_{I}^{2+}. This allows an unique opportunity for comparing our data to theories for *direct* double ionisation. One such theory is the so-called Wannier threshold theory which has recently been extended to double ionisation by positron impact. In this chapter we will start with an introduction to Wannier theory and continue by discussing the semiempirical model for single ionisation by Rost and Pattard. Finally we will present the modified Rost-Pattard model we have developed for double ionisation and compare it to our data.

3.1 Wannier theory

Wannier theory was originally developed to describe the threshold behaviour in single ionisation of atoms and ions by electron impact[1] [1]. It was inspired by the corresponding law for two-particle break-up derived by Wigner [2] and was based on some of the same ideas: In the fragmentation of a system into charged particles, one can separate the process into a 'reaction zone' and a 'Coulomb zone'. In the reaction zone the detailed mechanics of the ionisation

[1] Despite not being discussed in the original paper, the theory can also describe double ionisation by photon impact.

process take place. A complete treatment of this part of the process would require an intricate quantum mechanical calculation. On the other hand in the Coulomb zone the fragments are drifting apart and only interacting through long-range Coulomb forces allowing for a classical treatment of their motion. Following Wigner, Wannier assumed that in near-threshold ionisation the energy dependence of the cross section was determined entirely by the behaviour in the Coulomb zone. The reaction zone however was important for determining the absolute magnitude of the cross section. Even though Wannier ignored the reaction zone, he could still predict the energy dependence of the near-threshold cross section.

In near-threshold ionisation the available phase-space in the Coulomb zone is very limited. This is because the outgoing fragments have to be arranged into special configurations which allow for optimum usage of the scarce excess energy available for escape. For the classic example of single ionisation by electron impact the two electrons have to escape along a straight line, in opposite directions away from the ion, while always keeping equal distances to it. This configuration as well as those of other systems are characterised by being in 'equilibrium'. In the classic case just described, it is the ion that is held at equilibrium midway between the two electrons. The ion has to stay here until both electrons escape (to infinity) for the ionisation to proceed successfully. In terms of the potential one often talks about a Wannier 'saddle' or 'ridge' upon which the system is in a unstable equilibrium. How the systems get arranged into these equilibrium configurations is not of concern to Wannier theory as this takes place within the reaction zone. Wannier theory only predicts that they are necessary for the complete fragmentation (direct ionisation) to occur. For the configuration above Wannier found through classical calculations of the break-up the famous power-law $\sigma_{\mathrm{I}}^{+} \propto E^{1.127}$, where E is excess energy above the ionisation potential E_{I}^{+}. The exponent in the power-law is usually referred to as the Wannier exponent or index. The result has later been confirmed quantum mechanically [3,4].

In more recent papers concerning Wannier theory (see e.g. Poelstra *et al.* [5]) it has been realised that the mechanisms that govern the threshold power-law are the instabilities of the equilibrium configurations. These instabilities describe ways in which two or more fragments can end up in a bound state and thereby lead to a *failure* of complete fragmentation. By the simple laws of probability in quantum mechanics the chance of *success* is therefore also determined by the same instabilities. In a second order expansion of the system potential, the instabilities are described as inverted oscillators. The 'eigenfrequencies' of these oscillators determine the Wannier exponent through formulae derived quantum mechanically. Calculating Wannier exponents for various systems therefore comes down to identifying the equilibrium configurations and then determining eigenvalues for small deviations from these.

Approaches to finding the Wannier exponent of various systems are numerous. One of the most recent, and probably more elegant, has been published by Kuchiev and Ostrovsky [6]. Using what they call 'scaling configurations', they capture the essence of equilibrium configurations and the deviations from these in a very general way. After formulating the eigenvalue problem it is only a question of a numerical calculation to solve it. Of the eigenvalues some are identified as belonging to the overall translation, rotation and expansion of the system. Of the remaining values, those which are negative describe unstable modes. Another approach is that of Feagin *et al.* [5,7–9]. Using Jacobi coordinates to describe specific systems, they arrive at the eigenvalue problem through a number of rather tedious transformations. During these translation, rotation, overall expansion and sometimes also stable modes are removed 'by hand' leaving behind a reduced eigenvalue problem for the small deviations from equilibrium. However it is important to realise that no matter which approach is used, the resulting eigenvalues should be the same. We will return to discuss this later.

Generalisation of Wannier theory to systems with three escaping electrons was first done by Klar and Schlecht [10]. The generalisation to systems with even more electrons is obvious as seen from the discussion in the previous paragraph. The same goes for systems with other particles than electrons and an ion. Klar was the first to introduce positrons [11]. Looking at direct ionisation of atomic hydrogen by positron impact (or equivalently direct ionisation of positronium by proton impact) he found the threshold law to be $\sigma_{\mathrm{I}}^{+} \propto E^{2.651}$. In more general systems than those containing only electrons and one ion, the center of mass and center of charge do not necessarily coincide. The effect of this is that the equilibrium configurations do not necessarily have the high degree of symmetry as observed for systems with only electrons and one ion. Also for some systems more than one equilibrium configuration is possible. In these cases it is the configuration with the lowest Wannier exponent that determines the threshold power-law.

The first result for direct double ionisation by positron impact was calculated by Poelstra *et al.* [5]. Looking at double ionisation of H^{-} they found a Wannier exponent of 3.124 for this process. Upon request from us, Mendez and Feagin extended this result to Z = 2 i.e. double ionisation of a noble gas.[2] They found that $\sigma_{\mathrm{I}}^{2+} \propto E^{3.613}$ at threshold [12]. E is still excess energy above the relevant threshold energy i.e. E_{I}^{2+}. Partially motivated by our work as well, Kuchiev and Ostrovsky also looked at the process in their paper, finding a value of 3.838 [6]. An explanation for the disagreement can not be given as Mendez and Feagin have not published the details of their calculation. However Kuchiev and Ostrovsky also looked at double ionisation of H^{-} for which comparison

[2]The mass of the target atom is taken to be infinite. The result should be valid within a good approximation for all the noble gases.

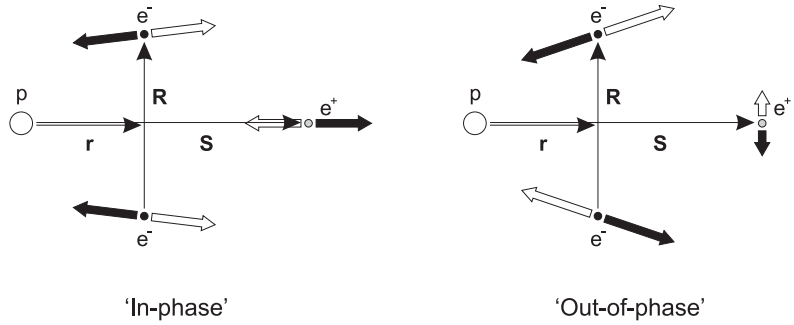

Figure 3.1: Unstable normal modes in the plane break-up configuration of e^+ on H^-. Thin arrows are the Jacobi coordinates **r**, **R** and **S** used by Poelstra *et al.* [5]. Thick arrows indicate the direction of oscillation (eigenvectors) in the two unstable modes of the system.

can be made with the results by Poelstra *et al.* Both groups find initially the same equilibrium configurations: Two linear and one plane. For the linear configurations they agree on the eigenvalues and therefore also on the partial Wannier exponents these give rise to. However in calculating the final exponent Kuchiev and Ostrovsky just add the partial exponents while Poelstra *et al.* multiply the sum by a phase-space factor. In this system this factor is equal to 2. Kuchiev and Ostrovsky dismiss this factor, which has partially been supported by a more recent paper (and erratum) by Pattard and Rost [13,14].

Regarding the plane configuration the two groups agree that it is this one that gives the lowest exponent and thereby the leading threshold law. In this configuration the electrons escape in opposite directions along a line which is at 90° with the line connecting the proton and positron in a cross-like way as indicated in figure 3.1. Apart from the phase-space factor discussed above, a second disagreement arises in this case. Kuchiev and Ostrovsky find two unstable modes while Poelstra *et al.* only find one of these. Kuchiev and Ostrovsky state that the reason for this disagreement remains unclear. However one can see either through an intuitive argument or a simple calculation, that it is the result of Poelstra *et al.* that is in error. In the intuitive picture one can imagine the proton and positron to be fixed in space. The instabilities of the electrons are that they can fall towards either of the positive particles. However this can happen in two ways: Either they fall toward the same particle or instead one falls toward the proton while the other falls toward the positron. In terms of oscillations, these two ways represent two unstable normal modes. These could be denoted as 'in-phase' and 'out-of-phase' respectively.

The intuitive argument can be confirmed by a calculation. Following the approach of Kuchiev and Ostrovsky, one can extend the calculation to not just finding the eigenvalues but also the eigenvectors. The results for the two unstable modes are illustrated in figure 3.1. One observes that the calculation introduces oscillation for the positron as well, which was fixed in the previous argument. This does not change the fact that there are two unstable modes behaving as discussed in the previous paragraph.

In figure 3.1 are also shown the Jacobi coordinates used by Poelstra *et al.* to describe the system. The mistake they commit during their calculation is to fix $\mathbf{r}$ along $\mathbf{S}$ and also at the same time keep the angle between $\mathbf{R}$ and $\mathbf{S}$ fixed at 90°. By doing so they 'freeze out' the out-of-phase motion. Only through changes in the length of $\mathbf{r}$ can the electrons move toward either the proton or the positron. However they are confined to move toward the *same* particle. This is confirmed by the fact that the single eigenvalue which Poelstra *et al.* find, corresponds to the in-phase mode. If Poelstra *et al.* had not made this mistake, their final Wannier exponent would have been equal to twice the value found by Kuchiev and Ostrovsky due to the phase-space factor.

Returning to double ionisation of the noble gases by positron impact, one could fear that the exponent by Mendez and Feagin suffers from problems similar to those seen in H^-. In this case it is also the plane configuration that gives the dominant power-law. Yet it is also clear that the problem is not exactly the same. The result by Mendez and Feagin is *not* equal to twice the value of any of the partial exponents found by Kuchiev and Ostrovsky, so something else is going on as well. From an experimental point of view there is not much difference between the two results as they are numerically nearly equal. However as can be seen from our discussion, more trust should be put in the exponent of Kuchiev and Ostrovsky. Finally it should be mentioned that a third value of 3.764 has been published by Pattard and Rost [15]. However, this value should have been in agreement with the one by Kuchiev and Ostrovsky according to one of the authors, who believe that the deviation comes down to numerical inaccuracy on their part [16].

Wannier theory has over the years been tested by a multitude of experiments using either electron or photon impact ionisation (see e.q. [17–21]). In general good agreement is found between the experimentally determined exponents and theory. However views are divided when it comes to the range of validity i.e. how high above threshold the power-law should be valid. Theory does not provide any definite answer to this, but estimates are a few eV. The direct experimental tests indicate in general ranges from below 1 eV and up to ∼5 eV with a few claiming ranges as high as ∼50 eV [22]. Only one test using positrons exists [23]. This has indicated that the range of validity for positron impact could be smaller than for electrons (< 1 eV). Finally one should, as always, remember that other threshold theories exist. Of these the Coulomb-dipole model by

Temkin [24] is the one most often mentioned. This model predicts a cross section which exhibits oscillatory structure at threshold. For a recent review of threshold theories in general, see Sadeghpour *et al.* [25].

3.2 Rost-Pattard theory

The Wannier theory only provides a parameterisation of direct ionisation cross sections in the near-threshold region. Attempts to describe cross sections over a larger energy range by semiempirical formulae are numerous. One example is the Lotz formula mentioned in section 2.3.2. It is characteristic for these parameterisations that they mostly focus on the behaviour at high energies and around the cross section maximum. The behaviour at threshold is rarely accounted for in any detailed way. One formula that does so for single ionisation has been published by Rost and Pattard [26]. The idea behind their model is to merge the threshold behaviour of Wannier theory with the high-energy behaviour of the first Born approximation in such a way that it also provides a good description of the cross section at intermediate energies.

As mentioned at the end of section 3.1, the range of validity is very limited for Wannier theory. At first it may therefore seem an odd choice of threshold theory to incorporate. Here one has to remember that the range of validity is the range within which the cross section follows the power-law *closely*. However this does not mean that the slow onset at threshold dictated by the power-law can not influence the behaviour of the cross section up to much higher energies. For the high-energy behaviour, Rost and Pattard choose to use the classical version of the first Born result, i.e. $\sigma^+ \propto E^{-1}$, which does not contain the logarithmic term (see (2.8)). As they argue, this term only becomes important at keV energies (for electron/positron impact) and can therefore be ignored for this purpose. Rost and Pattard base their parameterisation on the function

$$\begin{aligned} f(E) &= \frac{1}{E+E_0} \cdot \left(\frac{E}{E+E_0} \right)^{\alpha} \\ &\rightarrow \begin{cases} E^{\alpha} & \text{for } E \rightarrow 0_+ \\ E^{-1} & \text{for } E \rightarrow \infty \end{cases} , \end{aligned} \tag{3.1}$$

where $E_0 = E_{\mathrm{M}}/\alpha$. One identifies α to be the Wannier exponent in order for $f(E)$ to have the right threshold behaviour. The behaviour at high energies is also seen to be as desired. The energy E_{M} is a free parameter. However it is easily shown that $f(E)$ has its maximum at $E = E_{\mathrm{M}}$ and that E_{M} should therefore be chosen to be equal to the energy at the cross section maximum. Both E and E_{M} are excess energies above E_{I}^+. The cross section is given by

$$\sigma^+(E) = \sigma_{\mathrm{M}} \cdot \frac{f(E)}{f(E_{\mathrm{M}})} , \tag{3.2}$$

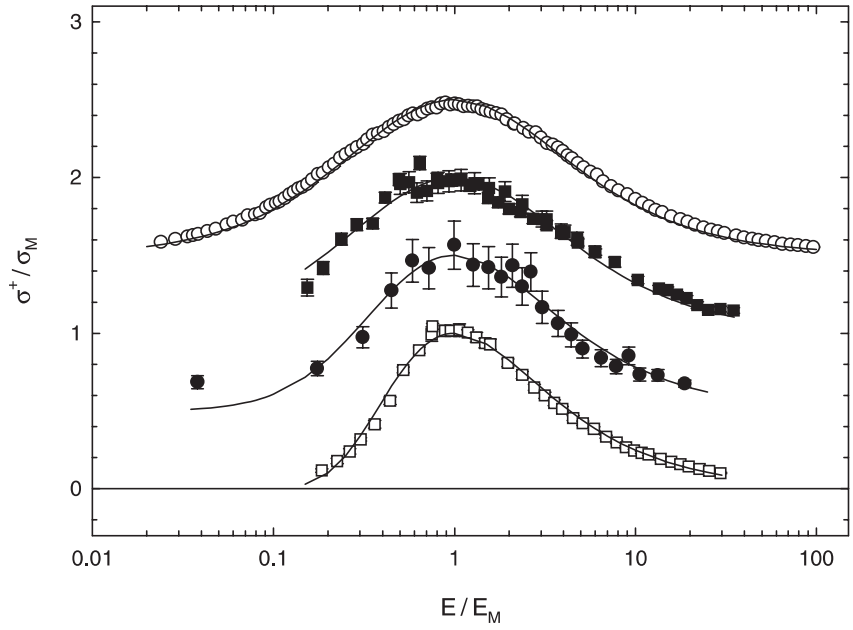

Figure 3.2: Direct single ionisation cross sections for hydrogen (helium) plotted in the scaled coordinates $x = E/E_{\mathrm{M}}$ and $y = \sigma^+/\sigma_{\mathrm{M}}$. (□) y for proton impact [27,28], (●) $y+0.5$ for positron impact [29], (■) $y+1$ for antiproton impact on helium [30,31], (○) $y+1.5$ for electron impact [32], (——) Rost-Pattard parameterisation (3.3) for the various projectiles. These curves only depend on the Wannier exponent of the respective systems.

where $\sigma_{\mathrm{M}} = \sigma^+(E_{\mathrm{M}})$ is the value of the cross section at its maximum. For a specific cross section the two parameters E_{M} and σ_{M} are found through a fit to experimental data. Apart from these two parameters, the cross section in (3.2) *only* depends on the Wannier exponent. To emphasise this, one can transform the cross section into the reduced coordinates $x = E/E_{\mathrm{M}}$ and $y = \sigma^+/\sigma_{\mathrm{M}}$. In these coordinates (3.2) reduces to

$$y(x) = \frac{\alpha+1}{\alpha\cdot x+1}\cdot\left(\frac{\alpha+1}{\alpha\cdot x+1}\cdot x\right)^{\alpha}\,, \tag{3.3}$$

which clearly only depends on the Wannier exponent. Viewed this way the Rost-Pattard model has therefore *no free* parameters. Figure 3.2 shows how well the model compares to experimental data for impact ionisation by a wide range of different projectiles. This figure is nearly identical to the figure presented by Rost and Pattard in their paper. The Wannier exponents used to plot the Rost-

Pattard curves are those found by Rost and Pattard i.e. 1.127, 2.650, 1.199 and 69.74 for e^-, e^+, $\bar{p}$ and p impact respectively. The value of α for antiproton impact is not entirely correct to use in figure 3.2 as it is the value for antiproton impact on hydrogen and not helium. However, as can be seen in the paper by Rost and Pattard, this is less than $\sim$4% from the correct value.

One remarkable feature of the Rost-Pattard model is that for light projectiles (electrons or positrons) the scaling into coordinates x and y makes the parameterisation *independent* of the specific target as α is virtually the same for all targets. The cross sections σ_I^+ of different targets under for example electron impact, should therefore transform onto one common curve. This is what Rost and Pattard observe. However this observation is of a more general kind as it does not depend on the specific parameterisation. It shows that the natural scale of energy for σ_I^+ should be relative to E_M rather than to E_I^+ which is the scale most widely used in parameterisations. The same statement is not necessarily true for heavy projectiles like protons and ions. At least according to the Rost-Pattard model there could still be some target dependence in (3.3) through the Wannier exponent α. This is because when calculating α one can not assume the target mass to be infinite relative to the projectile mass as is the case for electron and positron impact. The Wannier exponent has therefore some target dependence for these heavy projectiles. However the Wannier exponents for proton and ion impact are generally large (e.g. 69.74 for p on H). One can show that

$$y(x) \to \frac{1}{x} \cdot \exp\left(1 - \frac{1}{x}\right) \quad \text{for} \quad \alpha \to \infty \,. \tag{3.4}$$

This means that provided that α is sufficiently large for all targets, $y(x)$ is independent of its value, making the observation on the scaling true for proton and ion impact as well. For antiprotons the dynamics of the break-up configuration are such that α is nearly the same for all targets anyway ($\sim$1.2). The observation on the scaling should therefore be true for antiproton impact ionisation cross sections as well.

The Rost-Pattard model of course also has its limitations. Its description of direct single ionisation cross sections can not be applied to all types of targets and projectiles. The parameterisation describes a smoothly varying cross section. Cross sections exhibiting any kind of structure will therefore not be described well by the model. Rost and Pattard themselves characterise the model as applicable to cross sections which are dominated by ionisation of target electrons with the same ionisation potential. This will ensure a unique determination of the excess energy. In 'standard' ionisation experiments, like ours, this would mean cross sections dominated by outer shell ionisation.

Finally it has to be discussed whether or not the Rost-Pattard model has any implications for our understanding of the cross sections it describes. The parameterisation in itself gives no real further insight into ionisation mechanisms

as it has not been 'derived' in any stringent way such as through quantum mechanics. However the fact that so many cross sections can be fitted to the same simple formula seems to be a sign of some common underlying mechanisms. It is the opinion of Rost [16] that the model should apply to σ_{I}^{+} of any 'simple' target which behaves in accordance with the discussion above. If an uncharacterised cross section fits the model, this serves as an *indication* that the cross section is dominated by direct ionisation. However if a cross section does *not* fit the model it should be a clear sign that the cross section contains other channels than that of outer shell direct ionisation. These points will be important for the discussion of our modified Rost-Pattard model in the next section.

3.3 MRP theory and discussion

As mentioned already in the beginning of this chapter, it was our hope to be able to make a comparison between our data and Wannier theory. However as discussed at the end of section 3.1, the energy range over which such a comparison could be made, would probably be very limited. Inspired by the success of the Rost-Pattard model we set out to develop a *modified* Rost-Pattard (MRP) theory, that could describe our data over a wider energy range.

The Rost-Pattard model contains two aspects: A scaling law and a parameterisation. Our model contains the same two aspects. The scaling law is basically the same with $x = E/E_{\mathrm{M}}$ and $y = \sigma^{2+}/\sigma_{\mathrm{M}}^{2+}$, except that E and E_{M} now are both excess energies above E_{I}^{2+}. Just like in the Rost-Pattard model the scaling is crucial. If we want to have any hopes of describing our data by a simple target independent formula like (3.3) the cross sections *have* to scale onto a common curve. As can be seen in figure 3.3 this is actually the case with our data for $\sigma_{\mathrm{tot}}^{2+}$ for helium and neon. The two sets of data are observed to agree extremely well when scaled into the coordinates x and y. With respect to the parameterisation further modifications are needed. As discussed in section 2.1.2 the energy dependence in the range corresponding to our high-energy data is not expected to follow the first Born approximation due to the interplay between the different double ionisation mechanisms. We therefore replace the E^{-1} high-energy behaviour of the Rost-Pattard model with a more general $E^{-\beta}$ behaviour. The specific choice of the constant β will be discussed in a moment. As a result we base our parameterisation on the function

$$\begin{aligned} f(E) &= \frac{1}{(E+E_0)^{\beta}} \cdot \left(\frac{E}{E+E_0}\right)^{\alpha} \\ &\rightarrow \begin{cases} E^{\alpha} & \text{for } E \rightarrow 0_{+} \\ E^{-\beta} & \text{for } E \rightarrow \infty \end{cases}, \end{aligned} \tag{3.5}$$

where $E_0 = E_{\mathrm{M}} \cdot \beta/\alpha$ in order for E_{M} to retain the meaning of being the energy at the cross section maximum. α should now be the Wannier exponent for

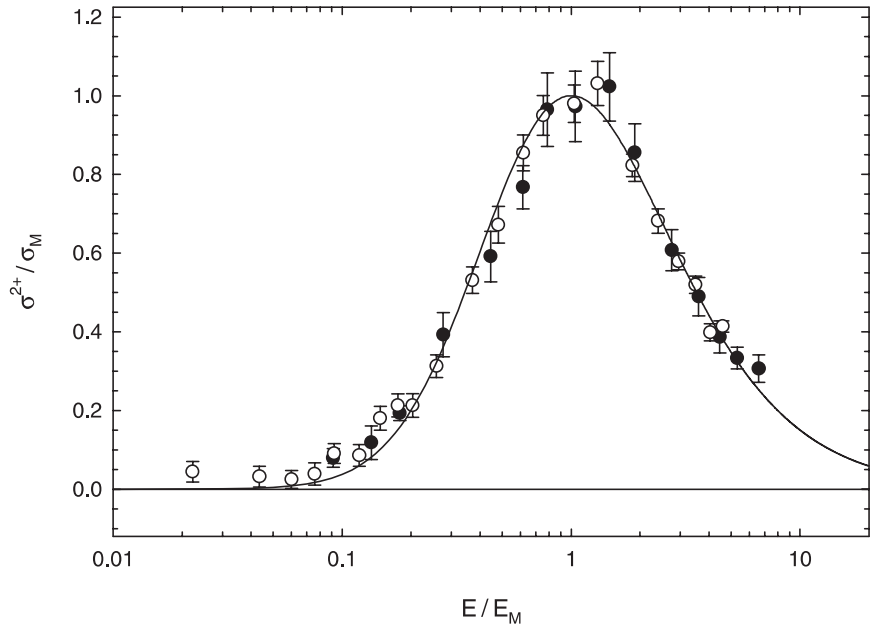

Figure 3.3: Double ionisation cross sections for helium and neon plotted in the scaled coordinates $x = E/E_{\mathrm{M}}$ and $y = \sigma^{2+}/\sigma_{\mathrm{M}}$. (●) present results for helium, (○) present results for neon, (——) modified Rost-Pattard parameterisation (3.7) for positron impact with $\alpha = 3.838$ and $\beta = 1.5$.

double ionisation. The cross section is as before given by

$$\sigma^{2+}(E) = \sigma_{\mathrm{M}} \cdot \frac{f(E)}{f(E_{\mathrm{M}})} \,, \tag{3.6}$$

where $\sigma_{\mathrm{M}} = \sigma^{2+}(E_{\mathrm{M}})$ again is the value of the cross section at its maximum. When expressed in the scaled coordinates x and y (3.6) reduces to

$$y(x) = \left(\frac{\alpha+\beta}{\alpha\cdot x+\beta}\right)^{\beta} \cdot \left(\frac{\alpha+\beta}{\alpha\cdot x+\beta}\cdot x\right)^{\alpha} \,, \tag{3.7}$$

which is independent of any specific target as long as α and β are constants. One also sees that (3.7) reduces to the Rost-Pattard parameterisation (3.3) when $\beta = 1$, as expected.

In our model we use the Wannier exponent value of $\alpha = 3.838$ found by Kuchiev and Ostrovsky [6] because we, as discussed in section 3.1, consider this most reliable. The value of β is determined by the different high-energy

double ionisation mechanisms. Returning briefly to section 2.1.2, we find that (ignoring logarithmic terms) the cross section due to SO or TS1 alone would behave in a manner corresponding to $\beta = 1$ while that of TS2 would have a $\beta = 2$ high-energy behaviour. In order to account for the interference between these mechanisms, we therefore chose an intermediate value of $\beta = 1.5$ for our model.

The parameterisation (3.7) is compared in figure 3.3 to the present results for double ionisation of helium and neon. One observes a very good agreement between the data and the curve. As discussed at the end of section 3.2, this may indicate that both cross sections are predominantly due to direct ionisation in accordance with the conclusions of chapter 2. To test the MRP model further we also compare it to the present results for argon and krypton. In chapter 2 we found a contribution from double ionisation with positronium formation to $\sigma_{\mathrm{tot}}^{2+}$ for these two gases. One would therefore expect some sort of deviation for these data from the MRP model as this should only describe direct ionisation. The scaled cross sections for argon and krypton are plotted in figure 3.4, which is similar to figure 3.3. One observes that there is a clear deviation between the data and the curve. At low x (< 1) the points seem to lie above the curve. This could be due to the Ps formation at near-threshold energies. Secondly one sees that at high values of x (> 1) the data and the curve exhibit different energy dependencies, indicating that maybe $\beta = 1.5$ is not the ideal choice for these data. As a result of this bad fit, the maxima of the cross sections are shifted to values of x and y slightly less than 1. One could therefore say that there is an observable influence from the positronium channel.

The conclusions above should however be taken with reservation. One has to remember that the MRP model contains the parameter β, the value of which is chosen more or less 'arbitrarily'. Another value of β could possibly change the outcome. To test this, one can perform fits in which not just E_{M} and σ_{M}, but also β are fitted. For helium and neon this yields a value $\beta = 1.32 \pm 0.06$. This is not much below the 1.5 we had chosen. Also one does not gain any real improvement in the overall fit of the curve compared to that with $\beta = 1.5$. For argon and krypton one finds $\beta = 1.11 \pm 0.05$. This value is in clear disagreement with the one we found for helium and neon confirming that the high-energy behaviours are different. The value for argon and krypton is actually more in agreement with the $\beta = 1$ for the original Rost-Pattard model. This new fit gives much better agreement between the curve and data at high energies and also around the maximum, but the deviations at low x persists. So there is still an observable influence from positronium formation. Finally one can fit the MRP model to our data by varying all of parameters of the model, including α. This yields $\alpha = 2.43 \pm 0.24$ and $\beta = 1.70 \pm 0.15$ for helium and neon, and $\alpha = 2.16 \pm 0.38$ and $\beta = 1.23 \pm 0.09$ for argon and krypton. In both cases the lower value of α gives a slightly better fit at low x. One sees that the

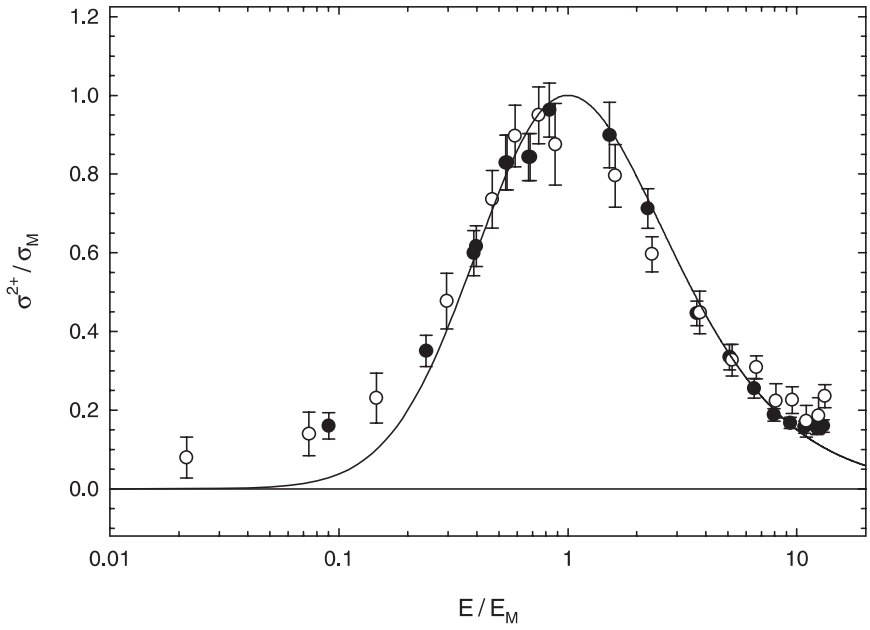

Figure 3.4: Double ionisation cross sections for argon and krypton plotted in the scaled coordinates $x = E/E_M$ and $y = \sigma^{2+}/\sigma_M$. (●) present results for argon, (○) present results for krypton, (——) modified Rost-Pattard parameterisation (3.7) for positron impact with $\alpha = 3.838$ and $\beta = 1.5$.

value of β becomes larger than before. This is because the 'width' of the cross sections is determined by both α and β. The lower value of α is compensated by a higher value of β. For helium and neon this nearly keeps the shape of the parameterisation fixed as compared to before. However for argon and krypton the new β is still consistent (within the combined uncertainty) with the 1.11 found before. This means that the curve is broader now as compared to before due to the much lower α. One should be careful about drawing too many conclusions from these kinds of fits. By fitting the Wannier exponent α one loses the connection there is between MRP theory and 'real' threshold theory, thereby reducing the parameterisation to a purely empirical fitting formula. However it is certain that the cross sections of argon and krypton exhibit a broader shape than that of helium and neon. In conjunction with our findings in chapter 2 this is most likely due to the suppression of positronium formation in the two light gases.

Finally it should be remarked that the present results for double ionisation of xenon can not be compared to the MRP model due to the bump observed in

$\sigma_{\mathrm{tot}}^{2+}$ at high energies (see figure 2.15 and the discussion in section 2.3.2). This structure could never be satisfactorily accounted for in a comparison with the parameterisation (3.7). This is also in accordance with the expectation of Rost and Pattard for the original model, as discussed in section 3.2.

Ways to further test the modified Rost-Pattard theory presented here, would be to compare it to double ionisation cross sections for something else than positron impact. Electron impact data would probably provide the most critical tests, as high quality data exist from high energies and down to threshold. However as the interference between SO, TS1 and TS2 influence electron cross sections conversely to positron cross sections, it is not certain that electron results are directly transferable to the positron case. Another option is comparison with proton data. This could shed some light on how well one can discern capture channels from direct ionisation using a comparison to the Rost-Pattard theory. These kinds of comparisons are however beyond the scope of this thesis, but it should be noted that Pattard and Rost [15] have already published similar considerations using a slightly different parameterisation. The same two authors have also successfully applied their original theory to double ionisation of negative ions by electron impact [33].

References

[1] G. H. Wannier, Phys. Rev. **90**, 817 (1953).

[2] E. P. Wigner, Phys. Rev. **73**, 1002 (1948).

[3] R. Peterkop, J. Phys. B: At. Mol. Phys. **4**, 513 (1971).

[4] A. R. P. Rau, Phys. Rev. A **4**, 207 (1971).

[5] K. A. Poelstra, J. M. Feagin, and H. Klar, J. Phys. B: At. Mol. Opt. Phys. **27**, 781 (1994).

[6] M. Yu. Kuchiev and V. N. Ostrovsky, Phys. Rev. A **58**, 321 (1998).

[7] J. M. Feagin, J. Phys. B: At. Mol. Phys. **17**, 2433 (1984).

[8] J. M. Feagin and R. D. Filipczyk, Phys. Rev. Lett. **64**, 384 (1990).

[9] J. M. Feagin and M. J. Goddard, J. Phys. B: At. Mol. Opt. Phys. **30**, 693 (1997).

[10] H. Klar and W. Schlecht, J. Phys. B: At. Mol. Phys. **9**, 1699 (1976).

[11] H. Klar, J. Phys. B: At. Mol. Phys. **14**, 4165 (1981).

[12] J. C. Mendez and J. M. Feagin, private communication.

[13] T. Pattard and J. M. Rost, Phys. Rev. Lett. **80**, 5081 (1998).

[14] T. Pattard and J. M. Rost, Phys. Rev. Lett. **81**, 2618 (1998).

[15] T. Pattard and J. M. Rost, Phys. Scrip. **T80**, 295 (1999).

[16] J. M. Rost, private communication.

[17] S. Cvejanović and F. H. Read, J. Phys. B: At. Mol. Phys. **7**, 1841 (1974).

[18] F. Pichou, A. Huetz, G. Joyez, and M. Landau, J. Phys. B: At. Mol. Phys. **11**, 3683 (1978).

[19] H. Kossmann, V. Schmidt, and T. Andersen, Phys. Rev. Lett. **60**, 1266 (1988).

[20] J. A. R. Samson and G. C. Angel, Phys. Rev. Lett. **61**, 1584 (1988).

[21] R. Wehlitz, M.-T. Huang, I. A. Sellin, and Y. Azuma, J. Phys. B: At. Mol. Opt. Phys. **32**, L635 (1999).

[22] M. Kamm, W. Weber, and W. Mehlhorn, J. Phys. B: At. Mol. Opt. Phys. **27**, 2585 (1994).

[23] P. Ashley, J. Moxom, and G. Laricchia, Phys. Rev. Lett. **77**, 1250 (1996).

[24] A. Temkin, Phys. Rev. Lett. **49**, 365 (1982).

[25] H. R. Sadeghpour, J. L. Bohn, M. J. Cavagnero, B. D. Esry, I. I. Fabrikant, J. H. Macek, and A. R. P. Rau, J. Phys. B: At. Mol. Opt. Phys. **33**, R93 (2000).

[26] J. M. Rost and T. Pattard, Phys. Rev. A **55**, R5 (1997).

[27] M. B. Shah and H. B. Gilbody, J. Phys. B: At. Mol. Phys. **14**, 2361 (1981).

[28] M. B. Shah, D. S. Elliott, and H. B. Gilbody, J. Phys. B: At. Mol. Phys. **20**, 2481 (1987).

[29] G. O. Jones, M. Charlton, J. Slevin, G. Laricchia, Á. Kövér, M. R. Poulsen, and S. Nic Chormaic, J. Phys. B: At. Mol. Opt. Phys. **26**, L483 (1993).

[30] L. H. Andersen, P. Hvelplund, H. Knudsen, S. P. Møller, J. O. P. Pedersen, S. Tang-Petersen, E. Uggerhøj, K. Elsener, and E. Morenzoni, Phys. Rev. A **41**, 6536 (1990).

[31] P. Hvelplund, H. Knudsen, U. Mikkelsen, E. Morenzoni, S. P. Møller, E. Uggerhøj, and T. Worm, J. Phys. B: At. Mol. Opt. Phys. **27**, 925 (1994).

[32] M. B. Shah, D. S. Elliott, and H. B. Gilbody, J. Phys. B: At. Mol. Phys. **20**, 3501 (1987).

[33] J. M. Rost and T. Pattard, J. Phys. B: At. Mol. Opt. Phys. **32**, L457 (1999).

Chapter 4

Ionisation of atomic deuterium

4.1 Introduction

Ionisation of atomic hydrogen by charged particle impact is considered to be among one of the most fundamental atomic collision processes. Being the archetype of the Coulomb three-body problem, the process has great theoretical interest. Particularly since the wave function of hydrogen is known exactly, it has also been favoured as a test-bench for atomic scattering theories. From an experimental point of view, atomic hydrogen has always been one of the more elusive targets, mainly due to problems with producing sufficiently high (pure) target densities. This problem has been resolved with the invention of reliable RF discharge sources (Slevin source) [1]. However for positron impact ionisation the problem was twofold as the intensities available from the earliest positron beam lines made ionisation experiments on hydrogen practically impossible. Therefore up until 1990, no data had been published on positron-hydrogen collisions.

Ionisation of hydrogen by positron impact can either take place through direct ionisation or ionisation with positronium formation i.e. the processes

$$\mathrm{e}^+ + \mathrm{H} \rightarrow \mathrm{H}^+ + \mathrm{e}^- + \mathrm{e}^+, \tag{4.1}$$

$$\mathrm{e}^+ + \mathrm{H} \rightarrow \mathrm{H}^+ + \mathrm{Ps}. \tag{4.2}$$

Following the notation from chapter 2 the partial ionisation cross sections corresponding to these two processes are denoted σ_{I}^+ and σ_{Ps}^+ respectively and similarly the threshold energies $E_{\mathrm{I}}^+ = 13.6$ eV and $E_{\mathrm{Ps}}^+ = 6.8$ eV. The total ionisation cross section σ_{tot}^+ is equal to the sum of σ_{I}^+ and σ_{Ps}^+, counting ion contributions irrespectively of the fate of the positron in either (4.1) or (4.2).

The first measurement of σ_I^+ for atomic hydrogen by positron impact was performed in 1990 at Bielefeld by Spicher *et al.* [2] using an electrostatic crossed beams technique. Discrimination against (4.2) was attained through coincidence detection of the ions with positrons scattered in the forward direction into a $\pm 30^\circ$ cone. Time-of-flight was used to separate H^+ ions from H_2^+ ions, the latter stemming from ionisation of H_2 present in the target due to incomplete dissociation in the RF source. Dissociative ionisation of H_2 was found to contribute negligibly to the H^+ count rate. Calibration and normalisation were attained through measurements for electron impact, which were compared to cross sections from the literature. To correct for the incomplete collection of the scattered positrons Spicher *et al.* used a calculation based on the first Born approximation.

The cross section obtained by Spicher *et al.* agreed in shape but not in absolute magnitude with the theoretical predictions at the time. However after the publication of their data, a more recent calculation by Acacia *et al.* [3,4] showed better overall agreement with the data. This was however questioned by Jones *et al.* [5], who at UCL also measured σ_I^+ for atomic hydrogen. Their experiment was performed using a magnetic positron beam line, which should give nearly complete collection of the scattered positrons. Their results were lower by 30–80% as compared to those of Spicher *et al.* and were in better agreement with previous theoretical results. The σ_I^+ by Jones *et al.* also showed a better merger with electron data at high energies, as expected from the first Born approximation (see section 2.1.1).

Around the same time, the Bielefeld experiment was moved to the high-intensity positron beam at Brookhaven National Laboratory. Supplementing the old data with new measurements and doing a more careful data analysis, Weber *et al.* [6] recalculated the σ_I^+ by Spicher *et al.* However for normalisation Weber *et al.* still had to rely somewhat on the old Bielefeld results. The outcome of the recalculation yielded a better agreement in shape with the σ_I^+ by Jones *et al.* but still an overall difference of $\sim$30% in absolute magnitude.

Further support was however gained for the data by Jones *et al.* First of all Stein *et al.* [7] pointed out that the σ_I^+ by Spicher *et al.* (and thereby also the σ_I^+ by Weber *et al.*) was in disagreement with data for the total *scattering* cross section for atomic hydrogen by positron impact measured by Zhou *et al.* [8]. The σ_I^+ by Jones *et al.* showed better agreement. Secondly Knudsen *et al.* [9] measured σ_I^+ for atomic hydrogen by antiproton impact. When plotted on a velocity scale these (and proton) data showed a better merger at high impact velocities with the data by Jones *et al.*, in accordance with the discussion in section 2.1.1.

Finally Hofmann *et al.* [10] repeated the Bielefeld-Brookhaven experiment using an improved version of the apparatus. Instead of using the first Born approximation, a calculation by Acacia and Stauffer [10] was used to correct for

the incomplete collection of scattered positrons. Their results for σ_{I}^{+} were now in full agreement with those by Jones *et al.* The previous disagreement were attributed to the electron data obtained by Spicher *et al.* for normalisation. Apparently the electron beam used did not possess the same characteristics (phase-space) as the positron beam. The disagreement surrounding σ_{I}^{+} therefore seemed resolved.

Concurrent with the measurements of σ_{I}^{+}, experiments to determine σ_{Ps}^{+} for atomic hydrogen were performed. The first results for σ_{Ps}^{+} were published in 1992 by the Bielefeld-Brookhaven group in a paper by Sperber *et al.* [11]. In this experiment σ_{Ps}^{+} was essentially found as the difference between σ_{I}^{+} and $\sigma_{\mathrm{tot}}^{+}$. The results were in reasonable agreement with theory at the time. However using the same equipment as Spicher *et al.* [2] these data also had to be corrected for incomplete positron collection. Secondly Sperber *et al.* used the results by Spicher *et al.* for absolute normalisation. The determination of σ_{Ps}^{+} was thereby closely linked to that of σ_{I}^{+} and therefore affected somewhat by the changes in σ_{I}^{+} discussed above.

The recalculation by Weber *et al.* [6] yielded together with a better determination of a detector efficiency from supplementing data a $\sim$30% reduction in absolute magnitude of σ_{Ps}^{+}. As theory at the time exhibited a fairly wide spread in absolute magnitudes, agreement with calculations remained reasonably good. More recent theories showed even better agreement. The reduction of σ_{Ps}^{+} was also in agreement with the conclusions of Stein *et al.* [7], who showed that the original data by Sperber *et al.* would cause disagreement with the total scattering cross section measured by Zhou *et al.* [8] by being too large. Hofmann *et al.* [10] also remeasured σ_{Ps}^{+} in their experiment. They found the ratio $\sigma_{\mathrm{Ps}}^{+}/\sigma_{\mathrm{I}}^{+}$ to be the same as that found by Weber *et al.* However with the 30% reduction in absolute magnitude of σ_{I}^{+}, σ_{Ps}^{+} was further reduced, breaking the good agreement observed between theory and the results by Weber *et al.*

Finally Zhou *et al.* [12] measured σ_{Ps}^{+} directly. Their experiment did not use crossed beams like the previous studies, but a specially built gas cell. By observing 511 keV annihilation radiation emanating from the gas cell, they measured a lower limit of σ_{Ps}^{+}. Normally the group would also have measured an upper limit of the cross section. This could be done by measuring the amount of unscattered as well as scattered positrons transmitted through the gas cell. Any attenuation in this number would be due to positrons lost due to positronium formation in (4.2) or positrons scattered in the backward direction in the gas cell. This way an upper limit of σ_{Ps}^{+} could be determined. However this was not done due to too large uncertainties arising in the measurements. Instead Zhou *et al.* provided what they believed to be the best estimate of the 'true' σ_{Ps}^{+}. Both this and the lower limit were higher than the σ_{Ps}^{+} found by Hofmann *et al.* The results showed instead good agreement with the σ_{Ps}^{+} by Weber *et al.* and the most recent theory.

In conclusion a disagreement therefore persists, in that the σ_{I}^{+} and σ_{Ps}^{+} (or $\sigma_{\mathrm{tot}}^{+}$) by the Bielefeld-Brookhaven group one way or the other are in disagreement with other measurements and the most recent theory. The results by Zhou *et al.* indicate that the problem lies with σ_{Ps}^{+}. To resolve this, new measurements of σ_{I}^{+} and σ_{Ps}^{+} (or $\sigma_{\mathrm{tot}}^{+}$) for atomic hydrogen should be performed. This should preferably be done on the same experimental system in order to avoid systematic errors in e.g. the absolute normalisation. This has been the aim of the present experiment.

4.2 Experimental technique

The primary objective of the present experiment has been to measure $\sigma_{\mathrm{tot}}^{+}$ for atomic hydrogen by positron impact. The experimental system and the techniques used are similar to those previously used in other positron ionisation experiments at UCL [13–15]. At the same time measurements of σ_{I}^{+} have been performed in order to ensure that the experiment can yield data consistent with the previous results by Jones *et al.* [5] and Hofmann *et al.* [10]. The technique used for these measurements is the same as used by Kara *et al.* [15] for obtaining σ_{I}^{+} for the noble gases. It will not be described in any detail here. All measurements have been performed using the deuterium isotope in order to discriminate better against hydrogen ions created in e.g. ionisation of the residual background gas.

4.2.1 Experimental equipment

A schematic of the UCL hydrogen ionisation experiment is shown in figure 4.1. Positrons emitted by a 37 MBq (1 mCi) ^{22}Na source are moderated in a moderator made from annealed tungsten mesh. The beam is confined along the entire experiment by an axial magnetic field of 50–150 Gauss. This is generated by Helmholtz coils placed along the outside of the vacuum tubing. The intensity of the beam has been measured to be around 10^4 e^{+}/s and has an energy resolution of $\sim$2 eV (FWHM). The moderator also emits secondary electrons, which are confined by the magnetic field as well. These are removed from the beam by keeping the lens element R1 at a potential of -1 keV. An $\mathbf{E} \times \mathbf{B}$ velocity filter with trochoidal electrodes serves to remove any remaining high-energy positrons from the beam and also shifts it out of the direct line of sight to the source. This prevents gamma radiation emitted by the source from reaching the interaction region. During measurements the velocity filter was also used to chop the beam by pulsing the applied voltages at a rate of $\sim$8.3 kHz. The duration of the positron pulse was of the order of 100 μs with the beam only being switched off for $\sim$6 μs during ion detection.

Before entering the interaction region the beam passes through a retarding

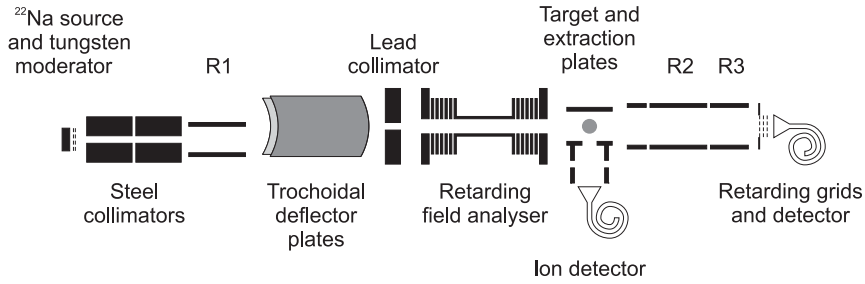

Figure 4.1: Schematic of UCL experiment. The positrons are confined by an axial magnetic field generated by Helmholtz coils placed along the outside of the vacuum tubing. R1–R3 are electrostatic lens elements. In the interaction region the target is generated by a Slevin source forming a jet of atomic deuterium at 90° with the plane of the paper.

field analyser (RFA). The RFA can be used to reflect positrons scattered in the backward direction from the interaction region back toward the positron detector at the end of the beam line. However during the measurements of $\sigma^+_{\rm tot}$ we did not need to detect the scattered positrons. The RFA was therefore used to minimise the flight time between the velocity filter and the interaction region by accelerating the positrons instead.

In the interaction region the beam was intersected at 90° by a deuterium target in the form of a jet. This was produced by a Slevin RF discharge source. The source was fed with D_2 at a pressure of ∼3.8 mTorr. The flow of the gas was controlled and purified by a hot palladium leak valve. During runs the source was operated at an RF power of ∼14 W of which ∼85% was absorbed by the source. This yielded a dissociation fraction of ∼30%, meaning that the resulting target jet contained roughly equal amounts of D and D_2. Better dissociation could have been achieved by raising the RF power. However this led to an undesired increase in the background in the final spectra, due to photons emitted by the source being detected by the ion detector. The pressure of the target jet emerging from the source was around 0.5 μTorr.

The interaction region is situated between two parallel extraction plates. After the passage of a positron pulse, ±150 V were applied to these plates. This pulsing was controlled by the same generator that chopped the beam. A suitable delay ensured that there were no positrons present in the interaction region while the voltages were applied. The acceleration of the positrons in the RFA mentioned before helped to minimise this delay. The generated electric field across the interaction region extracted any ions created through a grid-covered hole in the negative plate and accelerated them towards an ion detector. The extraction pulse lasted ∼3.4 μs after which the potentials of the plates

were returned to ground. Ions were identified through a time-of-flight (TOF) method similar to that described in section 2.2.1. The method of extraction and detection of all ions meant that count rates were proportional to the total ionisation cross section, $\sigma^+_{\rm tot}$.

At the end of the beam line a second detector was mounted for positron detection. During measurements of direct ionisation this detector was used to detect the scattered positrons. Lens elements R2 and R3 were then held at potentials that helped extract the positrons from the interaction region. Retarding grids in front of the detector could be used to distinguish scattered and unscattered positrons. However in the measurements of $\sigma^+_{\rm tot}$ the detector was only used to monitor the beam intensity before and after each run. Lens elements R2 and R3 were therefore held at 0 V and -15 V potentials respectively. A measurement of the beam intensity at the interaction region was performed. This was done by slotting in an aluminum plate immediately before the interaction region, stopping the positrons. The radiation from the annihilating positrons was measured with a NaI detector. This measurement showed that as much as 10% of the low-energy positrons relative to those at intermediate energies were lost after the interaction region and therefore not detected by the detector at the end of the beam line. Relative to the intensity at the highest energies (> 500 eV) the fraction of low-energy positrons not transported to the end was even larger. Therefore the beam intensity measured with the NaI detector was the one used in the final data analysis, while those of the other detector were only used to ensure that beam intensities were stable and similar in all runs.

Both the ion and positron detector were channeltron electron multipliers (CEM's). These were used rather than Ceratrons as the latter had been found to deteriorate when exposed to atomic hydrogen.

The peak energy of the beam energy distribution was given by $E = {\rm e}V_{\rm mod}+\phi$, where $V_{\rm mod}$ is the moderator potential and ϕ is an energy shift primarily arising from the negative positron work function of the tungsten moderator (see section 1.2.2). A rather good calibration of the beam energy was needed in this experiment as the threshold energy $E^+_{\rm Ps}$ is only 6.8 eV. Systematic deviations in E e.g. of the order of 1 eV could therefore shift the energy scale in a way that would induce significant disagreements in the final cross sections. Therefore instead of relying entirely upon retarding spectra, which can be affected by for example contact potentials, a novel time-of-flight method was used to determine ϕ. For this purpose a four-grid retarder was installed in the beam line immediately after the lead collimator and before the RFA. The RFA and the remainder of the the beam line were kept at ground potential during these investigations, so the positrons would not be accelerated by any electric fields during their flight. The axial magnetic field was maintained as usual during these measurements. The potential of the two central grids in the retarder was normally held at $V_{\rm mod} + 9$ V, thus stopping the beam. Using a pulser this

barrier could however very rapidly be lowered to ground potential, letting the positrons through. The time it took the positrons to traverse the distance from the retarder to the CEM detector at the end was measured using a time-to-amplitude converter. For a given V_{mod} the *shortest* flight times had to belong to the positrons in the beam with the *highest* axial energy. This flight time would be proportional to the inverse of the positron axial velocity v. The velocity v would in turn be proportional to $\sqrt{\mathrm{e}V_{\mathrm{mod}} + \delta}$, where δ is the energy by which the highest energy positrons are shifted above $\mathrm{e}V_{\mathrm{mod}}$ in the beam energy distribution. The two energies ϕ and δ could be related to each other through a retarding spectrum of the beam energy distribution. By measuring flight times for a range of different moderator voltages, δ could be found through a fit hence providing a calibration of the energy scale. Using this method, the value of ϕ was found to be 2.4 ± 0.1 eV.

4.2.2 Data analysis

Data were collected by an automated system. During a run the moderator voltage V_{mod} and hence the beam energy E was stepped over a range of values by a computer. At each step the number of counts in the window in the ion TOF spectrum corresponding to the D^+ ions were recorded. The steps in energy (V_{mod}) in a given run were chosen to cover the whole energy range from around E^+_{Ps} to $\sim$1 keV or at least to have a suitable overlap with other runs within this range. Measurements were also made to ensure that the D^+ ion count rate, N^+_{D}, did not contain significant contributions from processes such as dissociative ionisation of D_2 or ionisation of D by fast positrons or gamma radiation from the source. The first of these contributions was investigated by measuring N^+_{D} with the RF power for the Slevin source turned off, hence only admitting pure D_2 into the interaction region. The latter contribution was investigated by turning off the beam at the trochoidal deflector while keeping the rest of the experiment running as normal. In both cases negligible contributions to N^+_{D} were found.

The count rate N^+_{D} always contained a contribution N_γ from random coincidences from photons being detected by the ion detector. These photons were emitted by the deuterium source. Steps were taken to reduce this background by coating the entire interaction region in light absorbing carbon and by keeping the RF power low as mentioned in the previous section. The photon background could however not be fully eliminated. The TOF spectra showed the photon background to be flat i.e. random. The value of N_γ could therefore be found by either monitoring regions in the TOF spectrum away from any ion peaks or by performing measurements at energies below E^+_{Ps}.

At each energy an ion yield, Y, was calculated as

$$Y = \frac{N^+_{\mathrm{D}} - N_\gamma}{n_+}, \tag{4.3}$$

where n_+ is the positron beam intensity as measured with the NaI detector. Experimental conditions were kept as stable as possible during all runs, yet small variations were observed in the absolute magnitude of the yields between different runs. This was probably due to, for example, small variations in the target density or drifts in the ion detection system. Therefore the different yields were scaled to each other before being suitably binned into the final data. The absolute normalisation of the measured $\sigma^+_{\rm tot}$ was obtained through normalisation to data for $\sigma^+_{\rm I}$ for electron impact by Shah *et al.* [16] at energies above 200 eV. At those energies one would expect $\sigma^+_{\rm Ps}$ to have fallen to zero as also found by Zhou *et al.* [12]. One would therefore expect $\sigma^+_{\rm I}$ for positrons and electrons to be equal as discussed in section 2.1.1.

4.3 Results and discussion

The present results for the three cross sections $\sigma^+_{\rm tot}$, $\sigma^+_{\rm I}$ and $\sigma^+_{\rm Ps}$ for atomic deuterium are presented in figures 4.2, 4.3 and 4.4 respectively. Included in all the figures are the results by Hofmann *et al.* [10]. In figure 4.3 is also presented the $\sigma^+_{\rm I}$ by Jones *et al.* [5] while in figure 4.4 the $\sigma^+_{\rm Ps}$ by Zhou *et al.* [12] is shown as well. Finally in figures 4.2 and 4.3 the electron impact data for $\sigma^+_{\rm I}$ by Shah *et al.* [16], used for normalisation of our data, has been included.

A multitude of theoretical calculations have also been included in all three figures. One of these is the pseudo-state close-coupling (CC) calculation by Kernoghan *et al.* [17]. This calculation employs a 33-state approximation consisting of the 1s, 2s and 2p eigenstates of both positronium and hydrogen and 27 hydrogen pseudo-states for $n = 3$–9. This work is an improvement of a previous 18-state calculation by Kernoghan *et al.* [23]. The new calculation is superior to the old one in that the larger basis makes the results free of the pseudo-structure observed in the 18-state calculation. Furthermore by using only single-centre pseudo-states double counting between contributions coming from positronium and hydrogen states is avoided. A second CC calculation included in the figures is the one by Mitroy [18,19] using a large L^2 basis. It consists of a 21-state calculation (CC($\overline{13}$,$\overline{8}$)) below $E^+_{\rm I}$ and a 31-state calculation (CC($\overline{28}$,3)) above $E^+_{\rm I}$. In figure 4.3 it is therefore only the CC($\overline{28}$,3) results that are included for $\sigma^+_{\rm I}$. In the notation of Mitroy, the calculation by Kernoghan *et al.* would be denoted CC($\overline{30}$,3). The third theoretical calculation shown in all three figures is the hidden crossing theory (HCT) by Janev and Solov'ev [20]. This calculation allows for the formation of the quasi-bound molecular ion PsH^+. This results in a non-zero $\sigma^+_{\rm tot}$ ($\sigma^+_{\rm Ps}$) even below $E^+_{\rm Ps}$. Finally in figure 4.4 two other calculations have been included. These are the 6-state CC R-matrix calculation by Higgins and Burke [21] and the hyperspherical coupled-channel calculation by Igarashi and Toshima [22]. The collection of theoretical calculations presented here is by no means complete. Other calculations which either agree or disagree

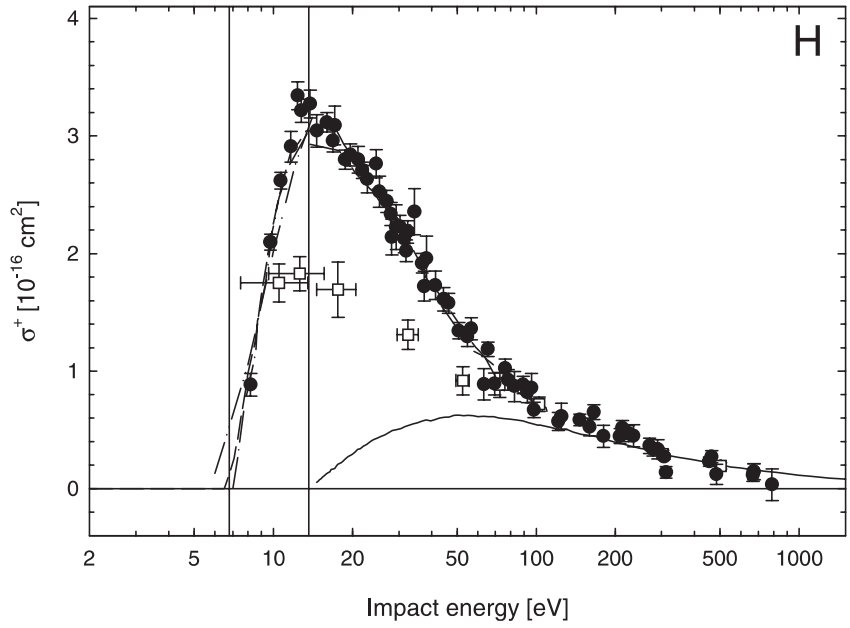

Figure 4.2: Single ionisation of atomic hydrogen (deuterium). Positron impact: (●) $\sigma^+_{\rm tot}$ present results, (□) $\sigma^+_{\rm tot}$ by Hofmann *et al.* [10], (- - - -) $\sigma^+_{\rm tot}$ CC($\overline{30}$,3) calculation by Kernoghan *et al.* [17], (—·—) $\sigma^+_{\rm tot}$ CC($\overline{13}$,$\overline{8}$) and CC($\overline{28}$,3) calculations by Mitroy [18,19], (—··—) $\sigma^+_{\rm tot}$ HCT calculation by Janev and Solov'ev [20]. Electron impact: (——) $\sigma^+_{\rm I}$ by Shah *et al.* [16]. The two vertical lines indicate $E^+_{\rm Ps}$ and $E^+_{\rm I}$ respectively.

with those above (e.g. [24–26] and [3,4] respectively) could have been included. However in order not to make the figures too crowded these have been left out.

In figure 4.2 one observes the present results to be in agreement with those by Hofmann *et al.* at the highest energies, as both sets merge with the electron data. However below ∼70 eV the $\sigma^+_{\rm tot}$ by Hofmann *et al.* falls increasingly below the present results and finally reach a maximum value which is only around 60% of that of the present results. The two CC calculations by Kernoghan *et al.* and Mitroy are in very good agreement with each other and also with the present results. Only around the maximum do a few points show a minor, if any at all, deviation from the theories. The HCT calculation shows good agreement within the narrow energy range it covers. The only deviation of the HCT calculation from the CC results is seen at energies below $E^+_{\rm Ps}$ due to the molecular effect discussed before.

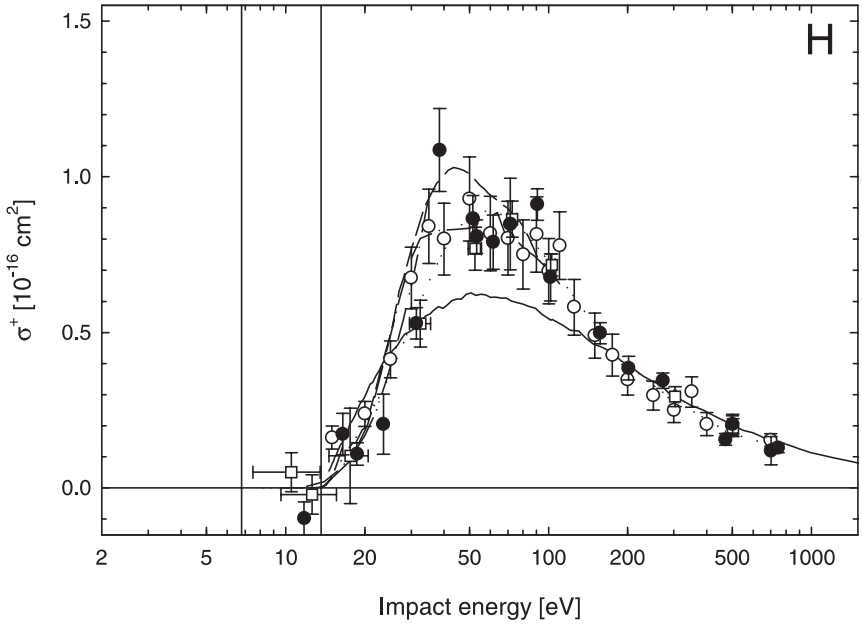

Figure 4.3: Direct single ionisation of atomic hydrogen (deuterium). Positron impact: (●) σ_I^+ present results, (○) σ_I^+ by Jones *et al.* [5], (□) σ_I^+ by Hofmann *et al.* [10], (– – – –) σ_I^+ CC($\overline{30}$,3) calculation by Kernoghan *et al.* [17], (—·—) σ_I^+ CC($\overline{28}$,3) calculation by Mitroy [19], (—··—) σ_I^+ HCT calculation by Janev and Solov'ev [20], (·····) smooth curve fitted through the present data and those by Jones *et al.* Electron impact: (——) σ_I^+ by Shah *et al.* [16]. The two vertical lines indicate E_{Ps}^+ and E_I^+ respectively.

In figure 4.3 one observes that the few points measured for σ_I^+ in the present experiment exhibit an overall good agreement with the previous results by Jones *et al.* and Hofmann *et al.* This is an important verification of our experimental technique. Good agreement is also found with theory. A small exception could be the present results and those by Hofmann *et al.* being slightly lower than theory and the results by Jones *et al.* between threshold and 40 eV. Included in figure 4.3 is a smooth curve fitted through the present results and those by Jones *et al.* This curve provided the estimate of σ_I^+ that has been subtracted from the result for σ_{tot}^+ in figure 4.2 in order to deduce the present σ_{Ps}^+ shown in figure 4.4.

In figure 4.4 one observes the present results for σ_{Ps}^+ to be in good agreement with those by Zhou *et al.* The present data seem slightly higher in absolute magnitude at energies between 10 and 40 eV. However remembering that Zhou

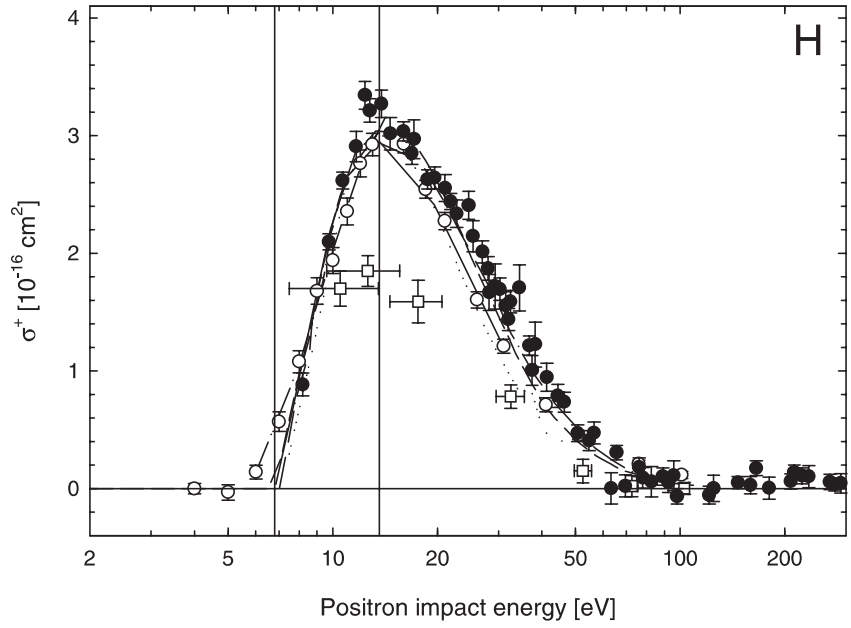

Figure 4.4: Positronium formation in single ionisation of atomic hydrogen (deuterium) by positron impact. (●) $\sigma^+_{\rm Ps}$ present results, (○) $\sigma^+_{\rm Ps}$ by Zhou *et al.* [12], (□) $\sigma^+_{\rm Ps}$ by Hofmann *et al.* [10], (– – – –) $\sigma^+_{\rm Ps}$ CC($\overline{30}$,3) calculation by Kernoghan *et al.* [17], (— · —) $\sigma^+_{\rm Ps}$ CC($\overline{13}$,$\overline{8}$) and CC($\overline{28}$,3) calculations by Mitroy [18,19], (— ·· —) $\sigma^+_{\rm Ps}$ HCT calculation by Janev and Solov'ev [20], (·····) $\sigma^+_{\rm Ps}$ calculation by Higgins and Burke [21], (——) $\sigma^+_{\rm Ps}$ calculation by Igarashi and Toshima [22]. The two vertical lines indicate $E^+_{\rm Ps}$ and $E^+_{\rm I}$ respectively.

et al. did not provide an upper limit on their results (see discussion in section 4.1), but rather their best estimate of $\sigma^+_{\rm Ps}$, the agreement is considered good. From our observations in figures 4.2 and 4.3 it is not surprising to find that the $\sigma^+_{\rm Ps}$ by Hofmann *et al.* falls significantly below the present results. Good agreement is found with the CC and HCT calculations. The small deviation observed at around the maximum in $\sigma^+_{\rm tot}$ in figure 4.2 is inherited by $\sigma^+_{\rm Ps}$. The calculation by Higgins and Burke as well as that by Igarashi and Toshima seem to be a little bit low at energies above $E^+_{\rm I}$ as compared to both the experimental data and the other calculations. Finally one remarks that the $\sigma^+_{\rm Ps}$ by Zhou *et al.* at energies around $E^+_{\rm Ps}$ seems to follow the HCT calculation by Janev and Solov'ev. This could be an indication of the formation of the quasi-bound molecular ion PsH^+ as suggested by Janev and Solov'ev.

In conclusion the disagreement that existed between the previous measurements of the ionisation cross sections of atomic hydrogen by positron impact now seems to have been resolved. As suggested already in section 4.1 it is the measurements of $\sigma^+_{\rm tot}$ (and $\sigma^+_{\rm Ps}$) by the Bielefeld-Brookhaven group that appear to be flawed.

Before concluding this chapter it should be noted that the results presented here are also a most excellent example of cross sections behaving in accordance with the standard picture of single ionisation as discussed in section 2.1.1. For example in figure 4.3 one observes that the positron cross section rises above the electron one at intermediate energies and down to around 25 eV where a cross-over takes place. It is also noted that the positronium channel is clearly the dominant channel at low energies, with $\sigma^+_{\rm Ps}$ (and $\sigma^+_{\rm tot}$) exhibiting a sharp rise within the gap between $E^+_{\rm Ps}$ and $E^+_{\rm I}$ (the Ore gap).

References

[1] J. Slevin and W. Stirling, Rev. Sci. Instrum. **52**, 1780 (1981).

[2] G. Spicher, B. Olsson, W. Raith, G. Sinapius, and W. Sperber, Phys. Rev. Lett. **64**, 1019 (1990).

[3] P. Acacia, R. I. Campeanu, M. Horbatsch, R. P. McEachran, and A. D. Stauffer, Phys. Lett. A **179**, 205 (1993).

[4] P. Acacia, R. I. Campeanu, M. Horbatsch, R. P. McEachran, and A. D. Stauffer, Hyperfine Interact. **89**, 95 (1994).

[5] G. O. Jones, M. Charlton, J. Slevin, G. Laricchia, Á. Kövér, M. R. Poulsen, and S. Nic Chormaic, J. Phys. B: At. Mol. Opt. Phys. **26**, L483 (1993).

[6] M. Weber, A. Hofmann, W. Raith, W. Sperber, F. Jacobsen, and K. G. Lynn, Hyperfine Interact. **89**, 221 (1994).

[7] T. S. Stein, W. E. Kauppila, C. K. Kwan, and S. Zhou, Hyperfine Interact. **89**, 461 (1994).

[8] S. Zhou, W. E. Kauppila, C. K. Kwan, and T. S. Stein, Phys. Rev. Lett. **72**, 1443 (1994).

[9] H. Knudsen, U. Mikkelsen, K. Paludan, K. Kirsebom, S. P. Møller, E. Uggerhøj, J. Slevin, M. Charlton, and E. Morenzoni, Phys. Rev. Lett. **74**, 4627 (1995).

[10] A. Hofmann, T. Falke, W. Raith, M. Weber, D. P. Becker, and K. G. Lynn, J. Phys. B: At. Mol. Opt. Phys. **30**, 3297 (1997), and references within.

[11] W. Sperber, D. Becker, K. G. Lynn, W. Raith, A. Schwab, G. Sinapius, G. Spicher, and M. Weber, Phys. Rev. Lett. **68**, 3690 (1992).

[12] S. Zhou, H. Li, W. E. Kauppila, C. K. Kwan, and T. S. Stein, Phys. Rev. A **55**, 361 (1997).

[13] P. Ashley, J. Moxom, and G. Laricchia, Phys. Rev. Lett. **77**, 1250 (1996).

[14] J. Moxom, P. Ashley, and G. Laricchia, Can. J. Phys. **74**, 367 (1996).

[15] V. Kara, K. Paludan, J. Moxom, P. Ashley, and G. Laricchia, J. Phys. B: At. Mol. Opt. Phys. **30**, 3933 (1997).

[16] M. B. Shah, D. S. Elliott, and H. B. Gilbody, J. Phys. B: At. Mol. Phys. **20**, 3501 (1987).

[17] A. A. Kernoghan, D. J. R. Robinson, M. T. McAlinden, and H. R. J. Walters, J. Phys. B: At. Mol. Opt. Phys. **29**, 2089 (1996).

[18] J. Mitroy, Aust. J. Phys. **48**, 645 (1995).

[19] J. Mitroy, J. Phys. B: At. Mol. Opt. Phys. **29**, L263 (1996).

[20] R. K. Janev and E. A. Solov'ev, in *Photonic, Electronic and Atomic Collisions, Proc. of XX ICPEAC*, edited by F. Aumayr and H. Winter (World Scientific, Singapore, 1998), p. 393.

[21] K. Higgins and P. G. Burke, J. Phys. B: At. Mol. Opt. Phys. **26**, 4269 (1993).

[22] A. Igarashi and N. Toshima, Phys. Rev. A **50**, 232 (1994).

[23] A. A. Kernoghan, M. T. McAlinden, and H. R. J. Walters, J. Phys. B: At. Mol. Opt. Phys. **28**, 1079 (1995).

[24] C. J. Brown and J. W. Humberston, J. Phys. B: At. Mol. Phys. **18**, L401 (1985).

[25] T. T. Gien, J. Phys. B: At. Mol. Opt. Phys. **30**, L23 (1997).

[26] S. Kar and P. Mandal, J. Phys. B: At. Mol. Opt. Phys. **33**, L165 (2000).

Chapter 5

Ionisation of molecules

5.1 Introduction

In the previous chapters of this thesis we have investigated ionisation of atomic targets. As mentioned in section 1.1, very few experimental studies exist of excitation of atoms by positron impact, due to experimental difficulties. As an alternative one can turn to study ionisation of simple molecules instead. In the interaction of a charged particle with a molecule, the target can be left in an excited (electronic) state that may lead to dissociation of the molecule into charged fragments. This kind of process can be studied by the same means as used to study ionisation of atoms. The aim of the present experiments has been to study positronium formation in molecules through measurements of total ionisation cross sections. The molecules that have been studied are N_2, CO, CO_2 and CH_4.

By direct non-dissociative (single) ionisation of a general molecule, AB, by positron impact, we mean the process

$$e^+ + AB \quad \rightarrow \quad AB^+ + e^- + e^+. \tag{5.1}$$

Changing our notation slightly as compared to that of the previous chapters, the cross section corresponding to (5.1) is denoted $\sigma(AB^+)_I$ and its threshold energy $E(AB^+)_I$. Similarly we have a non-dissociative ionisation channel with positronium formation:

$$e^+ + AB \quad \rightarrow \quad AB^+ + Ps, \tag{5.2}$$

with the partial cross section and threshold energy denoted $\sigma(AB^+)_{Ps}$ and $E(AB^+)_{Ps}$ respectively. As usual $E(AB^+)_{Ps}$ lies 6.8 eV below $E(AB^+)_I$ and a kind of molecular Ore gap exists between them. Also, as always, both (5.1) and

(5.2) contribute to the total non-dissociative ionisation cross section, $\sigma(AB^+)_{tot}$, which is equal to the sum of $\sigma(AB^+)_{Ps}$ and $\sigma(AB^+)_I$.

In the dissociation of a molecule several different processes can occur. In direct dissociative ionisation of the molecule AB, some of the processes leading to the production of an A^+ ion could be

$$e^+ + AB \rightarrow A^+ + B + e^- + e^+, \tag{5.3}$$

$$e^+ + AB \rightarrow A^+ + B^- + e^+, \tag{5.4}$$

where both A and B may represent fragments consisting of one or several atoms. The cross section corresponding to the sum of all such processes resulting in an A^+ ion is denoted $\sigma(A^+)_I$ and the appearance potential $E(A^+)_I$. The energy $E(A^+)_I$ corresponds to the lowest value among the threshold energies of all the direct ionisation processes yielding an A^+ ion. The process (5.4) cannot occur for all molecules as the negative ion fragment, B^-, does not exist. This is the case for example for N_2. As before there is also a positronium formation channel in dissociative ionisation that lead to the production of an A^+ ion:

$$e^+ + AB \rightarrow A^+ + B + Ps. \tag{5.5}$$

The corresponding cross section is denoted $\sigma(A^+)_{Ps}$. The appearance potential is denoted $E(A^+)_{Ps}$. Formally $E(A^+)_{Ps}$ lies 6.8 eV below the threshold energy of the process (5.3) which is not always equal to $E(A^+)_I$. However for our gases it is only for the production of C^+ ions from CO_2 that there is a significant difference (of ∼3.6 eV) between $E(C^+)_I$ and the threshold energy of (5.3). This reduces the gap between $E(C^+)_{Ps}$ and $E(C^+)_I$ to merely 3.2 eV.[1] The total dissociative ionisation cross section, $\sigma(A^+)_{tot}$, is equal to the sum of $\sigma(A^+)_{Ps}$ and $\sigma(A^+)_I$ and contains contributions from all the processes yielding an A^+ ion. Apart from the processes (5.3)–(5.5) one can envision additional processes of the type

$$e^+ + AB \rightarrow A^+ + B^+ + 2e^- + e^+, \tag{5.6}$$

$$e^+ + AB \rightarrow A^+ + B^+ + e^- + Ps, \tag{5.7}$$

in which two (or even more) positively charged fragments are produced. As will be discussed in section 5.2.3, these may cause problems due to the experimental technique used in our experiment. However it will be shown that we do not need to consider these processes any further. Furthermore we do not pay any special attention to processes resulting in more 'exotic' reaction products, like e.g. Ps^- or PsH, in this chapter.

The first comparative studies of particle/antiparticle impact ionisation and dissociation of small molecules were performed by Hvelplund *et al.* [2] and Knudsen *et al.* [3] using protons and antiprotons. They found that much of what was

[1] All values used for $E(A^+)_{Ps}$ and $E(A^+)_I$ are from Frandsen [1] and references within.

known from ionisation of atoms could be transfered to the molecular case. Not surprisingly, non-dissociative ionisation behaves in the same way as single ionisation of a noble gas, as discussed in section 2.1.1. Dissociative ionisation on the other hand shares features in common with double ionisation of a noble gas. Particularly the interference model discussed in section 2.1.2 can be used in a qualitative way for the molecular case as well. As illustrated above, several different processes may lead to the production of an A^+ ion. Some of these might even represent several different processes involving excitation into different electronic dissociative states leading to the same reaction products. These processes can either be the result of one or multiple projectile interactions with the target electrons. The picture is not quite as clear as in high-energy double ionisation of a noble gas, nonetheless similar behaviour is observed. Interference of the different processes gives rise to a difference between the dissociative ionisation cross sections of positive and negative projectiles. In the present study we are also interested in whether or not some of the observed behaviour of positronium formation in double ionisation of the noble gases is present in dissociative ionisation as well.

The amount of previous work on positron impact ionisation of molecules is limited. Most is concerned with non-dissociative ionisation of H_2, e.g. [4–7]. Of these some are relevant as precursors to the atomic hydrogen experiments discussed in chapter 4, rather than as molecular experiments. In Århus, Frandsen performed a systematic study of direct non-dissociative and dissociative ionisation by positron impact of the molecules N_2, CO, CO_2 and CH_4 for his master's thesis [1]. However apart from a preliminary report [8], these results remained unpublished at the time. They have now been published together with the present results in two papers by Bluhme *et al.* [II,V]. It is however beyond the scope of this thesis to discuss how these direct ionisation data were obtained. They will only be used for comparison with the present results in section 5.3. In more recent studies Moxom *et al.* [9,10] have measured the total non-dissociative and dissociative cross sections for CH_3F and CH_3Cl. Furthermore Kwan *et al.* [11] have studied total positronium formation in a few different molecules. Finally it should be mentioned that there exists a range of beam attenuation experiments, as e.g. [12,13], measuring the total *scattering* cross section for different molecules by positron impact. These are however not relevant to use for comparison in this chapter.

5.2 Experimental technique

The experimental technique for measuring the total non-dissociative and dissociative ionisation cross sections for N_2, CO, CO_2 and CH_4 by positron impact was very similar to the technique used in the mixed gas experiments on the noble gases discussed in chapter 2. The mixed gas technique was used for the

molecular targets before it was used on the noble gases as these molecular measurements were performed between the pure gas and mixed gas experiments from chapter 2. As the technique is virtually the same we will not discuss it in any detail but rather refer to section 2.2. There are however a few differences that need to be discussed here.

5.2.1 Experimental equipment

The experiments were performed using the Århus electrostatic slow positron beam line shown in figure 2.5. The only changes made in order to run the molecular targets were in the pulsing system. The positron pulse was reduced from 1 μs to 100 ns. As the repetition time was maintained at $\sim$10 μs this meant a reduction of the effective beam intensity by a factor of 100 as compared to a DC beam. However this reduction was necessary. In dissociative ionisation the ion fragments can be created having kinetic energies of several eV. Unlike the noble gases, in which the ions have thermal energies, it is important to extract the molecular ion fragments as quickly as possible after their creation before they can drift out of the interaction region. For the same reason the extraction field was applied only 50 ns after the passage of the positrons. This meant that at the most it would take 150 ns from the creation of an ion until it was extracted. By varying the delay between the positron pulse and the onset of the extraction field, it was found that as long as this total time was below $\sim$200 ns, full extraction of all ion fragments was attained.

The ion fragments were identified by time-of-flight (TOF). For N_2 this gives rise to a problem. In N_2 one can create a N_2^{2+} ion through non-dissociative *double* ionisation. As this ion has the same M/Q value as the N^+ ion created in dissociative ionisation, the two can not be separated by TOF. The ratio of N_2^{2+} to N^+ ions created from N_2 by positron impact has never been measured. However Hałas and Adamczyk [14] measured the ratio $\sigma(N_2^{2+})/\sigma(N^+)$ for electron impact ionisation using heteroisotropic N_2 ($^{14}N^{15}N$). They found the ratio to have a maximum value of $\sim$13% at 150 eV. Similarly one could make comparison with the ratio $\sigma(CO^{2+})/(\sigma(C^+)+\sigma(O^+))$ for CO. Using the proton data by Knudsen *et al.* [3] this yields a value of 2–6%, while the electron impact data by Tian and Vidal [15] gives a value of less than 2%. As we can not discern the N^+ and N_2^{2+} ions in our experiment, we have to say that whenever in the remainder of this chapter we discuss N^+, we mean the *sum* of N^+ and N_2^{2+}. However we expect the contribution from N_2^{2+} to the sum to be less than $\sim$10%.

Finally it should be mentioned that the ground potential ($V_{\mathrm{f.gnd}}$) of the resistive chain during these experiments sometimes was floated to a *positive* voltage, allowing measurements with positron impact energies all the way up to 2 keV.

5.2.2 Data analysis

The data analysis is based on the same principles as used in section 2.2.2. However some of the calculations can in this case be performed in a more straight forward manner than for the noble gases. In section 2.2.2 we used complicated ratios, like (2.22), as they were independent of experimental parameters like accumulation time, gas pressure, the geometry of the interaction region and even the beam intensity as long as the ratio of the positron to electron current, n_+/n_-, remained a known function of the positron impact energy. This was important as the data for a noble gas were obtained over periods of several months. However for a molecular target each run only lasted a few hours and all data for a specific cross section were obtained in no more than a few weeks. This means that some of the experimental parameters, like gas pressure and the induced electron current, n_-, safely can be assumed to be the same for all runs. This allows one to make the correction of the ion count rates for electron induced background *before* any ratios are taken.

For non-dissociative ionisation of the molecule AB, the number of counts, $N(\mathrm{AB}^+)$, is obtained from the AB^+ peak in the TOF spectrum after correction for the general background. This is furthermore corrected for the electron induced background, $N(\mathrm{AB}^+)_{\mathrm{e}^-}$, to yield

$$N(\mathrm{AB}^+)_{\mathrm{corr}} = N(\mathrm{AB}^+) - N(\mathrm{AB}^+)_{\mathrm{e}^-}. \tag{5.8}$$

The number $N(\mathrm{AB}^+)_{\mathrm{e}^-}$ is, as for the noble gases, found using data obtained at positron impact energies below the threshold $E(\mathrm{AB}^+)_{\mathrm{Ps}}$ suitably corrected for the electron cross section using known values from the literature. For N_2 the electron data by Krishnakumar and Srivastava [16] is used. For CO, CO_2 and CH_4 the similar data by Orient and Srivastava [17] could have been used. However Knudsen *et al.* [3] have questioned the reliability of these data and also in particular those for dissociative ionisation from the same paper, as they do not show a good merger with antiproton data at high energies as expected. Therefore for CO, CO_2 and CH_4 we use the electron data by Tian and Vidal [15] and Straub *et al.* [18,19] respectively as they show better merger with the antiproton data. For each TOF spectrum the same procedure is used to obtain the corrected number of counts in the He^+ peak, $N(\mathrm{He}^+)_{\mathrm{corr}}$, using the electron data by Krishnakumar and Srivastava [20] for correction. The corrected numbers are used to calculate the ratio

$$R(\mathrm{AB}^+)_{\mathrm{tot,ABHe}} \equiv \frac{\sigma(\mathrm{AB}^+)_{\mathrm{tot}}}{\sigma(\mathrm{He}^+)_{\mathrm{tot}}} = \epsilon(\mathrm{AB}^+)\rho_{\mathrm{ABHe}}\frac{N(\mathrm{AB}^+)_{\mathrm{corr}}}{N(\mathrm{He}^+)_{\mathrm{corr}}}, \tag{5.9}$$

where the factor $\epsilon(\mathrm{AB}^+)$ corrects for the difference in the Ceratron detector efficiency for the AB^+ and He^+ ions. The factor ρ_{ABHe} is, as in the noble gases, the ratio between the targets densities of the molecular gas and helium. This

arises from the 30% molecular gas and 70% helium mixture in the gas bottle used and the difference in diffusion velocity of the two gases out of the gas cell (see discussion in section 2.2.2). Unlike in single ionisation of the heavy noble gases, the entire factor of $\epsilon(AB^+)\rho_{ABHe}$ is *not* determined through direct normalisation of our data to electron cross sections. Instead we rely upon the detector efficiencies found by Andersen *et al.* [21] for calculating $\epsilon(AB^+)$. These were also used by Frandsen [1] in obtaining the $\sigma(AB^+)_I$ with which we are going to make comparison in section 5.3. The final absolute cross section, $\sigma(AB^+)_{tot}$, is deduced from the ratio $R(AB^+)_{tot,ABHe}$ by multiplication with the known total single ionisation cross section for helium, $\sigma(He^+)_{tot}$, shown in figure 2.3. A few of the points measured in our experiments were obtained at positron impact energies below the threshold energy of helium, $E(He^+)_{Ps}$. As these points cannot be normalised using $\sigma(He^+)_{tot}$, a different method is used. We had found the positron intensity, n_+, to be constant below ∼50 eV (see section 2.2.1). The near-threshold points can therefore be normalised by comparing the molecular ion count rate, $N(AB^+)_{corr}$, of these points to the count rate of a point at slightly higher energy ($E = 20$–30 eV), where we expect the deduced cross section to be reliable. This procedure induces some extra experimental error for the near-threshold points.

For dissociative ionisation the procedure for obtaining $\sigma(A^+)_{tot}$ is the same as above for finding $\sigma(AB^+)_{tot}$. In all the calculations the ion AB^+ is just replaced by A^+, yielding

$$R(A^+)_{tot,ABHe} \equiv \frac{\sigma(A^+)_{tot}}{\sigma(He^+)_{tot}} = \epsilon(A^+)\rho_{ABHe}\frac{N(A^+)_{corr}}{N(He^+)_{corr}}. \tag{5.10}$$

The factor ρ_{ABHe} stays the same as before as it only concerns the target densities and not the ions.

In section 5.3.2 we present our results for dissociative ionisation of N_2, CO and CO_2. No dissociative cross sections are presented for CH_4. Several ion fragments such as CH_3^+, CH_2^+ and H^+ were easily observed in the TOF spectra. However due to the small mass difference the CH_3^+ and CH_2^+ peaks overlapped with each other and the non-dissociative CH_4^+ peak. Therefore in order to deduce the ion count rates a fitting procedure had to be employed. Unfortunately it was found that the resulting count rates, $N(CH_3^+)$ and $N(CH_2^+)$, were heavily dependent on the details of the fit. The reliability of the resulting cross sections would therefore be questionable. The variations in $N(CH_3^+)$ and $N(CH_2^+)$ also influenced the non-dissociative count rate, $N(CH_4^+)$. However as these variations were found to be within the statistical uncertainty on $N(CH_4^+)$, we proceeded to deduce $\sigma(CH_4^+)_{tot}$, which we consider reliable within the accumulated experimental uncertainty. For the H^+ ion fragment the extraction of the count rates from the TOF spectra caused no problem. Yet the resulting cross section looked spurious, particularly at energies above 200 eV, where $\sigma(H^+)_{tot}$

was observed to fall below the $\sigma(H^+)_I$ by Frandsen [1]. In dissociation of CH_4 a light fragment like H^+ will recoil with most of the energy released in the process, making it hard to collect. We therefore suspect our observations to be due to incomplete extraction and collection of this particular ion fragment, hence rendering the resulting cross section unreliable.

5.2.3 'Light-before-heavy' effect

In our experiments the TOF of the molecular ions were recorded by a time-to-amplitude converter (TAC). The start pulse was provided by the trigger for the onset of the ion extraction field, while the stop pulse came from the ion Ceratron detector. With such a system, processes like (5.6) and (5.7), in which two (or more) positively charged fragments are created, may cause problems. When these ion fragments are extracted, it will be the one with the lowest value of M/Q and hence the shortest flight time which will reach the Ceratron detector first, stopping the TAC (see section 2.2.1). Therefore only the TOF of this ion fragment is recorded, leading to the so-called 'light-before-heavy' (LBH) effect. This effect may cause an underestimation of the number of heavy ion fragments as they get 'shadowed' by lighter fragments. Experiments looking at MeV ion impact on molecules [3,22–24] have shown that it can be important to correct for the LBH effect. Since the ions in these experiments had impact *velocities* of the same order as our positrons, we also have to consider the LBH effect here.

For N_2 the processes (5.6) and (5.7) do not give rise to any LBH effect as the ions A^+ and B^+ are the same. It may be discussed whether or not the channels (5.6) and (5.7) should be counted as contributing once or twice to the cross section $\sigma(N^+)_{tot}$. Turning to the proton impact experiments by Knudsen *et al.* [3], they found the $C^+ + O^+$ channel in CO to contribute ~7% to $\sigma(O^+)_{tot}$. If this is the same for N_2, it could mean that we have an potential underestimation of $\sigma(N^+)_{tot}$ as our system only counts contributions from (5.6) and (5.7) once. Furthermore for N_2, processes in which for example a N^+ and a N^{2+} ion are created together may be subject to the LBH effect. From the proton impact experiments by Knudsen *et al.* it is known that the ratio N^{2+}/N^+ is less than 5%. Within the experimental uncertainty of our results this channel can therefore probably be ignored.

For our measurements on CO, CO_2 and CH_4 we decided to test the influence from the LBH effect experimentally. This was done using a fast timing signal sorter and two TACs which both recorded ion flight times. The signal from the ion Ceratron detector was fed into the sorting unit. In the case of the detection of an ion, this would send a stop pulse to the first TAC, recording the TOF as usual. However if a second (heavier) ion was detected later within the same extraction period, a stop pulse would be sent by the signal sorter to the second TAC, recording the TOF of this ion. By comparing the TOF spectra from the two TACs, the importance of the LBH effect could be estimated.

The results of this investigation were similar for all three gases. The TOF spectra of the second TAC always seemed to be a weak reminiscence of the 'real' TOF spectra as recorded by the first TAC. Firstly the low number of total counts indicated that there was no significant influence from the LBH effect in our experiments. This is contrary to what was observed in the experiments using MeV ion impact mentioned above. We believe this can only be due to the fundamental difference between the projectile energies used in those experiments and in ours. Secondly the fact that the TOF spectra of the second TAC were mainly dominated by a non-dissociative peak made us suspect that these spectra were all together due to another effect than LBH. In non-dissociative ionisation there is no LBH effect as only one ion fragment is created. The observed TOF spectra could therefore be explained by 'after pulsing' of the Ceratron detector, which generates a 'false' secondary pulse rapidly after the detection of an ion. Such effect has been observed to be due to ion back-streaming within the Ceratron detector when used at high pressure. In our experiments these secondary pulses could at times even be observed directly in the signal from the Ceratron using an oscilloscope.

In conclusion we can ignore the LBH effect in our results for CO, CO_2 and CH_4. This also serves as a good indication that the effect can safely be ignored in N_2 as well.

5.3 Results and discussion

In sections 5.3.1 and 5.3.2 respectively are presented the present results for the total non-dissociative and dissociative ionisation cross sections of N_2, CO, CO_2 and CH_4 by positron impact. Error bars represent the accumulated experimental uncertainty from counting statistics, subtraction of the electron induced background and the normalisation to an absolute scale. This includes the uncertainty in the cross section $\sigma(He^+)_{tot}$ from figure 2.3 used for this purpose.

5.3.1 Non-dissociative ionisation

The present results for the total non-dissociative ionisation cross sections of N_2, CO, CO_2 and CH_4 are presented in figures 5.1–5.4 respectively. Included in all of the figures are the cross sections for direct non-dissociative ionisation by Frandsen [1]. Also plotted in the figures are the electron impact data used for the background correction. These are by Krishnakumar and Srivastava [16], Tian and Vidal [15], and Straub *et al.* [18,19] respectively. Furthermore is included a second set of electron data in each figure, namely those by Straub *et al.* [25] for N_2 and those by Orient and Srivastava [17] for the remaining three gases.

The cross sections for the four gases generally exhibit the same behaviour. At high energies the present results are observed to merge with the direct ion-

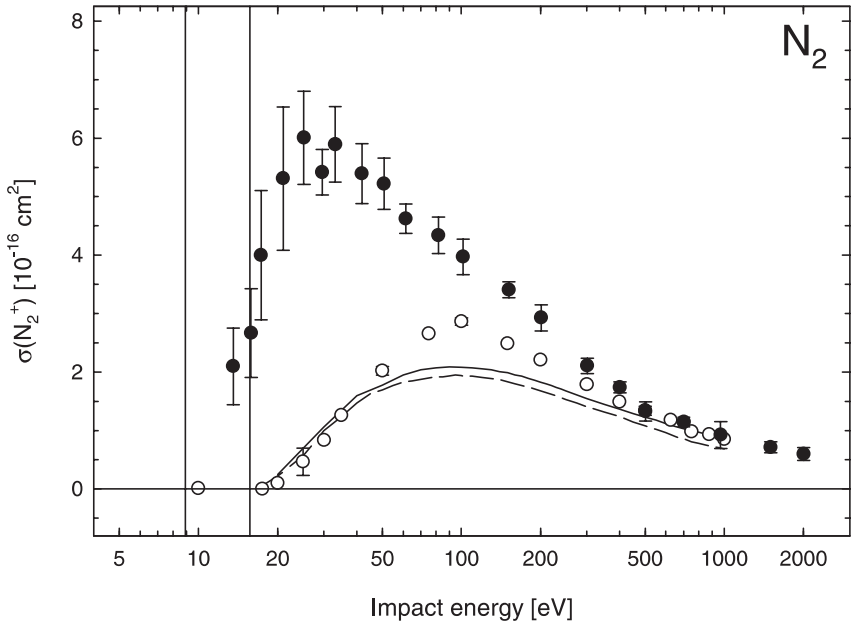

Figure 5.1: Non-dissociative ionisation of N_2. Positron impact: (●) $\sigma(N_2^+)_{\rm tot}$ present results, (○) $\sigma(N_2^+)_{\rm I}$ by Frandsen [1]. Electron impact: (——) $\sigma(N_2^+)_{\rm I}$ by Krishnakumar and Srivastava [16], (- - - -) $\sigma(N_2^+)_{\rm I}$ by Straub *et al.* [25]. The two vertical lines indicate $E(N_2^+)_{\rm Ps}$ and $E(N_2^+)_{\rm I}$ respectively.

isation data by Frandsen, as expected since positronium formation should not contribute to the total non-dissociative ionisation cross section at these energies. Both the total and the direct cross sections are seen to merge with the electron data at these energies. Particularly good merger is observed with the electron impact cross sections by Srivastava and co-workers. This is however indirectly due to the normalisations used. The direct ionisation data by Frandsen are normalised directly to these electron data. The present results on the other hand are normalised through the helium data in figure 2.3, which in turn are normalised to the electron impact helium data by Krishnakumar and Srivastava [20]. This yields consistent normalisations of all the cross sections. As in single ionisation of the noble gases this is based on the assumption of the validity of the first Born approximation. Support for its validity is found in the observation that the shapes of the cross sections agree as well at these energies.

Going down in energy one observes in all four figures $\sigma(AB^+)_{\rm tot}$ to start rising above $\sigma(AB^+)_{\rm I}$ for positron impact at around 100–200 eV, as positronium formation begins to make a significant contribution to the total non-dissociative

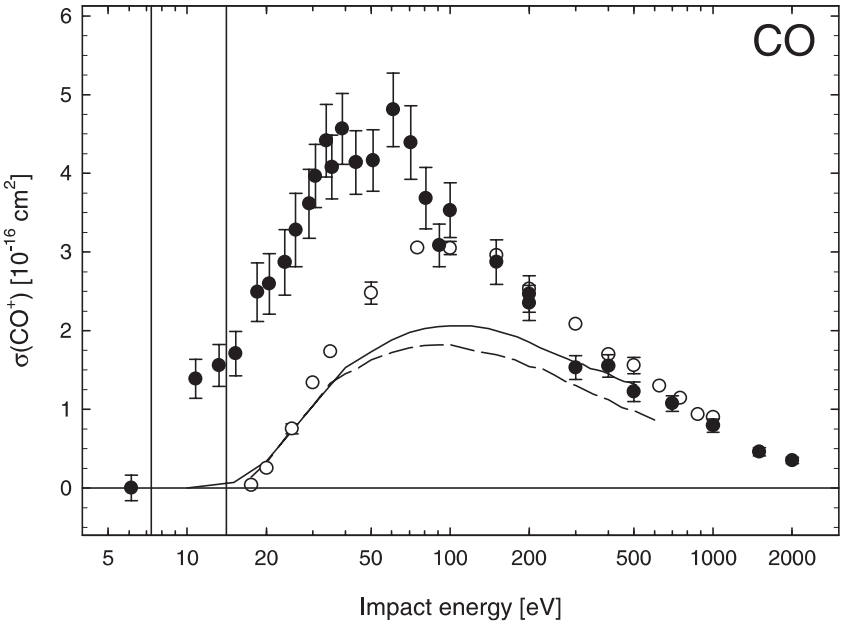

Figure 5.2: Non-dissociative ionisation of CO. Positron impact: (●) $\sigma(CO^+)_{tot}$ present results, (○) $\sigma(CO^+)_I$ by Frandsen [1]. Electron impact: (——) $\sigma(CO^+)_I$ by Orient and Srivastava [17], (- - - -) $\sigma(CO^+)_I$ by Tian and Vidal [15]. The two vertical lines indicate $E(CO^+)_{Ps}$ and $E(CO^+)_I$ respectively.

ionisation cross section. The significance of the contribution grows larger as one goes to even lower energies. At around the maximum of the total cross section, the positronium formation contributes from 40 to 85%, depending on the target gas, to $\sigma(AB^+)_{tot}$. Even as the direct ionisation cross section falls to zero at $E(AB^+)_I$ the total ionisation cross section has a significant value at $E(AB^+)_I$ as compared to its maximum value. The total cross section falls to zero at $E(AB^+)_{Ps}$. From the present data it is not quite clear whether the final decent of $\sigma(AB^+)_{tot}$ proceeds by a sharp or slow decrease. Nevertheless it is clear for all four gases that positronium formation is significant within the gap between $E(AB^+)_{Ps}$ and $E(AB^+)_I$.

The behaviour described above is completely analogous to that observed in section 2.3.1 for single ionisation of the noble gases. Our results for the total non-dissociative ionisation cross section of molecules are thereby in accordance with the standard picture of single ionisation, as discussed in section 2.1.1. As mentioned in section 5.1, this is also what was concluded from the antiproton experiments by Hvelplund *et al.* [2] and Knudsen *et al.* [3]. One also notes that

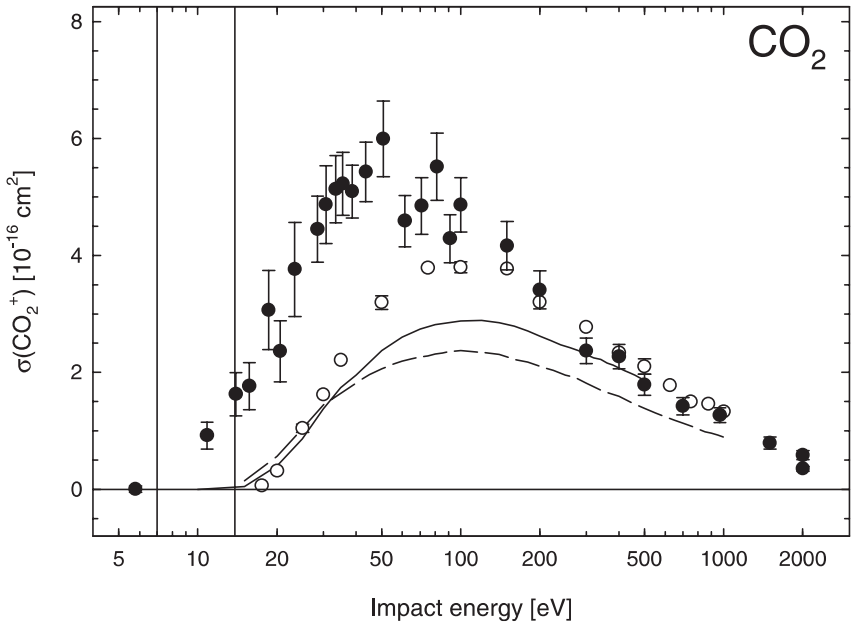

Figure 5.3: Non-dissociative ionisation of CO_2. Positron impact: (●) $\sigma(CO_2^+)_{\rm tot}$ present results, (○) $\sigma(CO_2^+)_{\rm I}$ by Frandsen [1]. Electron impact: (——) $\sigma(CO_2^+)_{\rm I}$ by Orient and Srivastava [17], (- - - -) $\sigma(CO_2^+)_{\rm I}$ by Straub *et al.* [18]. The two vertical lines indicate $E(CO_2^+)_{\rm Ps}$ and $E(CO_2^+)_{\rm I}$ respectively.

the behaviour of the direct ionisation data by Frandsen fits this picture, by $\sigma(AB^+)_{\rm I}$ for positron impact being larger than $\sigma(AB^+)_{\rm I}$ for electron impact at intermediate energies. Furthermore one observes a possible cross-over at lower energies as expected (see discussion in section 2.1.1). This is best observed in the cross sections for CH_4 in figure 5.4.

5.3.2 Dissociative ionisation

The present results for the total dissociative ionisation cross sections of N_2, CO and CO_2 are presented in figures 5.5–5.7 respectively. As discussed in section 5.2.2, no results are presented for dissociative ionisation of CH_4. For N_2 we present the cross section for the ion fragment N^+ (and N_2^{2+}, see section 5.2.1), for CO the cross sections for the ion fragments O^+ and C^+, while for CO_2 we present cross sections for the ion fragments CO^+, O^+ and C^+. Several other ion fragments were at times observed for some of the gases. However the counting statistics were too poor for the cross sections of these fragments to

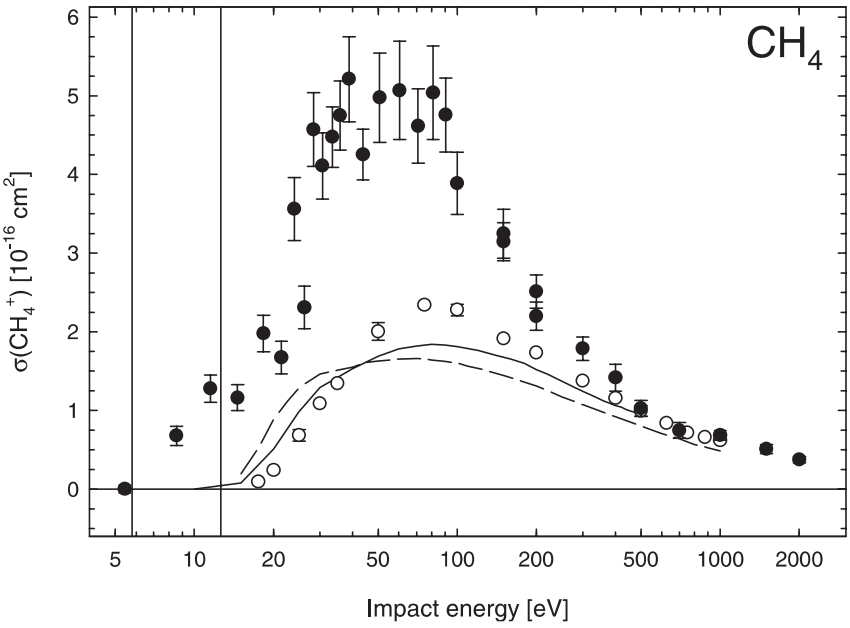

Figure 5.4: Non-dissociative ionisation of CH_4. Positron impact: (●) $\sigma(CH_4^+)_{\rm tot}$ present results, (○) $\sigma(CH_4^+)_{\rm I}$ by Frandsen [1]. Electron impact: (——) $\sigma(CH_4^+)_{\rm I}$ by Orient and Srivastava [17], (- - - -) $\sigma(CH_4^+)_{\rm I}$ by Straub *et al.* [19]. The two vertical lines indicate $E(CH_4^+)_{\rm Ps}$ and $E(CH_4^+)_{\rm I}$ respectively.

be deduced. Corresponding to figures 5.1–5.3, in figures 5.5–5.7 we include the direct dissociative ionisation data for positron impact by Frandsen [1] and for the respective gases the electron impact data by Tian and Vidal [15], Krishnakumar and Srivastava [16], Orient and Srivastava [17] and Straub *et al.* [18,25].

One starts by noting that in figure 5.6 for CO and in particular in figure 5.7 for CO_2 there is a discrepancy between the electron impact data by Orient and Srivastava and those by Tian and Vidal and Straub *et al.* respectively. Of these experiments it is only the latter two that demonstrate full collection of all ion fragments. The data by Tian and Vidal and Straub *et al.* should therefore be considered the most reliable. The observed difference could be explained by an incomplete ion collection in the experiment by Orient and Srivastava, as their data are lower than those of the other two experiments. This is also supported by the observations by Knudsen *et al.* [3] as discussed in section 5.2.2. It is the large recoil energies with which the ion fragments are created in dissociative ionisation that makes them hard to collect. Similarly the measurement of electron impact dissociative ionisation of N_2 by Krishnakumar

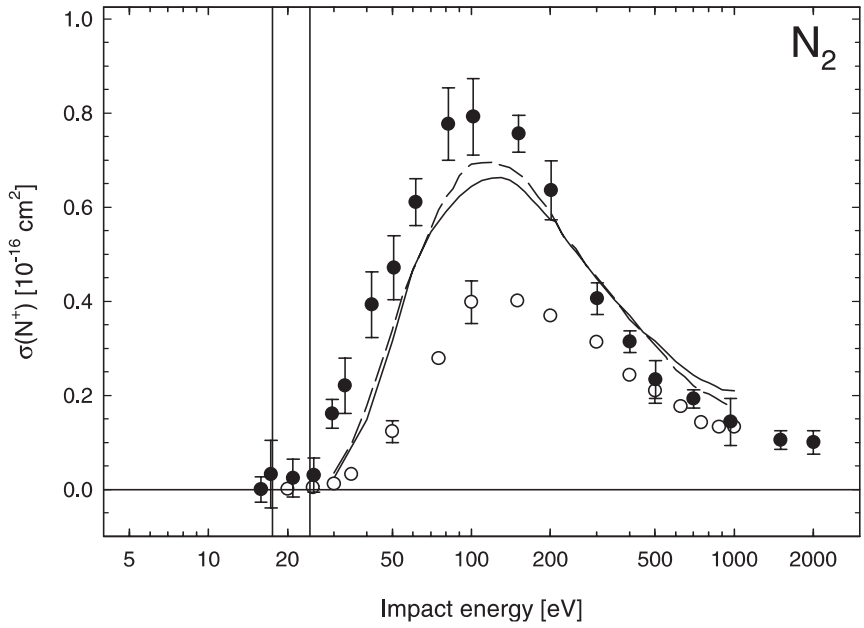

Figure 5.5: Dissociative ionisation of N_2 into N^+ (and N_2^{2+}). Positron impact: (●) $\sigma(A^+)_{tot}$ present results, (○) $\sigma(A^+)_I$ by Frandsen [1]. Electron impact: (——) $\sigma(A^+)_I$ by Krishnakumar and Srivastava [16], (----) $\sigma(A^+)_I$ by Straub *et al.* [25]. The two vertical lines indicate $E(A^+)_{Ps}$ and $E(A^+)_I$ respectively.

and Srivastava in figure 5.5 did not demonstrate full ion collection. However in this case good agreement is observed with the electron impact data by Straub *et al.* which have full ion collection.

As with the non-dissociative ionisation cross sections, the behaviour of the present results for dissociative ionisation of the three gases N_2, CO and CO_2 are similar. Starting at the highest energies one observes the present results for $\sigma(A^+)_{tot}$ to be merged with the $\sigma(A^+)_I$ by Frandsen. Unlike in non-dissociative ionisation, this is not related to some common normalisation, but shows directly that there is no significant contribution from positronium formation to $\sigma(A^+)_{tot}$ at these energies. Also at the highest energies or slightly above, the positron data seem to merge with the most reliable electron data, indicating that above these energies the dissociative cross sections are independent of the sign of the projectile charge. This happens at energies that are somewhat lower than those expected from results on e.g. double ionisation of the noble gases.

In figures 5.5 and 5.6 for N_2 and CO respectively, one observes the positron data to fall below the most reliable electron data at energies between 200 and

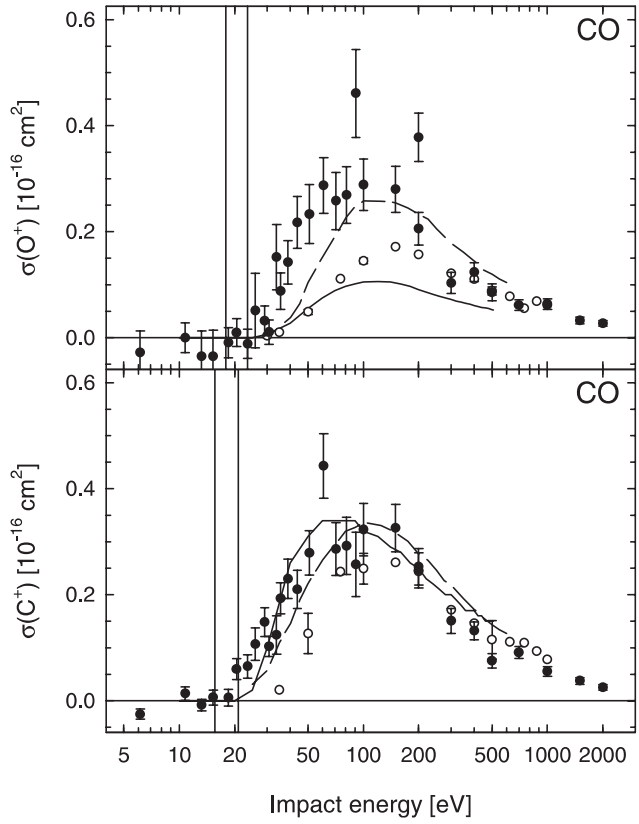

Figure 5.6: Dissociative ionisation of CO into O^+ and C^+ respectively. Positron impact: (●) $\sigma(A^+)_{tot}$ present results, (○) $\sigma(A^+)_I$ by Frandsen [1]. Electron impact: (——) $\sigma(A^+)_I$ by Orient and Srivastava [17], (----) $\sigma(A^+)_I$ by Tian and Vidal [15]. The two vertical lines indicate $E(A^+)_{Ps}$ and $E(A^+)_I$ respectively.

500 eV. The effect is most clearly observed when comparing the electron data to $\sigma(A^+)_I$ by Frandsen, but it can also be seen for the present results as long as these are merged with the direct ionisation data. This effect is an indication of the quantal interference model discussed in section 5.1 and is the same effect as observed for double ionisation of the noble gases in section 2.3.2. The direct ionisation data by Frandsen continues to lie below the electron data for energies below 200 eV. The same difference becomes apparent in CO_2 as well at low energies.

At intermediate energies the present results for $\sigma(A^+)_{tot}$ rise above $\sigma(A^+)_I$ by Frandsen, showing that for all the measured ion fragments there is a contribu-

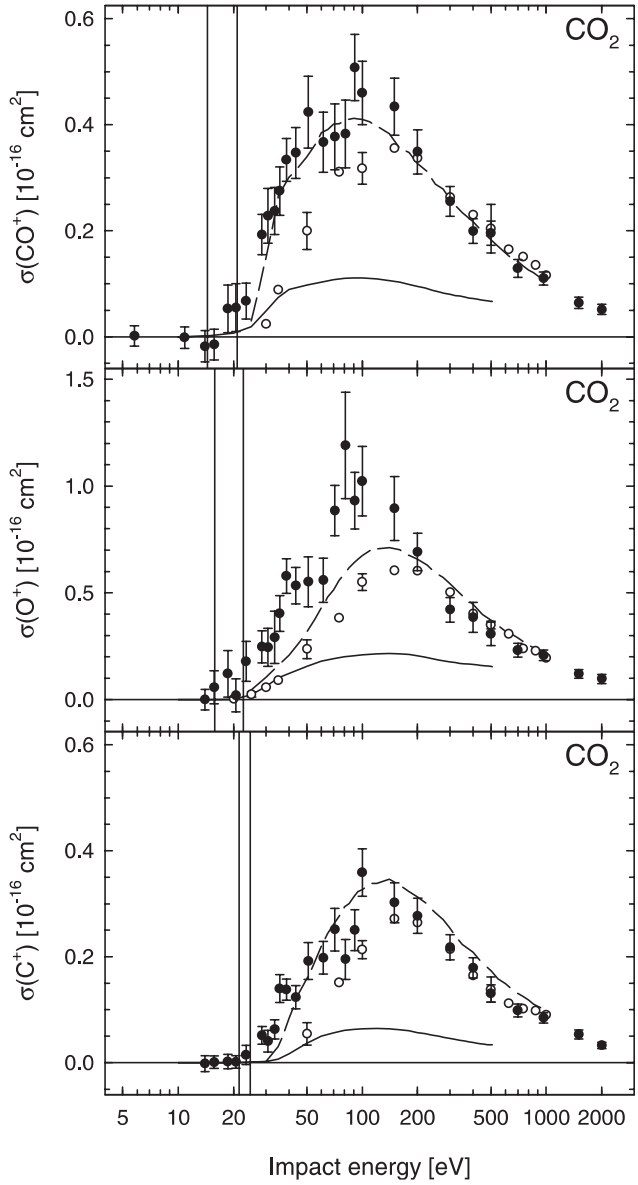

Figure 5.7: Dissociative ionisation of CO_2 into CO^+, O^+ and C^+ respectively. Positron impact: (●) $\sigma(A^+)_{tot}$ present results, (○) $\sigma(A^+)_I$ by Frandsen [1]. Electron impact: (——) $\sigma(A^+)_I$ by Orient and Srivastava [17], (- - - -) $\sigma(A^+)_I$ by Straub *et al.* [18]. The two vertical lines indicate $E(A^+)_{Ps}$ and $E(A^+)_I$ respectively.

tion from dissociative ionisation with positronium formation. The significance of the contribution varies from a clear one in $\sigma(N^+)_{tot}$ for N_2 to nearly none in $\sigma(C^+)_{tot}$ for CO_2.

Near threshold and in the gap between $E(A^+)_{Ps}$ and $E(A^+)_I$ one sees that $\sigma(A^+)_{tot}$ for all fragments falls to zero within the entire gap. This shows that there is virtually no contribution from positronium formation to dissociative ionisation at these near-threshold energies. Exceptions are found for a few fragments, like for example C^+ from CO or O^+ from CO_2, where single data points within the gap or the general trend of $\sigma(A^+)_{tot}$ above $E(A^+)_I$ could indicate a possible small contribution. Nevertheless there is clearly a suppression of positronium formation within the gap as compared to non-dissociative ionisation. This behaviour is the same as observed in double ionisation of the light noble gases helium and neon in section 2.3.2. On the other hand the contribution from the positronium channel at intermediate energies, as found above, is more similar to that seen in double ionisation of the heavy noble gases. With respect to positronium formation the present results for dissociative ionisation therefore seem to form a kind of intermediate case.

The observed suppression of positronium formation at near-threshold energies makes one speculate whether or not this could somehow be explained by the recapture model proposed by Humberston and Van Reeth [26] for the noble gases (see discussion in section 2.3.2). Looking at a process like the dissociative positronium formation process (5.5) it might be true that it shares two-electron features in common with double ionisation of e.g. helium. However the ion fragment created in this process is still only singly charged. Any recapture process would therefore be more like a recapture process in single ionisation of a noble gas, where there is no observable suppression. It is therefore not quite clear how, if at all, the ideas of the recapture model by Humberston and Van Reeth could be applied to the molecular case [27].

Qualitatively one can however make one observation on the behaviour of the positronium formation channel. Looking at figure 5.7 for CO_2 one notes that the least significant contribution from the positronium channel is found in $\sigma(C^+)_{tot}$. Since the carbon atom sits in the middle of the linear triatomic CO_2 molecule, both oxygen atoms have to be stripped away in order to create a C^+ ion. This makes the production of a C^+ ion from CO_2 a more 'violent' dissociation than e.g. production of a CO^+ ion, in that more molecular bonds have to be broken. The small contribution from positronium formation to $\sigma(C^+)_{tot}$ in CO_2 could therefore be related to the observed lack of positronium formation in double ionisation of helium and neon, since double ionisation of these two gases are characterised by being 'violent' as well, i.e. by having the highest threshold energies among the noble gases. Further studies on either the molecular targets discussed in this chapter or on other gases, might help quantify some of these considerations.

References

[1] N. P. Frandsen, Master's thesis, University of Aarhus, 1993.

[2] P. Hvelplund, H. Knudsen, U. Mikkelsen, E. Morenzoni, S. P. Møller, E. Uggerhøj, and T. Worm, J. Phys. B: At. Mol. Opt. Phys. **27**, 925 (1994).

[3] H. Knudsen, U. Mikkelsen, K. Paludan, K. Kirsebom, S. P. Møller, E. Uggerhøj, J. Slevin, M. Charlton, and E. Morenzoni, J. Phys. B: At. Mol. Opt. Phys. **28**, 3569 (1995).

[4] D. Fromme, G. Kruse, W. Raith, and G. Sinapius, J. Phys. B: At. Mol. Opt. Phys. **21**, L261 (1988).

[5] F. M. Jacobsen, N. P. Frandsen, H. Knudsen, and U. Mikkelsen, J. Phys. B: At. Mol. Opt. Phys. **28**, 4675 (1995).

[6] P. Ashley, J. Moxom, and G. Laricchia, Phys. Rev. Lett. **77**, 1250 (1996).

[7] J. Moxom, P. Ashley, and G. Laricchia, Can. J. Phys. **74**, 367 (1996).

[8] M. R. Poulsen, N. P. Frandsen, and H. Knudsen, Hyperfine Interact. **89**, 73 (1994).

[9] J. Moxom, J. Xu, G. Laricchia, L. D. Hulett, D. M. Schrader, Y. Kobayashi, B. Somieski, and T. A. Lewis, Nucl. Instr. and Meth. B **143**, 112 (1998).

[10] J. Moxom, D. M. Schrader, G. Laricchia, L. D. Hulett, and J. Xu, Appl. Surf. Sci. **149**, 244 (1999).

[11] C. K. Kwan, W. E. Kauppila, S. Nazaran, D. Przybyla, N. Scahill, and T. S. Stein, Nucl. Instr. and Meth. B **143**, 61 (1998).

[12] O. Sueoka, H. Takaki, A. Hamada, H. Sato, and M. Kimura, Chem. Phys. Lett. **288**, 124 (1998).

[13] O. Sueoka, A. Hamada, M. Kimura, H. Tanaka, and M. Kitajima, J. Chem. Phys. **111**, 245 (1999).

[14] St. Hałas and B. Adamczyk, Int. J. Mass. Spec. Ion Phys. **10**, 157 (1972–73).

[15] C. Tian and C. R. Vidal, J. Phys. B: At. Mol. Opt. Phys. **31**, 895 (1998).

[16] E. Krishnakumar and S. K. Srivastava, J. Phys. B: At. Mol. Opt. Phys. **23**, 1893 (1990).

[17] O. J. Orient and S. K. Srivastava, J. Phys. B: At. Mol. Phys. **20**, 3923 (1987).

[18] H. C. Straub, B. G. Lindsay, K. A. Smith, and R. F. Stebbings, J. Chem. Phys. **105**, 4015 (1996).

[19] H. C. Straub, D. Lin, B. G. Lindsay, K. A. Smith, and R. F. Stebbings, J. Chem. Phys. **106**, 4430 (1997).

[20] E. Krishnakumar and S. K. Srivastava, J. Phys. B: At. Mol. Opt. Phys. **21**, 1055 (1988).

[21] L. H. Andersen, P. Hvelplund, H. Knudsen, S. P. Møller, A. H. Sørensen, K. Elsener, K.-G. Rensfelt, and E. Uggerhøj, Phys. Rev. A **36**, 3612 (1987).

[22] I. Ben-Itzhak, S. G. Ginther, and K. D. Carnes, Phys. Rev. A **47**, 2827 (1993).

[23] I. Ben-Itzhak, K. D. Carnes, S. G. Ginther, D. T. Johnson, P. J. Norris, and O. L. Weaver, Phys. Rev. A **47**, 3748 (1993).

[24] U. Mikkelsen, Master's thesis, University of Aarhus, 1994.

[25] H. C. Straub, P. Renault, B. G. Lindsay, K. A. Smith, and R. F. Stebbings, Phys. Rev. A **54**, 2146 (1996).

[26] J. W. Humberston and P. Van Reeth, J. Phys. B: At. Mol. Opt. Phys. **33**, L97 (2000).

[27] J. W. Humberston, private communication.

Chapter 6

Summary

The purpose of the experiments presented in this thesis has been to study the total ionisation cross section of atoms and molecules by positron impact. Through these measurements information about positronium formation has been obtained. This has been done both directly through near-threshold measurements and through comparison of the present total ionisation cross sections with known cross sections for direct ionisation.

In chapter 2 measurements of the total single ionisation cross section of argon, krypton and xenon and measurements of the total double ionisation cross section of helium, neon, argon, krypton and xenon are presented. It has been found that while positronium formation is significant in single ionisation at both near-threshold and intermediate energies this not true for double ionisation. In helium and neon a suppression of double ionisation with positronium formation has been observed at all energies. In argon, krypton and xenon a small contribution from positronium formation has been found at both low and intermediate energies. However even in these three heavy gases it is clear from the threshold behaviour of the cross sections that positronium formation is not as significant a channel at near-threshold energies in double ionisation as in single ionisation.

In chapter 3 Wannier theory and the semiempirical Rost-Pattard parameterisation are discussed. As the present experiments on the noble gases have provided the first near-threshold data for double ionisation of atoms by positron impact, a modified Rost-Pattard model have been developed to describe this case. It has successfully been applied to our data for double ionisation of helium and neon, showing that this kind of model can be extended from single to double ionisation.

In chapter 4 measurements of both the direct and total single ionisation cross sections of atomic deuterium are presented, settling the dispute existing within the literature between previous measurements of these cross sections.

Comparison has been made with the most recent theoretical calculations and good agreement has been found.

Finally in chapter 5 measurements of the total non-dissociative single ionisation cross section of the molecules N_2, CO, CO_2 and CH_4 are presented. For the first three there are also presented the total dissociative ionisation cross sections for fragmentation into several different types of ion fragments. It has been found that the non-dissociative ionisation cross sections exhibit a behaviour which is similar to that observed for single ionisation of the noble gases in chapter 2. The dissociative ionisation cross sections on the other hand have a behaviour which is closer to that observed in double ionisation of the noble gases. With respect to positronium formation the dissociative cross sections exhibited a suppression of this channel at near-threshold energies, but at the same time also exhibited a clear contribution at intermediate energies. The behaviour of the dissociative ionisation cross sections can therefore best be classified as somewhere between the double ionisation cross sections of the light noble gases, helium and neon, and those of the three heavy noble gases.

Prior to the present studies it was believed that the contribution to the total ionisation cross section from positronium formation would exhibit a similar behaviour irrespective of the target and the degree of ionisation. This picture was mainly based on observations of single ionisation. The present studies of single ionisation of atoms and non-dissociative single ionisation of molecules in chapters 2, 4 and 5 confirm this picture. However with the present results for double ionisation of the noble gases and for dissociative ionisation of the small molecules, a far more complex behaviour of ionisation with positronium formation has been uncovered. Particularly the behaviour observed in double ionisation of helium and neon seems unique even compared to that of both the heavy noble gases and dissociative ionisation of the molecules. This could indicate an importance for positronium formation of the strong correlation between target electrons prior to the collision as in helium and neon. In chapter 2 the observed behaviour of the near-threshold cross sections of the noble gases is discussed in terms of the recapture model by Humberston and Van Reeth. While this model concerns a post-collisional mechanism for the suppression of positronium formation in double ionisation, it does not deal with the actual initial positronium formation. The present results show that such considerations could be very important in order to explain the observed behaviour. A complete understanding of positronium formation in multi-electron ionisation processes has therefore not yet been reached.

As a conclusion of this thesis are given a few brief remarks on some of the future research within the field of atomic collisions with positrons that would help clarify some of the results presented within this thesis. First of all, much of our discussion of positronium formation in double ionisation has been based on comparisons between direct and total ionisation cross sections. For a more

quantitative discussion than the one presented here, there is a need for better data for direct ionisation, particularly at near-threshold energies. Despite that these will be elaborate and time consuming to measure, they can be obtained with the positron beam intensities available today.

Secondly one could wish for more theoretical investigations into some of the phenomena observed. Apart from those presented in chapter 4, there is a general lack of calculations for ionisation processes, particularly for those that are more complex. For example numerical calculations of positronium formation in double ionisation would be desirable. Today there already exist coupled state calculations of positronium formation in single ionisation of e.g. helium. Expanding these calculations to double ionisation is a question of including the appropriate states in the calculation and is hence a question of computational power. As a start one could maybe limit the calculations to within the second Ore gap, where the number of extra states to be included is more limited. One can only hope that advances in algorithms and computer power will make such calculations feasible in the near future. Also more investigations into models like the Rost-Pattard model are needed, as this seems to point toward some sort of common underlying ionisation mechanism.

Thirdly with respect to our molecular studies there is a multitude of other small molecules, like e.g. O_2, C_2H_2 and CF_4, that could be interesting to investigate. One could also try to measure the total non-dissociative *double* ionisation cross section of e.g. CO and CO_2 in order to get a better understanding of how the present results for non-dissociative and dissociative ionisation of molecules fit in with respect to our noble gas data.

Finally one can only hope that advances in positron beam intensities and in the experimental technique in general will help in the future to produce better and more easily obtainable results.

Dansk resumé

Denne afhandling er en præsentation af resultaterne af et 4-årigt forskningsarbejde udført ved Institut for Fysik og Astronomi ved Århus Universitet. Nogle af resultaterne er også opnået under et ophold ved University College London i England. Det overordnede emne for det udførte arbejde har været eksperimentel atomfysik, nærmere bestemt atomare kollisioner med positroner.

'Atomfysik' står for mange almindelige mennesker som indbegrebet af moderne fysik. Af fysikere betragtes atomfysik som værende den gren inden for fysikken, der har sit væsentligste udspring i Niels Bohrs atommodel fra 1913. Det Bohr gjorde, var at lave en teoretisk beskrivelse af det simple brintatom. I brint kredser én enkelt elektron rundt om en atomkerne bestående af kun én proton. Bohrs fortjeneste var, at han postulerede, at elektronen kun kan bevæge sig rundt om protonen i nogle helt bestemte 'energitilstande'. I dag vil man sige, at det Bohr gjorde, var at beskrive brintatomets 'struktur'. Bohrs atommodel blev udgangspunkt for det, vi i dag kalder kvantemekanik. Kvantemekanikken er den teori, der bruges til at beskrive atomers struktur. Sideløbende med udviklingen af teorien for atomer har det også været vigtigt at lave eksperimentelle undersøgelser af atomernes struktur. Der har altid i fysikken været et nært samspil imellem teori og eksperiment. Selv Bohrs teori var inspireret af eksperimentelle observationer af det lys, atomer kan udsende. I dag bruges eksperimenter til enten at teste teoretiske forudsigelser eller til at give inspiration til nye retninger og muligheder inden for teorien, som burde udforskes.

En af de måder man med eksperimenter kan undersøge atomers struktur, er via atomare kollisioner. I atomare kollisioner skyder man partikler på atomer og observerer, hvordan de spredes. Disse partikler kan være enten elektroner, protoner, andre atomer osv. Måden hvorpå sådanne projektiler spredes, afhænger af strukturen af det atom, man skyder dem på. Man har dog også fundet, at spredningen afhænger af hvilken slags partikel, man bruger som projektil. Sammenligner man f.eks. spredning af elektroner og protoner, ser man en forskel. Dette skyldes bl.a., at elektronen har negativ ladning, mens protonen er positivt ladet, samt at protonen vejer 1836 gange mere end elektronen. Spredningen

afhænger altså af samspillet imellem projektilets egenskaber og atomets struktur. At forstå dette samspil er af stor interesse for atomfysikken.

Traditionelt har man i eksperimenter med atomare kollisioner ofte brugt elektroner eller protoner som projektiler, da disse fra natures hånd er let tilgængelige. Sammenligner man spredning af elektroner og protoner, er der dog det problem, at man ikke helt kan sige om den forskel, man observerer, skyldes, at de to projektiler har forskellig ladning, eller om den skyldes deres forskellige masse. For at afklare dette spørgsmål har eksperimentalfysikere søgt at bruge andre og mere 'eksotiske' projektiler. Et sådan projektil er positronen.

Positronen er elektronens antipartikel. Hvad en antipartikel og mere generelt antistof præcist er, skal vi ikke komme ind på her, men blot nævne at antistof ikke findes i ret store mængder i universet omkring os. Hvorfor det er sådan, er et af fysikkens store ubesvarede spørgsmål. Det er dog heldigt, at det er sådan, da antistof kan annihilere med almindeligt stof. Det betyder, at hvis en positron støder direkte ind i en elektron, vil de begge forsvinde i et slags lysglimt. Store mængder antistof i universet kunne derfor være ret så ubehageligt. Der findes dog radioaktive kilder, der udsender små mængder af positroner. Sådanne kilder er ofte hovedkomponenten i de eksperimentelle opstillinger, der bruges til at lave atomare kollisioner med positroner. Fordi positronen er elektronens antipartikel, har den som projektil de smarte egenskaber, at den vejer det samme som en elektron, men har en ladning med modsat fortegn, dvs. at den er positiv. Sammenligner man derfor spredning af elektroner med spredning af positroner, kan en evt. forskel *kun* skyldes forskellen i ladning. Af tekniske årsager har det kun rigtigt været muligt at lave denne slags kollisionsforsøg med positroner siden starten af 1970'erne. Siden da har man dog lært en masse om spredningsmekanismer fra disse forsøg. En del af arbejdet præsenteret i denne afhandling vedrører den slags undersøgelser med sammenligning af positroners spredning med bl.a. elektroners og protoners spredning.

Tingene er dog ikke altid så simple som beskrevet ovenfor. Fra atomare kollisioner ved man, at nogle projektiler har nogle ganske særlige spredningsmekanismer. For eksempel har elektroner det, der på engelsk kaldes 'exchange', hvilket kan oversættes med 'ombytning' eller 'udveksling'. Ved denne spredningsmekanisme bytter elektronen, som er projektil, plads med en elektron i atomet. Da elektronerne er ens, kan man ikke umiddelbart se, om denne ombytning finder sted eller ej. Med protoner som projektil kan der ske det, der kaldes 'indfangning'. Ved denne mekanisme stjæler protonen en elektron fra det atom, man skyder på, og danner et brintatom. Atomet, der nu mangler en elektron, siges at være blevet enkelt ioniseret. Protonen kunne også have enkelt ioniseret atomet ved blot at slå en elektron af uden at indfange den. Disse to mekanismer kan dog skelnes fra hinanden. Når man studerer atomare kollisioner, er det vigtigt at være opmærksom på sådanne særlige mekanismer som f.eks. indfangning. Især i teoretiske beregninger skal man ofte huske at tage hensyn til

dem. Eksperimentelt kan man tit tage forbehold, der gør, at man enten kan undgå disse mekanismer eller ligefrem vælge direkte at studere dem.

Positronen har den samme positive ladning som protonen. Derfor har positronen også den samme indfangningsmekanisme som protonen. Når en positron indfanger en elektron, danner de et slags pseudoatom kaldet positronium. I positronium er der ingen atomkerne som f.eks. i brint. I stedet kredser positronen og elektronen nærmest om hinanden. Positronium er meget ustabilt og lever højst i ca. én 10 milliontedel af et sekund. Det er fordi positronen og elektronen før eller siden opdager, at de er hinandens antipartikler og annihilerer med hinanden. Som med protoner bliver atomet enkelt ioniseret af denne mekanisme. Skønt positronium atomet hurtigt forsvinder, kan man godt med eksperimenter måle, hvor vigtig indfangning er ved ionisering i kollisioner af positroner med atomer. Den centrale del af denne afhandling handler om målinger af positronens indfangningsmekanisme ved ionisering.

Ved enkelt ionisering af et atom er den vigtigste betingelse for at indfangning kan finde sted, at det positivt ladede projektil og den løsrevne elektron flyver bort fra kollisionen sammen i cirka samme retning og med omtrent den samme fart. Dette betyder, at indfangning især sker, når projektilet kommer ind mod atomet med lav hastighed[1], da elektronen så har nemmere ved at 'følge med'. Det betyder også, at indfangning er relativt mere vigtig i enkelt ionisering med positroner end med protoner. Det er fordi protonen er så tung, at den kun afbøjes ganske lidt i en kollision. Det er derfor op til en løsreven elektron at indrette sig efter protonen for at indfangning kan finde sted. Da positronen er 1836 gange lettere end protonen, kan den afbøjes langt mere. Det gør det relativt mere sandsynligt for at positronen og en løsreven elektron ender med at følges ad. Alt dette har været kendt relativt længe både teoretisk og eksperimentelt. Nogle af resultaterne fra denne afhandling bekræfter også, at det forholder sig sådan.

Et af de vigtigste spørgsmål, der er undersøgt i denne afhandling, er dog, hvordan det forholder sig med indfangning, hvis man *dobbelt* ioniserer atomet i stedet, dvs. slår to elektroner af under en kollision. Før resultaterne fra denne afhandling blev kendt, troede man at indfangning ville betyde lige så meget i dobbelt ionisering med positroner som i enkelt ionisering. For det første er der to elektroner at vælge imellem, og for det andet er dobbelt ionisering en mere 'voldsom' kollision end enkelt ionisering, så positronen kan stadig afbøjes mindst lige så meget som før. Vores resultater har vist, at det *ikke* forholder sig sådan.

Fra et eksperiment, hvori vi har set på kollisioner af positroner med det simpleste to-elektron atom, nemlig ædelgassen helium, har vi fundet, at indfangning *ikke* kan finde sted ved dobbelt ionisering. Det samme gælder i ædelgassen

[1] Lav hastighed betyder i denne sammenhæng en hastighed sammenlignelig med den, elektronerne har i atomet, dvs. i størrelsesorden af ca. 1% af lysets hastighed.

neon. For de tre tungere ædelgasser argon, krypton og xenon har vi fundet, at nogen indfangning finder sted. Dog ved de laveste projektilhastigheder finder der mindre indfangning sted end umiddelbart forventet. Disse resultater betragtes som højst overraskende. Der findes endnu ikke nogen fuld teoretisk forklaring til dette fænomen. Det eneste forslag hidtil er en mekanisme, hvori den tilbageblevne ion efter ioniseringen af atomet selv udfører en slags omvendt indfangning af elektronen i positronium pseudoatomet. Resultatet bliver derved ikke en dobbelt ionisering med indfangning men en enkelt ionisering *uden* indfangning. Denne mekanisme skulle så være særlig favorabel i helium og neon, hvor vi overhovedet ingen dobbelt ionisering med indfangning ser. Om denne teori er korrekt, eller om tingene forholder sig anderledes, er dog stadig uvist.

Den forskning, der er udført til denne afhandling, hører ind under det man kalder grundforskning. Det betyder, bl.a. at resultaterne ikke har nogen umiddelbar teknologisk anvendelse. De studerede systemer bestående af f.eks. en atomkerne, to elektroner og en positron, kan virke meget simple. Det er dog igennem forståelsen af sådanne systemer, at man kan gøre sig håb om en bedre forståelse af mere generelle problemer i atomfysikken. Vores resultater har vist, at inden for den del af atomfysikken, der har med atomare kollisioner at gøre, er der stadig simple mekanismer, vi endnu ikke forstår fuldt ud. Forhåbentlig vil kommende forskning bibringe en forklaring til de observerede fænomener, og dermed give os en bedre forståelse af atomare kollisioner og atomer generelt.

List of Figures

1.1 Advantage of moderation 8

2.1 Capture in double ionisation of helium by proton impact 19
2.2 Single ionisation of helium [keV/amu] 21
2.3 Single ionisation of helium by positron impact 22
2.4 Ratio $R_{\mathrm{I}}^{(2)}$ for helium [keV/amu] 27
2.5 Schematic of the Århus electrostatic beam line and gas cell . . . 31
2.6 Time-of-flight MCA spectrum 34
2.7 Single ionisation of neon by positron impact 38
2.8 Single ionisation of argon 41
2.9 Single ionisation of krypton 42
2.10 Single ionisation of xenon 43
2.11 Double ionisation of helium 44
2.12 Double ionisation of neon 45
2.13 Double ionisation of argon 46
2.14 Double ionisation of krypton 47
2.15 Double ionisation of xenon 48
2.16 Threshold behaviour of $\sigma_{\mathrm{tot}}^{2+}$ for Ne, Ar, Kr and Xe 51
2.17 Double ionisation of argon [keV/amu] 53

3.1 Four-particle break-up configuration of e^+ on H^- 62
3.2 Rost-Pattard plot of σ_{I}^{+} for hydrogen (helium) 65
3.3 MRP plot of $\sigma_{\mathrm{tot}}^{2+}$ for helium and neon 68
3.4 MRP plot of $\sigma_{\mathrm{tot}}^{2+}$ for argon and krypton 70

4.1 Schematic of UCL experiment 79
4.2 Total single ionisation of atomic hydrogen 83
4.3 Direct single ionisation of atomic hydrogen 84
4.4 Positronium formation in atomic hydrogen 85

5.1 Non-dissociative ionisation of N_2 97
5.2 Non-dissociative ionisation of CO 98

5.3 Non-dissociative ionisation of CO_2 99
5.4 Non-dissociative ionisation of CH_4 100
5.5 Dissociative ionisation of N_2 101
5.6 Dissociative ionisation of CO 102
5.7 Dissociative ionisation of CO_2 103